


## REVIEW ARTICLE

# Avenues to molecular imaging of dying cells: Focus on cancer

Anna A. Rybczynska<sup>1,2</sup> | Hendrikus H. Boersma<sup>1,3</sup> | Steven de Jong<sup>4</sup> |  
Jourik A. Gietema<sup>4</sup> | Walter Noordzij<sup>1</sup> | Rudi A. J. O. Dierckx<sup>1,5</sup> |  
Philip H. Elsinga<sup>1</sup> | Aren van Waarde<sup>1</sup> 

<sup>1</sup>Molecular Imaging Center, Department of Nuclear Medicine and Molecular Imaging, University of Groningen, University Medical Center Groningen, Groningen, the Netherlands

<sup>2</sup>Department of Genetics, University of Groningen, Groningen, the Netherlands

<sup>3</sup>Department of Clinical Pharmacy & Pharmacology, University of Groningen, Groningen, the Netherlands

<sup>4</sup>Department of Medical Oncology, University of Groningen, Groningen, the Netherlands

<sup>5</sup>Department of Nuclear Medicine, Ghent University, Ghent, Belgium

## Correspondence

Aren van Waarde, Molecular Imaging Center, Department of Nuclear Medicine and Molecular Imaging, University Medical Center Groningen, University of Groningen, Hanzeplein 1, 9713GZ Groningen, the Netherlands.  
Email: a.van.waarde@umcg.nl

## Abstract

Successful treatment of cancer patients requires balancing of the dose, timing, and type of therapeutic regimen. Detection of increased cell death may serve as a predictor of the eventual therapeutic success. Imaging of cell death may thus lead to early identification of treatment responders and nonresponders, and to “patient-tailored therapy.” Cell death in organs and tissues of the human body can be visualized, using positron emission tomography or single-photon emission computed tomography, although unsolved problems remain concerning target selection, tracer pharmacokinetics, target-to-nontarget ratio, and spatial and temporal resolution of the scans. Phosphatidylserine exposure by dying cells has been the most extensively studied imaging target. However, visualization of this process with radiolabeled Annexin A5 has not become routine in the clinical setting. Classification of death modes is no longer based only on cell morphology but also on biochemistry, and apoptosis is no longer found to be the preponderant mechanism of cell death after antitumor therapy, as was earlier believed. These conceptual changes have affected radiochemical efforts. Novel probes targeting changes in membrane permeability, cytoplasmic pH, mitochondrial membrane potential, or caspase activation have recently been

Abbreviations:  $\gamma$ H2AX, phosphorylated X isoform of the histone H2A; ABC, ATP-binding cassette; ApoPep-1, apoptosis-targeting peptide-1; ATP, adenosine 5'-triphosphate; ATR kinase, ataxia telangiectasia and Rad3-related threonine serine kinase; Bcl-2, B-cell lymphoma 2; Caspase, cysteine-aspartic protease; CytC, Cytochrome C; DDC, *N,N'*-didansyl-L-cystine; DPA, dipicolylamine; ER, endoplasmic reticulum; FbNTP, fluorobenzyl triphenyl phosphonium; LysoPS, lyso-phosphatidylserine; mAb, monoclonal antibody; MIAPaCa-2, human pancreatic carcinoma cell line; mibi, methoxyisobutylisonitrile; ML, malonic acid; MMP, mitochondrial membrane potential; MW, molecular weight; PARP-1, poly (ADP-ribose) polymerase 1; PE, phosphatidylethanolamine; PET, positron emission tomography; PKC, protein kinase C; PS, phosphatidylserine; SA, streptavidin; SPECT, single photon emission computed tomography; TNF, tumor necrosis factor; TPP, tetraphenylphosphonium; TRAIL, TNF-related apoptosis inducing ligand; z-YVAD-fmk, caspase-1 inhibitor

This is an open access article under the terms of the Creative Commons Attribution License, which permits use, distribution and reproduction in any medium, provided the original work is properly cited.

© 2018 The Authors Medicinal Research Reviews Published by Wiley Periodicals, Inc.

explored. In this review, we discuss molecular changes in tumors which can be targeted to visualize cell death and we propose promising biomarkers for future exploration.

#### KEYWORDS

apoptosis, early treatment response, necrosis, positron emission tomography (PET), single photon emission computed tomography (SPECT)

## 1 | INTRODUCTION

A living organism can be considered as a complicated machine, which requires constant maintenance, modernization, and restructuring or reconstruction. Subunits of the organism, such as cells, are continuously produced, exploited, altered, utilized and exchanged. Billions of cells die daily as a part of natural processes in the adult human body, and even more cells die during embryonic development. Under physiological conditions, superfluous, dangerous, or damaged cells are killed and dismantled in a discrete and highly orchestrated manner. For instance, squamous epithelial cells are removed via cornification,<sup>1</sup> Müllerian duct in males or Wolffian duct in females via apoptosis, and pronephric kidney tubes also via apoptosis.<sup>2,3</sup> A mainstay of the body's homeostasis is a proper decision on cellular fate: death or survival.

It is thus not surprising that perturbations of cell death processes are an underlying factor of many pathologic conditions. Cell death is enhanced in ischemia,<sup>4</sup> sepsis,<sup>5</sup> type-1 diabetes,<sup>6</sup> transplant rejection,<sup>7</sup> neurodegenerative disorders,<sup>8</sup> and autoimmunity (e.g., AIDS).<sup>9</sup> In contrast, reduced cell death is observed in persistent inflammation (as occurs in chronic obstructive pulmonary disease and asthma),<sup>10,11</sup> autoimmunity (e.g., rheumatoid arthritis),<sup>12</sup> and cancer.<sup>13</sup> With nondestructive and minimally invasive medical imaging techniques like PET (positron emission tomography) and SPECT (single photon emission computed tomography), cell death in organs and tissues of the human body can be visualized and quantified. Such quantification may be important in cancer treatment, since monitoring of the increase in cell death early after the onset of antitumor therapy can serve as a predictor of the eventual therapeutic outcome.

In the following review, we describe molecular changes in tumors related to cell death and we provide an overview of the wide range of PET and SPECT tracers which have been developed to monitor these changes. We discuss the potential and the limitations of the existing tracers and we propose some promising biomarkers of dying cells which deserve to be explored in future imaging research.

### 1.1 | Canonical classification of cell death modes

There are many ways for a cell to die. In recent years our concepts of cell death have changed. In this chapter, we first describe the canonical classification of cell death modes and we subsequently summarize new observations which have led to a revised classification.

The classical concept of cell death (proposed in 1973) is based on morphologic features of dying cells and makes a distinction between three death types: apoptosis (type I), autophagic cell death (type II), and necrosis (type III) (see Table 1).<sup>14</sup> Even nowadays, cell death is still frequently classified in these three subroutines. Apoptosis and autophagy are considered as "regulated" and necrosis as "accidental" cell death.<sup>15</sup>

#### 1.1.1 | Apoptosis

Apoptosis was considered to be a noninflammatory, highly orchestrated, and inherently controlled process. Since its identification in 1972,<sup>16</sup> apoptosis has been the most investigated type of cell death. Apoptosis can be activated by intra- or extracellular stimuli and is then coined as "intrinsic" or "extrinsic" apoptosis. Both these apoptotic scenarios

**TABLE 1** Morphological classification of cell death

Apoptosis (Type I)	Autophagic cell death (Type II)	Necrosis (Type III)
Affects an individual cell	Affects an individual cell	Affects a group of cells
Cell rounding, shrinkage and detachment	Cytoplasmic vacuolization	Increased cell volume (oncosis), translucent and vacuolized cytoplasm
Cell membrane blebbing and shedding of apoptotic bodies, but membrane intact	Cell membrane intact	Cell membrane breakdown
Maintained organelles and cytoplasm condensation	Degradation of Golgi, polyribosomes and ER	Swollen organelles and cytoplasm
Chromatin condensation (pyknosis)	No/partial chromatin condensation	Chromatin condensation into small, irregular patches (karyolysis)
Nuclear fragmentation (karyorrhexis)	Appearance of autophagosomes and autolysosomes	Dilatation of the nuclear membrane
DNA fragmentation	Late DNA fragmentation	Late DNA fragmentation (after cell lysis)
Presence of phagocytosis, generally anti-inflammatory	No/little phagocytosis	Generally absence of phagocytosis, often pro-inflammatory

include extensive cellular remodeling by activated cysteine–aspartic proteases, called “caspases” (for more information, see 2.4.).

In intrinsic apoptosis, stimuli such as DNA damage and hypoxia lead to swelling or permeabilization of the mitochondrial outer membrane, dissipation of the mitochondrial membrane potential (MMP), and release of various apoptotic effectors. Apoptotic effectors serve either as activators of the proapoptotic cascade or inhibitors of the pro-survival cascade. Apoptosome complex forming compounds, such as caspase-9, cytochrome c (CytC), apoptotic peptidase-activating factor 1, deoxy-adenosine 5'-triphosphate (deoxy-ATP), and second mitochondria-derived activator of caspases (second mitochondria-derived activator of caspase/direct inhibitor of apoptosis-binding protein with low Isoelectric point (pI)) belong to the activator category, whereas B-cell lymphoma 2 (Bcl-2) family members and inhibitors of apoptosis proteins are in the inhibitor class.<sup>17–19</sup>

Extrinsic apoptosis is activated by the appearance of multiple members of a tumor necrosis factor (TNF) family of ligands via death receptors, or by the disappearance of specific ligands for dependence receptors. Death receptor ligands include TNF $\alpha$ , first apoptosis signal ligand which binds to the Fas receptor, and TNF-related apoptosis inducing ligand (TRAIL), which interacts with the TRAIL receptors.<sup>20,21</sup> An example of a ligand for a dependence receptor is netrin-1, which binds to the uncoordinated movement receptor gene 5B (mutations in this gene result in uncoordinated movement of *Caenorhabditis elegans*) receptor.<sup>22</sup> Main effectors activating the proapoptotic cascade are death-inducing signaling complex-forming: Fas-associated protein with death domain, caspase-8 and caspase-10, whereas main effectors inhibiting the proapoptotic cascade are cellular Fas-associated protein with death domain-like IL-1 $\beta$ -converting enzyme-inhibitory protein and x-linked inhibitor of apoptosis protein.<sup>23–25</sup> Extrinsic apoptosis is frequently linked to the response of the immune system to abnormalities.

Under certain circumstances (e.g., high x-linked inhibitor of apoptosis protein expression levels), components of the intrinsic apoptosis machinery can also become activated during extrinsic apoptosis. This interrelation of extrinsic and intrinsic signaling is mediated by a proapoptotic Bcl-2 member, Bcl-2 homology domain 3 interacting-domain death agonist, and serves for amplification of an apoptotic signal downstream death receptors.<sup>26</sup> Furthermore, intrinsic and extrinsic apoptosis converge through caspase-9 and caspase-8, which leads to activation of caspase-3 and cellular disassembly from within. Activation of caspase-3 is followed by cleavage of cytosolic and nuclear proteins, DNA fragmentation, cross-linking of proteins, formation of apoptotic bodies, expression of ligands for phagocytic cell receptors, and removal of apoptotic cells by phagocytosis.<sup>27</sup>

Evasion of cell death is considered to play an important role in oncogenesis and in development of treatment resistance in cancer.<sup>28</sup> One example of apoptosis evasion is a decrease in p53 signaling. P53 is a tumor suppressor protein, which can regulate the cell cycle and can induce cancer cell apoptosis in response to diverse stressful stimuli. Frequent

mutations in the *TP53* gene and/or defects in the p53 signaling pathway (e.g., upregulation of the p53 inhibitor mouse double minute 2, mouse double minute 2 homolog [E3 ubiquitin-protein ligase]) result in uncontrolled proliferation and a brake on apoptosis. This may have a subsequent impact on both initiation of oncogenesis and development of treatment resistance. Although apoptosis is the best-characterized cell death mechanism, in many cancers it is not the main cause of cell loss induced by DNA damaging agents.<sup>28</sup>

### 1.1.2 | Autophagic cell death

Autophagy is a natural, regulated process for disassembly of dysfunctional or damaged cellular organelles and proteins. Such damaged components are contained inside a double-membrane vesicle called an autophagosome. After fusion of an autophagosome and a lysosome to an autolysosome, the contents of the organelle are digested by acidic lysosomal hydrolases.<sup>29</sup>

Even today, there is much controversy on the question whether *in vivo* autophagy is a type of cell death or fulfills a pro-survival function, for example, by limiting cell constituents during nutrient starvation. This question is raised because most inhibitors of autophagy *accelerate* (and not retard) cell death.<sup>30–34</sup> For this reason, autophagic cell death has now been defined as cell death inhibited by inactivation of autophagy genes or by autophagy inhibitors, such as 3MA, rather than cell death judged by simple morphological classification.<sup>35</sup> This definition is based on studies which have elucidated molecular mechanisms of autophagic cell death.<sup>36,37</sup> Tissue-specific knockout models of genes controlling autophagy in mice have provided much information about the role of autophagy in the development and differentiation of mammalian tissues and organs.<sup>38</sup> In some tissues (e.g., mouse liver) autophagy seems to suppress tumorigenesis,<sup>39</sup> but in most cases, autophagy facilitates the formation of tumors and increases tumor growth and aggressiveness.<sup>40</sup> Autophagy seems to be particularly induced when cancers progress to metastasis.<sup>41</sup> Inhibitors of autophagy may thus be useful as adjuvants in cancer therapy.

### 1.1.3 | Necrosis

Necrosis is the consequence of irreversible damage to cells caused by factors such as mechanical trauma, infections, toxins, and shortage of oxygen and nutrients. Necrosis is traditionally thought to be an uncontrollable and accidental type of cell death, which is highly immunogenic and elicits an inflammatory response due to leakage of cytosolic contents. It was considered the death mode of cells which displayed no characteristics of apoptosis. In most cases necrosis affects not a single cell but spreads over a group of cells, as in gangrene or ischemia. Morphologic features of necrosis are listed in Table 1. At the biochemical level, necrosis is accompanied by a massive production of reactive oxygen species and reactive nitrogen species, besides a marked drop of cellular ATP.<sup>35</sup>

About 10 years ago, studies on genes that could control necrosis led to the conclusion that a regulated form of necrosis must exist. Regulated necrosis ("necroptosis") can occur as the result of activation of death receptors, for example, by TNF, first apoptosis signal ligand, or TRAIL,<sup>42</sup> and is controlled by two key regulators: TNF receptor-associated factor 2 and receptor-interacting protein kinases 1 and 3.<sup>35,43</sup> Besides the activation of death receptors, necroptosis requires inhibition of the apoptotic signaling.<sup>44</sup> This type of necrosis occurs not only in disease (e.g., in systemic inflammatory response syndrome), but also in normal physiology (e.g., in immunologically silent maintenance of T-cell homeostasis).<sup>45,46</sup> In cancer, necrosis occurs when rapid tumor growth is accompanied by insufficient vascularization or the cancer cell population becomes very dense.<sup>47</sup> It can also be a consequence of successful immunotherapy, for example, with oncolytic viruses.<sup>48</sup> The triggering of nonapoptotic cell death modes, such as regulated necrosis, is currently explored for treatment of apoptosis-resistant cancer cells.<sup>49</sup> However, clinical application of regulated necrosis in cancer treatment has not yet been achieved.

## 1.2 | Revised classification of cell death modes

Canonical (morphologic) features of a particular cell death mode can be inhibited while death is only deferred.<sup>15</sup> Under certain circumstances, a dying cell can even switch between different cell death programs, for example, the response to

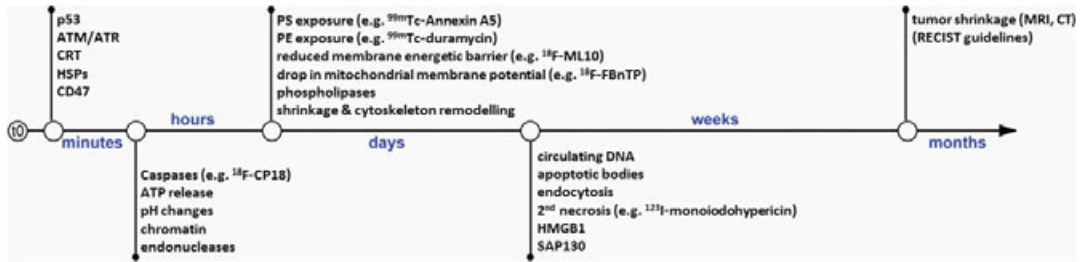


**FIGURE 1** Physiologic, molecular, and morphologic events during the time-course of cell death

DNA damage changes from apoptosis to mitotic catastrophe in p53-expressing ovarian cancer treated with cisplatin versus cisplatin and checkpoint kinase 2 (required for checkpoint-mediated cell cycle arrest) inhibitor<sup>50–52</sup> or from apoptosis to (secondary) necrosis in conditions of insufficient phagocytosis. This suggests that an interplay and/or a fluidic switch may exist between various types of cell death.<sup>53</sup> Apparently, cell death may differ not only in its main morphologic features but also in biochemical features, cell types involved, and activating mechanisms. Moreover, morphologic features are hardly quantifiable and do not take functional, biochemical, and immunological variables into account. Therefore, scientists have shifted from a morphological to a biochemical classification of cell death.<sup>35</sup> As a consequence, the canonical distinction of three different cell death modes has been revised and expanded to comprise 14 subroutines (see Table 2), of which ten play a proven role in treatment-induced cancer cell death.<sup>15,35,54</sup> These include: apoptosis (divided into: intrinsic caspase-dependent, intrinsic caspase-independent, extrinsic by death receptors, extrinsic by dependence receptors), unregulated necrosis, regulated necrosis (necroptosis), pyroptosis, autophagic cell death, mitotic catastrophe, and anoikis. It is still hotly debated whether some of these processes (e.g., autophagic cell death and mitotic catastrophe) are true subroutines or associated phenomena preceding cell death (for more information, see).<sup>35,55</sup> Furthermore, it is still not clear which of these subroutines predominates in cell death induced by antitumor treatment and which route should be activated for the most effective treatment of a particular type of cancer.<sup>28</sup> Nevertheless, this new classification of cell death allows a better separation of molecular pathways and the linking of pathways to functional consequences.

In order to properly classify cell death, several parameters should be determined since many biochemical processes that were initially considered to be hallmarks of apoptosis appear also in other death modes (Table 2). Despite this complexity, five main biochemical parameters appear to define dying cells: (1) changes of membrane asymmetry (exposure of phosphatidylethanolamine [PE] and phosphatidylserine [PS]), (2) loss of transmembrane potential, (3) permeabilization of the mitochondrial membrane with associated potential changes, (4) increased proteolysis, and (5) DNA fragmentation. We will discuss these in the following chapter.

## 2 | HALLMARKS OF CELL DEATH

As listed in Table 2, each of the five characteristics of apoptosis occurs in more than one cell death mode. However, the order of their appearance on the scenario of cell death is generally well preserved (see Figure 1).

### 2.1 | Changes in membrane asymmetry

The cell membrane is a highly specialized bilayer of asymmetrically distributed phospholipids. In the resting state, cationic phospholipids prevail in the outer, and anionic phospholipids in the inner membrane leaflet. The cell membrane functions as: a *barrier* (allowing passage of only a selected set of molecules), an *organizer* (assembling, co-localizing, and controlling activity of signaling components), and a *sensor and communicator* (processing and conducting signals between the cell and its environment).<sup>56</sup> Multiple cellular activities are accompanied by changes in morphology or

TABLE 2 Revised classification of cell death modes and their characteristics

Cell death mode	PS exposure	Decrease in MMP	Cell membrane rupture	Active caspases	DNA fragmentation/ hydrolysis	Hallmarks/markers	Inducer (example)	Inhibitor (example)
Caspase-dependent intrinsic apoptosis <sup>35,282</sup>	++	++	+	++	++	Bak (BCL-2 homologous antagonist/killer), Bax (BCL-2-associated X protein) activation CytC (second mitochondria-derived activator of caspase). SMAC/DIABLO (direct inhibitor of apoptosis-binding protein with low pl), HTRA2 release from mitochondria Caspase-9, -3, -6, -7 activation	Raptinal Cadmium	z-LEHD-fmk (caspase-8 inhibitor) Cyclosporin A
Caspase-independent intrinsic apoptosis <sup>35,283</sup>	++	++	+	-	++	BNIP-3 (BCL2/adenovirus E1B 19 kDa protein-i-interacting protein 3) overexpression EndoG (endonuclease G), AIF, HTRA2 release from mitochondria ROS production	Cadmium	Cyclosporin A
Extrinsic apoptosis by death receptors <sup>35</sup>	++	+	+	++	++	Death receptor activation Caspase-8, -10, -3, -7 activation CytC release, BID (Bcl-2 homology domain 3 interacting-domain death agonist) cleavage	FasL (first apoptosis signal ligand)	z-ITD-fmk (caspase-8 inhibitor)

(Continues)

TABLE 2 (Continued)

Cell death mode	PS exposure	Decrease in MMP	Cell membrane rupture	Active caspases	DNA fragmentation/hydrolysis	Hallmarks/markers	Inducer (example)	Inhibitor (example)
Extrinsic apoptosis by dependence receptors <sup>35,284</sup>	++	+	+	++	++	Dependence receptor activation (patched, uncoordinated movement receptor gene 5A, DCC [deleted in Colorectal Cancer gene]) Caspase-9, -3, -7 activation	Suboptimal netrin concentration	z-LEHD-fmk (caspase-8 inhibitor)
Autophagic cell death <sup>29,35</sup>	++	+	-	-	-/+	PE conjugated LC3 (LC3-II) Beclin-1 accumulation SQSTM1 (sequestosome1 [ubiquitin-binding protein p62])/p62 degradation	Rapamycin	3-methyl-adenine Atg5, Atg7, Beclin-1 VPS34 (Class III phosphoinositide 3-kinase) genetic inactivation
Necroptosis <sup>285</sup>	-	++	++	-	+	RIP1, RIP3 activation MLKL (mixed lineage kinase domain like pseudokinase) activation	TNF	Caspase-8 Necrostatin-1
Pyroptosis <sup>286,287</sup>	++	++	++	++	++	Caspase-1, -4, -5 activation IL1 $\beta$ (interleukin 1 beta), IL18 (interleukin 18) Gasdermin D cleavage	LPS (lipopolysaccharide)	z-YVAD-fmk (caspase-1 inhibitor)

(Continues)

TABLE 2 (Continued)

Cell death mode	PS exposure	Decrease in MMP	Cell membrane rupture	Active caspases	DNA fragmentation/hydrolysis	Hallmarks/markers	Inducer (example)	Inhibitor (example)
Mitotic catastrophe <sup>*,288,289</sup>	++	+	++	-	+	Cyclin B accumulation CDK1 (cyclin-dependent kinase 1) activation	Cytochalasin D Trichostatin A	Survivin
Anoikis <sup>*,290,291</sup>	++	++	+	++	++	Epidermal growth factor receptor downregulation BIM overexpression BMF (Bcl2-modifying factor) phosphorylation JNK (c-Jun N-terminal kinases) activation	Cell disengagement from the extracellular matrix	bFGF (basic fibroblast growth factor) z-VAD-fmk (cell-permeable, irreversible pan-caspase inhibitor)
Cornification <sup>292</sup>	n.d.	+	-	+	++	Transglutaminases, caspase-4 activation		
Netosis <sup>293</sup>	+	++	++	-	-	NADPH ( $\beta$ -nicotinamide adenine dinucleotide, reduced) oxidase activation ROS production	PMA (phorbol 12-myristate 13-acetate)	Diphenyl iodide
Parthanatos <sup>294</sup>	+	++	++	-	++	PARP1 activity increased PAR accumulation Mitochondria release AIF AIF translocates to nucleus MIF activity increased MIF translocates to nucleus	MNNG (methylnitrosotroganidine)	Niraparib

(Continues)



TABLE 2 (Continued)

Cell death mode	PS exposure	Decrease in MMP	Cell membrane rupture	Active caspases	DNA fragmentation/hydrolysis	Hallmarks/markers	Inducer (example)	Inhibitor (example)
Entosis <sup>295</sup>	-	-	-	-	DNA fragmentation/hydrolysis (+)	RhoA (Ras homolog gene family, member A), ROCK1/2 (Rho-associated, coiled-coil containing protein kinase 1/2) activation AMPK (5'-AMP-activated protein kinase) increased E-cadherin increased LC3 lipidation	Glucose starvation AICAR (5-aminoimidazole-4-carboxamide ribonucleotide)	Y-27632 (selective inhibitor of Rho-associated protein kinase p160ROCK) Compound C
Necrosis- oncosis <sup>*,296,297</sup>	-	-	++	-	-/+	Rapid decline of intracellular ATP Reduced activity of ion pumps (Ca <sup>2+</sup> , Na <sup>+</sup> /K <sup>+</sup> ATPases)	H <sub>2</sub> O <sub>2</sub>	
Ferroptosis <sup>298</sup>	-	++	-	-	-	Reduced cysteine uptake Production of ROS GPX4 (glutathione peroxidase 4) inhibition Glutathione depletion	Erastin	Ferrostatin-1

An asterisk (\*) indicates cell death modes known to apply to therapy-induced cancer cell death, ++ = process strongly increased, + = process increased, - = process not increased, n.d. = activity of process not determined.

AIF, apoptosis-inducing factor; Atg, genes controlling autophagy; fmk, fluoromethyl ketone; HTRA2, HTRA serine peptidase 2; LC3, microtubule-associated protein 1A/1B-light chain 3; MIF, macrophage migration inhibiting factor; ROS, reactive oxygen species.

composition of the cell membrane. These activities include the regulation of immunity, coagulation and bone formation, for example, by changing the conformation, interactions, localization, and destination of proteins.<sup>57–61</sup>

A hallmark of apoptosis is the disturbance of membrane asymmetry, and specifically, the translocation of phospholipids, such as PE and PS, from the inner to the outer leaflet of the membrane. Under basal conditions, PE is predominantly and PS is almost exclusively confined to the inner leaflet of the cell membrane (in erythrocytes, 80–85% and >96%, respectively).<sup>62</sup> Once on the cell surface, exposed PE may regulate actin-dependent blebbing and the formation of apoptotic bodies,<sup>63–65</sup> whereas exposed PS serves as a recognition and docking site, for example, for phagocytes, and facilitates the removal of apoptotic cells.<sup>66–68</sup>

Although disturbance of membrane asymmetry is a feature of apoptosis, disturbed asymmetry also appears early after activation of other cell death modes, such as anoikis, autophagic cell death, pyroptosis and mitotic catastrophe (Table 2).<sup>69–72</sup> In death modes such as necrosis, PE and PS may become accessible only at later time points, when cell membrane integrity has been lost.<sup>73</sup>

### 2.1.1 | Phosphatidylethanolamine exposure

PE is a neutral (zwitterionic) molecule which accounts for 40–50% of total membrane phospholipids.<sup>74</sup> Most PE molecules are cone-shaped and do not organize themselves into membrane bilayers in an artificial setting, but rather form monolayers,<sup>75</sup> although PE is kept in bilayer configuration in biological membranes by interaction with other phospholipids. This feature enables PE to “coat” lipophilic regions of membrane proteins and to participate in membrane fusion and fission. In hepatocytes, the presence of PE in the bilayer was shown to result in a less tight packing of the membrane lipids and increased membrane permeability.<sup>76</sup>

The dynamics of PE play a role in membrane reorganization during cytokinesis,<sup>77,78</sup> stress and apoptosis,<sup>63,79</sup> and possibly also in hemostasis<sup>80</sup> and the physiology of the mitochondrial inner membrane.<sup>81,82</sup> The appearance of PE on the surface may be a more sensitive biomarker of cell stress than PS, since PE is more abundant than PS and could deliver a stronger signal.<sup>64,82</sup> Moreover, PE is present on the luminal surface of tumor blood vessels. Exposed PE in the vessel wall may represent a biomarker for imaging response to antivasular cancer therapy.<sup>64</sup>

### 2.1.2 | Phosphatidylserine exposure

PS is an anionic molecule accounting for 2–10% of the total membrane phospholipids.<sup>83,84</sup> It has a cylindrical shape, which promotes formation of membrane bilayers. However, at elevated pH or  $[Ca^{2+}]$ , PS can adopt a conical shape to form hexagonal membrane structures.<sup>85–87</sup> PS is inhomogeneously distributed in the plasma membrane, forming 11 nm clusters.<sup>88</sup>

As mentioned above, PS exposure is a hallmark of apoptosis and an “eat me” signal for phagocytosis of dying cells. Many biochemical assays (e.g., *in vitro* staining of cells with Annexin A5) use PS exposure as a marker of apoptosis. Since annexin is not able to selectively identify apoptosis, Annexin A5 is then used in combination with propidium iodide to identify necrotic cells from apoptotic cells. Early in apoptosis,  $10^6$ – $10^9$  PS molecules become accessible to Annexin A5 after translocation to the outer leaflet of the cell membrane.<sup>89,90</sup>

However, PS exposure also occurs in normal physiology. For example, binding of proteins to intracellular PS can localize their signaling pathways to the proximity of the cell membrane (e.g., PS–PKC [protein kinase C] interaction)<sup>91,92</sup> and/or can promote membrane fusion and fission (e.g., PS–synaptotagmin-I interaction).<sup>93</sup> PS exposure plays a role in physiological processes such as cell activation (platelets in clotting cascade, lymphocytes in immune response), membrane fusion in phagocytosis,<sup>94</sup> release of membrane-encapsulated nuclei during maturation of erythroblasts,<sup>95</sup> and cellular stress responses.<sup>96,97</sup> Up to 50% of blood vessels in untreated tumors are positive for exposed PS, likely due to oxidative stress in their environment.<sup>98,99</sup> This fraction generally increases after anticancer treatment.<sup>100</sup>

In recent years it has become apparent that different forms of PS play unique and important signaling roles in the cell. Oxidized PS was shown to promote recognition of apoptotic cells by macrophages *via* interaction with CD36 (cluster of differentiation 36 [fatty acid translocase])<sup>101</sup> or the bridging protein lactadherin (aka milk fat

globule-epidermal growth factor 8 protein, MFGE8).<sup>102</sup> Up to 20% of the PS in neutrophils is endogenously converted to PS with only a single acyl chain lyso-phosphatidylserine (lysoPS), in a  $\beta$ -nicotinamide adenine dinucleotide (reduced) oxidase-dependent manner. LysoPS plays a role in the clearance of PS-expressing, nonapoptotic neutrophilic cells.<sup>103</sup>

1-Lyso-2-acyl-PS and 1-acyl-2-lyso-PS (PS with deletions of the first or second acyl chain) perform different cellular functions.<sup>104–106</sup> 1-Lyso-2-acyl-PS can signal platelet degranulation, mast cell activation, and T-cell growth suppression; and 1-acyl-2-lyso-PS may accompany histamine release from peritoneal mast cells and neuronal differentiation. However, our understanding of the role of different forms of lysoPS in cancer cell death is still rudimentary.

### 2.1.3 | Mechanism of PE and PS exposure

Currently, there are two models describing PS exposure during apoptosis: a recently proposed model of increased phospholipid vesicle trafficking (involving lysosomes,<sup>107</sup> or bidirectional endosomes<sup>108</sup>) and a widely accepted model of disturbed phospholipid transport.<sup>109–112</sup>

According to the first model, PS externalization reflects phospholipid vesicle trafficking between plasma membrane and cytoplasm rather than an activity of phospholipid transporters.<sup>108</sup> This model is supported by the finding that PS externalization during apoptosis is derived from a newly synthesized pool, and the rate of PS synthesis is then ~twofold increased.<sup>113,114</sup> Furthermore, altered lipid packing in shrinking cells can prompt PS exposure.<sup>115</sup>

According to the second model, localization of PE and PS is regulated by a common set of transporters, such as scramblases,<sup>116,117</sup> ATP-binding cassette (ABC) transporters,<sup>118</sup> and aminophospholipid translocases.<sup>119</sup> Scramblases carry out  $\text{Ca}^{2+}$ -dependent bidirectional and nonspecific transport of phospholipids, whereas ATP-dependent ABC transporters (floppases) and aminophospholipid translocases (flippases) transport PS and PE appropriately between the two leaflets of the cell membrane, that is, in outward or inward direction. The more specific localization of PS than PE to the intracellular leaflet under baseline conditions may be attributed to the fact that aminophospholipid translocases have a somewhat lower affinity for PE than for PS. It is generally accepted that apoptosis leads to deactivation of aminophospholipid translocases and activation of scramblases and ABC transporters.<sup>109–112</sup> Scramblases are activated by elevation of cytosolic  $\text{Ca}^{2+}$ , an upstream event in, for example, apoptosis and blood coagulation. However, the identity of the transporters that are activated during cancer cell apoptosis has been the subject of a long debate.

The speed, strength, persistence, and reversibility of the signal are the best-characterized features of PS exposure. Exposure of PS to the outer leaflet has been shown to occur within a few hours after induction of apoptosis.<sup>120</sup> In human promyelocytic leukemia cells and Jurkat cells (immortalized line of human T lymphocytes) treated with various apoptosis inducers (e.g., anti-Fas antibody or camptothecin), the content of PS in the outer leaflet increased 25–280-fold (from  $<0.9$  to  $>240$  pmole/million cells).<sup>67,120</sup> At least an eightfold increase in externalized PS had to be reached to initiate phagocytosis of these cells, which is in line with the threshold model.<sup>120</sup> In myocardial ischemia in mice, PS exposure on apoptotic cardiomyocytes was shown to persist for about 6 hours (hr) after reperfusion.<sup>121</sup>

The upstream signaling cascade leading to PE and PS externalization in apoptosis has also been examined. PS exposure is usually accompanied by other molecular events, such as caspase activation,<sup>121–123</sup> cathepsin D activation,<sup>124</sup> perturbed  $\text{Ca}^{2+}$  homeostasis,<sup>125–128</sup> and PKC activation.<sup>129,130</sup> Whether these processes may occur in parallel or are required in combination to initiate PE and PS exposure is not yet clear.<sup>108</sup> A direct role of caspases in PS exposure during apoptosis has been suggested by the discovery of Kell blood group precursor-related protein 8, which requires a caspase-3 cleavage site to support presentation of PS on the surface of a dying cell followed by phagocytosis.<sup>131</sup> In the human myeloid leukemia cell line KBM7, the P4-ATPases ATPase phospholipid transporting, type 11C and cell division cycle protein 50A were shown to act as flippases and to transport aminophospholipids from the outer to the inner leaflet of the plasma membrane.<sup>132</sup> ATPase phospholipid transporting, type 11C is a caspase substrate. Caspase-mediated apoptotic exposure of PS is irreversible and leads to cellular engulfment by macrophages.

PS exposure is not under all circumstances closely related to cell death and phagocytic removal. PS can be exposed by viable cells, but is then likely an insufficient trigger for phagocytosis.<sup>133</sup> However, blocking PS on dying cells can abrogate their clearance by phagocytosis. Therefore, phagocytes recognize cell surface PS on dying cells most likely only within strongly curved membrane areas (i.e., in blebs). However, little is known about membrane

morphology surrounding exposed PE and PS and how these phospholipids are engaged by specific receptors, for example, lactadherin.<sup>66,134,135</sup> Furthermore, several tumor cell lines have been identified that lack PS exposure during apoptosis<sup>108</sup> and PS exposure can be reversible.<sup>97,121,136,137</sup>

## 2.2 | Loss of cellular transmembrane potential

Scrambling processes in early apoptosis reduce the pH of the external membrane leaflet and cytoplasm (acidification), and reduce the energy barrier of the cell membrane (depolarization).<sup>138,139</sup> The mechanism of cytoplasm acidification is not yet completely understood. A change in PS localization during apoptosis may affect the function of H<sup>+</sup>-ATPases, increase proton (H<sup>+</sup>) transport across the cell membrane, and reduce cytoplasmic pH.<sup>140,141</sup> Under basal conditions the cytoplasm has a pH of about 7.2 which decreases by about 0.3 to 0.4 pH units in early apoptosis. This drop promotes the activity of important enzymes involved in cell death, such as proteases and DNase II.<sup>142</sup> A loss of plasma membrane potential can be due to a change in cationic and anionic phospholipid distribution, an altered balance between extracellular Na<sup>+</sup> and intracellular K<sup>+</sup> (e.g., impaired function of Na<sup>+</sup>/K<sup>+</sup>-ATPase) and export of intracellular Cl<sup>-</sup>. The impairment of Na<sup>+</sup>/K<sup>+</sup> ATPase function in apoptotic cells was shown to be caspase-dependent and coincided with mitochondrial depolarization.<sup>143</sup>

## 2.3 | Change in mitochondrial transmembrane potential ( $\Delta\psi_m$ )

Ca<sup>2+</sup> is a very powerful regulator of many biochemical processes. Therefore, its cellular concentration must be tightly controlled. Increases in cytoplasmic Ca<sup>2+</sup> (e.g., caused by calcium release from the endoplasmic reticulum [ER]) can be resolved by mitochondria.<sup>144</sup> Mitochondria are one of the largest stores of intracellular Ca<sup>2+</sup> (after the ER), and centers of cellular energy production by oxidative phosphorylation. The functioning electron transport chain facilitates the creation of an electrochemical gradient ( $\delta\text{pH}$ ) across the inner mitochondrial membrane and the creation of an MMP ( $\Delta\psi_m$ ). The highly negative charge generated at the inner mitochondrial membrane by oxidative phosphorylation is strongly reduced when cells are energetically compromised and on their way to death. Certain apoptotic stimuli (e.g., ER stressors, death receptors, DNA damage) may cause a mitochondrial Ca<sup>2+</sup> overload and spillage of Ca<sup>2+</sup> into the cytoplasm. Ca<sup>2+</sup> efflux is regulated by the Na<sup>+</sup>/Ca<sup>2+</sup> exchanger and the permeability transition pore complex formed by proapoptotic Bcl-2 family members. A disturbance in Ca<sup>2+</sup> homeostasis and transition pore formation was shown to result in inhibition of oxidative phosphorylation and electron transport, dissipation of  $\Delta\psi_m$  and/or generation of mitochondrial outer membrane permeability, a decrease in cellular ATP, release of proteins from the mitochondrial intermembrane space, and activation of cytoplasmic Ca<sup>2+</sup>-dependent endonucleases.<sup>145,146</sup> Factors which are then released from mitochondria include ATP, reactive oxygen species, and facilitators of caspase-9 activity, such as CytC, apoptosis-inducing factor, and second mitochondria-derived activator of caspase (see Section 1.1). The release of such factors is thought to be "a point-of-no-return" in the apoptotic cascade.<sup>147,148</sup>

Changes in mitochondrial transmembrane potential can be both the cause and a consequence of apoptosis. They are the cause if certain agents induce mitochondrial damage and downstream activation of caspase-9, and a consequence if mitochondria amplify the apoptotic cascade downstream death receptors and caspase-8 has already become activated. Depolarization (or, in rare cases, hyperpolarization) of the mitochondrial membrane occurs in response to a cellular insult.<sup>149,150</sup>

Changes in  $\Delta\psi_m$  are frequently monitored as an indicator of cell viability. Almost each form of cell death results in declined  $\psi_m$ , either at an earlier or a later stage, but an interesting study has shown that release of certain proapoptotic molecules (such as CytC) may occur in the absence of changes in mitochondrial outer membrane potential.<sup>151</sup>

## 2.4 | Increased caspase proteolysis

Cell death is frequently mediated by a proteolytic cascade, in which caspases play a pivotal role. Caspases have been demonstrated to cleave as much as 5% of the cellular proteome during apoptosis.<sup>152,153</sup> The caspases are a family of

enzymes with the ability to sever a myriad of peptides and proteins at residues C-terminally to aspartate (Asp, D). They contain a catalytic Cys-His pair with Cys285 acting as the nucleophile and His237 acting as the general base to abstract the proton from the catalytic Cys and promote the nucleophile. Caspases recognize and cleave proteins after the tetrapeptide motif Asp-x-x-Asp. The enzymes occur as dimers and are mostly present in the cytoplasmic compartment of the cell.

To date, at least 11 caspases (14 according to ref. 154) and 11 caspase-encoding genes were identified in the human genome and proteome. Although these proteases are generally known as executioners of apoptosis, nonapoptotic activities have also been reported.<sup>155</sup> Thus, they can be classified as apoptotic and nonapoptotic (inflammatory) caspases. The apoptotic caspases comprise apoptosis initiators (caspase-2, -8, -9, and -10) and apoptosis executors (caspase-3, -6, and -7). The executor caspases can cleave hundreds of substrates.<sup>156</sup> Caspase-3 is the main executor of apoptosis. Among its substrates are proteins participating in DNA repair (e.g., poly [ADP-ribose] polymerase 1, PARP-1), cytoskeletal proteins (e.g., fodrin), remodeling proteins (e.g., Rho-associated, coiled-coil containing protein kinase 1), and nuclear proteins (e.g., lamin B1). (Primarily) nonapoptotic caspases include caspase-1, -4, -5, and -14.

In the absence of a demand for proteolytic activity, caspases are present in an inactive zymogen form (procaspases). Upon specific cellular insults, two procaspases are cleaved in a highly controlled manner into two small and two large subunits, assembled into a heterotetramer and activated. By cleaving a specific range of assigned protein substrates, caspases render a controlled loss, gain, functional change, or altered localization of client proteins. This in turn leads to the appearance of typical apoptotic characteristics, such as disturbance of cell membrane lipid asymmetry, cell shrinkage, nuclear chromatin condensation, and DNA fragmentation.

Synthetic caspase-3/7 substrates should consist of at least five amino acid residues. Caspase substrates are selected based on protein primary, secondary, tertiary, and quaternary structure.<sup>152</sup> The design of synthetic caspase substrates is based on the preference of caspases for individual peptide sequences (subsite preference).<sup>157</sup>

## 2.5 | DNA fragmentation

DNA fragmentation is a major step of cellular disassembly. The process may be induced by cell death-inducing factors (e.g., cytolytic T-cells) or by irreparable errors or damage to DNA (e.g., radiation damage). Genomic DNA can be hydrolyzed either inside or outside a dying cell.<sup>158</sup> DNA hydrolysis occurs at different time points and has a different pattern in different cell death modes.

Cleavage of DNA is executed by certain enzymes, DNA endonucleases, which are also known as DNases. These DNases are divided into three groups: (a)  $\text{Ca}^{2+}/\text{Mg}^{2+}$  endonucleases (e.g., DNase I and DNase I3), (b)  $\text{Mg}^{2+}$  endonucleases (e.g., endonuclease G and DFF40/caspase-activated DNase), and (c) cation-independent/acid endonucleases (e.g., DNase II). The activity of these DNases is controlled by various means, such as protease activation (caspases or serine proteases), poly(ADP-ribosylation), phosphorylation, or ubiquitination, and by physicochemical conditions, such as a change of cytoplasmic pH.<sup>142,159</sup> Activation of various DNases results in different DNA fragmentation patterns.

(Inter)nucleosomal DNA fragmentation yielding low molecular weight (MW) DNA fragments ("laddering pattern") almost always accompanies apoptosis. Caspase-activated DNase (present in extrinsic and intrinsic apoptosis) and endonuclease G (present in intrinsic apoptosis) produce various laddering patterns.<sup>160-164</sup> The selection of a certain DNase seems to be stimulus- and cell type-dependent. DNA is processed in two steps during apoptosis. In the early stage, DNA is cleaved into high MW fragments (50–300 kb). Here DNA condensation takes place. Subsequently, these molecules are further broken up into oligonucleosome-sized fragments (repeats of 180–200 bp).<sup>165</sup> Free DNA termini present as a consequence of apoptosis can be detected by a TdT-mediated-dUTP nick end labeling assay.<sup>166</sup> However, DNA breaks detected by this assay need not to be a consequence of apoptosis. The TdT-mediated-dUTP nick end labeling assay cannot discriminate among apoptosis, necrosis, and autolytic cell death.

A more random form of DNA fragmentation, yielding a "smear pattern," is observed in nonapoptotic cell death modes, such as necrosis, or cellular disassembly after phagocytosis. This pattern results from the activity of lysosomal DNases, for example, DNase II.

### 3 | CELL DEATH IMAGING

Since the mechanisms underlying cell death are complex, the question arises how treatment-induced cell death, for example, in cancer, should be quantified with medical imaging. The majority of tracers monitoring cell death are designed to probe: (1) disturbances in membrane asymmetry, (2) reductions in the membrane energetic barrier, (3) changes in MMP, and (4) activation of apoptotic caspases. Although these phenomena were initially considered hallmarks of apoptosis, similar processes occur in other forms of cell death. Thus, most imaging probes are not selective for one particular form of cell death. Increased uptake of such probes may be the net result of cells dying by various mechanisms.

#### 3.1 | Membrane asymmetry

##### 3.1.1 | Exposure of PE

Several imaging probes have been developed to monitor the translocation of PE to the outer leaflet of the cell membrane during apoptosis. A few lantibiotics have been radiolabeled and tested for imaging of exposed PE; these include cinnamycin and duramycin.

##### Cinnamycin

Cinnamycin (Ro09-0198) is a small peptide (2,046 kDa, 19 amino acids) from a family of lantibiotics isolated from *Streptovorticillium cinnamoneus*, which binds selectively to PE.<sup>81</sup> A few in vitro assays have been performed with the fluorescein-streptavidin (SA)-labeled cinnamycin derivative fluorescein-SA-Ro, the iodine-125-labeled derivative (<sup>125</sup>I)-SA-Ro, or the AF546-SA-biotin-labeled derivative,<sup>63,77,78,167</sup> for results see Table 3.

##### Duramycin

Duramycin (PA48009, a peptide of 2,013 kDa and 19 amino acids) differs from cinnamycin by only one amino acid residue: Lys2 → Arg2.<sup>168,169</sup> Duramycin takes its name from being resistant to high temperatures and proteolysis. Soon after its discovery, duramycin was shown to interact with biological membranes and to have a high affinity ( $K_d$ , 4–11 nM) to PE.<sup>170</sup> The PE binding is specific and occurs in an equimolar and Ca<sup>2+</sup>-independent manner.<sup>171</sup> Duramycin binding to PE depends on membrane curvature and may alter both the curvature and permeability of the membrane. The mechanism by which duramycin induces these changes is unknown.<sup>172</sup> Studies of protein domains involved in membrane tubulation and vesicle formation (e.g., ENTH [epsin NH2-terminal homology] and BAR [protein dimerization domain named after the proteins Bin, Amphiphysin, and Rvs] domains) may provide clues on how duramycin can fold the membrane.<sup>173</sup>

The results presented in Table 3 suggest that radiolabeled duramycin but not cinnamycin is suitable for SPECT imaging of exposed PE. However, the tracer has not yet been tested in patients or in healthy human volunteers.

##### 3.1.2 | Exposure of PS

Since PS exposure accompanies apoptosis, PS has been extensively studied as a target for the imaging of dying cells. Thus far, five families of protein or peptide-based PS imaging probes have been employed: Annexin A5, the C<sub>2A</sub> domain of synaptotagmin I, lactadherin, PS-binding peptide 6, and bavituximab. Annexin A5 is the only probe that has proceeded to the clinical stage of testing. Imaging data for probes targeting exposed PS are presented in Tables 3 and 4.

##### Annexin A5

Annexin A5 (earlier called Annexin V or “placenta protein 4”) is an endogenous 36 kDa protein which was originally isolated from human placenta.<sup>174</sup> Other tissues, such as endothelial cells, kidneys, myocardium, skeletal muscle, skin, red blood cells, platelets, and monocytes contain lower quantities of the protein.<sup>175</sup> Annexin A5 was identified as a potent anticoagulant which could displace and inhibit coagulation factors from biological membranes.<sup>176</sup> Its binding

TABLE 3 Probes targeting altered membrane asymmetry (radiolabeled lantibiotics and annexin)

Probe/label	Target/ $K_d$	Preclinical evaluation	Human studies	Perspectives
Cinnamycin <sup>125</sup> I	Exposed PE 10–200 nM <sup>299</sup>	Accumulates in apoptotic blebs in a PE-specific manner <sup>78</sup> .	None	Little evaluated, perhaps because of toxicity. <sup>300</sup>
Duramycin <sup>99m</sup> Tc	Exposed PE 4 to 11 nM <sup>170</sup>	Jurkat cells <sup>171</sup> , COLO205 (human colon carcinoma cell line), MDA-MB-231 (human breast adenocarcinoma cell line), HT29 (human colon adenocarcinoma cell line) xenografts. <sup>301–304</sup>	None. A tracer production kit has been developed. <sup>305</sup>	Detects exposed PE in apoptotic cells and the early response of tumors to chemo- and radiotherapy (uptake seven- to 30-fold increased).
Duramycin <sup>18</sup> F	Exposed PE 11 to 21 nM <sup>172</sup>	S180 (mouse fibrosarcoma cell line) tumors, A549 (human lung adenocarcinoma cell line) and SPCA-1 (human lung adenocarcinoma cell line) xenografts. <sup>306</sup>	None	Only moderate (1.5-fold) increases in tumors treated with chemotherapy.
Annexin A5 <sup>99m</sup> Tc (HYNIC, tricarboxyl and various other labeling methods) <sup>111</sup> In	Exposed PS 1 to 7 nM <sup>307,308</sup>	PC12 (rat pheochromocytoma cell line), SHSY5Y (human neuroblastoma cell line) cells <sup>308</sup> . Rodent models of chemotherapy, <sup>182,309–320</sup> radiotherapy, <sup>312,314,315</sup> and photodynamic therapy. <sup>321</sup> Only limited preclinical data are available for [ <sup>111</sup> In]Annexin A5. <sup>322–326</sup>	Pilot study in 15 cancer patients. <sup>327</sup> Studies in 29, <sup>328</sup> 17, <sup>329</sup> 16, <sup>330</sup> and 38 patients <sup>331</sup> indicated significant correlations of the early increase of tracer uptake after chemo- or radiotherapy with treatment response during follow-up. Even a single baseline scan may be useful to predict tumor response to subsequent therapy. <sup>332,333</sup>	Detects exposed PS and the early response of tumors to antitumor therapy (uptake up to sixfold increased). Detected primary tumors but did not visualize most affected lymph nodes in a human study. <sup>334</sup> Uptake in non-necrotic tumors is correlated to TUNEL (TdT-mediated-dUTP nick end labeling) staining <sup>335</sup> and Fas ligand expression. <sup>336</sup> Acceptable test-retest reproducibility in head and neck cancer. <sup>337</sup> However, Annexin-SPECT has not become routine in the clinical setting for reasons discussed in Section 3.1.2. Tricarboxyl labeling results in better chemical stability of the probe than HYNIC labeling and precludes isomerization. <sup>338–342</sup> Site-specific labeling increases probe affinity <sup>342–351</sup> and improves pharmacokinetics (less kidney retention).

(Continues)

TABLE 3 (Continued)

Probe/label	Target/ $K_d$	Preclinical evaluation	Human studies	Perspectives
Annexin A5 $^{123}\text{I}$ , $^{131}\text{I}$	Exposed PS 7 nM <sup>352</sup>	Less renal uptake than [ $^{99m}\text{Tc}$ ]HYNIC-Annexin A5. <sup>353–362</sup>	None	Poor metabolic stability (rapid dehalogenation). <sup>353–362</sup>
Annexin A5 $^{18}\text{F}$	Exposed PS 2 to 10 nM <sup>363–366</sup>	Jurkat, TC32 (primitive neuroectodermal tumor cell line) cells. <sup>367,368</sup> UM-SCC-22B, A549 (human lung adenocarcinoma cell line) xenografts, <sup>363,369</sup> VX2 (rabbit anaplastic squamous cell carcinoma) tumors. <sup>369</sup>	None	Site-specific $^{18}\text{F}$ labeling increases probe affinity. <sup>369,370</sup> Uptake in tumors then up to 40-fold increased after treatment.
Annexin B1 $^{99m}\text{Tc}$	Exposed PS 50 nM <sup>371</sup>	Hepatic, thymus apoptosis models in mice. <sup>371,372</sup>	None	Increased uptake correlates with histologic evidence of apoptosis. Probe injection may cause immune response.
Annexin B1 $^{18}\text{F}$	Exposed PS 10 nM <sup>373</sup>	Jurkat cells, <sup>373</sup> W256 (Walker 256 carcinosarcoma cell line) tumors. <sup>373</sup>	None	Detects early response of tumors to chemotherapy (uptake sixfold increased). Risk of immune response.

HYNIC, hydrazinonicotinamide, Jurkat, immortalized line of human T lymphocytes.



**TABLE 4** Probes targeting altered membrane asymmetry (other than lantibiotics and annexin)

Probe/label	Target/affinity	Preclinical evaluation	Human studies	Perspectives
C <sub>2A</sub> -GST- <sup>99m</sup> Tc	Anionic phospholipids (PS) IC <sub>50</sub> 90 nM <sup>374</sup>	Jurkat cells, <sup>374</sup> H460 (human non-small-cell lung cancer cell line) xenografts. <sup>375</sup>	None	Can be used to visualize and quantify apoptosis after chemotherapy.
C <sub>2A</sub> -GST- <sup>18</sup> F	As above. IC <sub>50</sub> unknown.	Jurkat cells, <sup>202</sup> VX2 (rabbit anaplastic squamous cell carcinoma) tumors in rabbits. <sup>202</sup> Uptake similar to [ <sup>18</sup> F]Annexin A5.	None	As above. Strong increase after chemotherapy (>50-fold). Probe can cross the blood–brain barrier.
C <sub>2A</sub> -cH- <sup>99m</sup> Tc, <sup>111</sup> In	As above. IC <sub>50</sub> 55–71 nM <sup>201</sup>	Mouse models of lymphoma and human colorectal cancer. <sup>204</sup>	None. Kit-based production possible. <sup>376</sup>	<sup>99m</sup> Tc-labeled probe shows better tumor-to-muscle ratios than the <sup>111</sup> In-labeled derivative.
ATSE (diacetyl-bis[N4-ethylthiosemicarbazone])/AMal-C <sub>2A</sub> C, <sup>64</sup> Cu	As above. K <sub>d</sub> 760 μM <sup>377</sup>	None (only radiochemistry reported).	None	<sup>64</sup> Cu offers longer physical half-life than <sup>18</sup> F. But labeling results in probe with very low affinity.
HYNIC (hydrazinonicotinamide)-lactadherin <sup>99m</sup> Tc	Exposed PS. K <sub>d</sub> sub-nM <sup>378</sup>	HL60 cells, <sup>212</sup> HeLa (human cervix carcinoma cell line) cells. <sup>379</sup> Probe localizes mainly in the liver in mice and pigs. <sup>378,380</sup>	None.	Binds in HL60 cells only to PS, but may in tissues also bind to integrins. Labeling of the C2 domain may result in a probe which is specific for PS.
PSBP-6 <sup>99m</sup> Tc	Exposed PS. K <sub>d</sub> of Re analog 2.6 nM <sup>381</sup>	B16/F10 (mouse melanoma cell line) tumors. <sup>381</sup> 38C13 (mouse B-lymphoma cell line) xenografts. <sup>382</sup>	None	Can visualize apoptosis after chemotherapy.
NOTA (1,4,7-triazacyclononane-1,4,7-triacetic acid)-Ava-PSBP-6, <sup>64</sup> Cu	Exposed PS. IC <sub>50</sub> 23 μM <sup>218</sup>	EL4 cells. <sup>218</sup> EL4-tumors in mice. <sup>218</sup>	None	Very low affinity for PS because of labeling procedure; too low for successful imaging.

(Continues)

TABLE 4 (Continued)

Probe/label	Target/affinity	Preclinical evaluation	Human studies	Perspectives
Bavituximab <sup>111</sup> In	$\beta_2$ -glycoprotein 1 (binds to PS)	A549 (human lung adenocarcinoma cell line) xenografts. <sup>383</sup> Impact of antitumor therapy not examined.	None	Labeled antibody visualized tumors and showed specific binding in SPECT.
Bavituximab <sup>74</sup> As	$\beta_2$ -glycoprotein 1 (binds to PS)	Dunning R3227-AT1 (Dunning prostate carcinoma) prostate tumors. <sup>226</sup> Impact of antitumor therapy not examined.	None	Labeled antibody visualized tumors and showed specific binding in PET.
Bavituximab <sup>64</sup> Cu	$\beta_2$ -glycoprotein 1 (binds to PS)	LNCaP (human prostate carcinoma cell line) xenografts. <sup>384</sup>	None	Labeled antibody visualized tumors in PET.
PGN635 <sup>89</sup> Zr	$\beta_2$ -glycoprotein 1 (binds to PS)	KPL-4 (human breast cancer cell line), COLO205 (human colon carcinoma cell line), HT29 (human colon adenocarcinoma cell line), and NCI-H2122 (human nonsmall cell lung cancer cell line) xenografts. <sup>385</sup>	None	Seems useful for monitoring of the early response of tumors to chemo- or immunotherapy with PET.
PGN650 <sup>124</sup> I	$\beta_2$ -glycoprotein 1 (binds to PS)	PC3 xenografts. <sup>386</sup>	Trial in 12 patients with advanced solid tumors (NCT 01632696). Results not yet reported.	In an animal model of prostate cancer, tumor-to-muscle ratios of radioactivity were inversely correlated with tumor growth measured during a follow-up period of 28 days. <sup>386</sup>
KL15 betabody	Exposed PS	PC3 xenografts. <sup>228</sup>	None	Seems to bind also to (nonapoptotic) immune cells.

EL4, mouse lymphoma cell line; GST, glutathione S-transferase; Jurkat, immortalized line of human T lymphocytes; PC3, human prostate carcinoma cell line.

was attributed to a  $\text{Ca}^{2+}$ -dependent interaction with negatively-charged PS molecules on the cell surface. Annexin A5 has no absolute specificity for PS, but binds with lower affinities to other targets, such as PE,<sup>177</sup> membrane products of lipid peroxidation,<sup>178</sup> vascular endothelial growth factor receptor 2,<sup>179</sup> and integrin  $\beta 5$ .<sup>180</sup> For this reason, some Annexin A5 binding may be observed even in viable cells.

Although annexin A5 has been extensively tested in experimental animals and in cancer patients (see Table 3), for various reasons the original probe failed to meet clinical expectations<sup>181–183</sup>:

1. The radiolabeling procedures for Annexin A5 are rather elaborate and complex, which has limited application of the radiolabeled probe in a clinical setting.
2. Since Annexin A5 binds to exposed PS, an annexin scan cannot discriminate between apoptosis and necrosis. This caveat is true for all PS- and PE-binding radiotracers. In a treatment response setting, the lack of specificity is not necessarily a problem, and may rather be an advantage, since PS- and PE-probes can provide a stronger signal than pure apoptosis tracers and both apoptosis and necrosis can be desirable consequences of antitumor therapy.
3. Since the binding of Annexin A5 to exposed PS is calcium-dependent, fluctuations (or regional differences) of intracellular  $\text{Ca}^{2+}$  concentrations may affect the binding of the tracer. This impact of calcium may result in high intraindividual variability of probe binding and an impaired test-retest reproducibility of annexin scans.
4. The magnitude of Annexin A5 uptake in target lesions and the target-to-background (or signal-to-noise) ratios of Annexin A5 scans are usually rather low. Low uptake of the tracer may be partially due to poor penetration of Annexin A5 into tumor tissue. Poor image contrast may be caused by slow clearance of radiolabeled Annexin A5 from nontarget regions and blood, and by an increased uptake of the probe in normal tissues after antitumor therapy. In order to address this problem, Annexin V-128 was developed, which shows a significantly lower kidney retention than Annexin A5 and is currently being evaluated in clinical trials.
5. High nonspecific accumulation of Annexin A5 in the liver and the kidneys makes it hard to detect tumors in the abdomen.
6. Tracer accumulation in areas far from known tumor sites may indicate the presence of unknown tumors or metastases, but may also be false positives, since Annexin A5 can accumulate in various benign lesions, such as infections and inflammations, capillary haemangioma, platelet-rich thrombi, and unstable atherosclerotic plaques. Uptake of the tracer in such sites could be misinterpreted as indicating the presence of malignant lymph nodes.
7. The optimal timing of a post-therapy Annexin A5 scan is frequently unknown or uncertain (which is true for all existing cell death-targeting tracers), and a complex protocol with multiple scans may be necessary for correct evaluation of the response of a tumor to therapy. A protocol involving three separate injections of radiolabeled annexin and six whole-body SPECT scans has been proposed for studies in cancer patients, in order not to miss an early response of the tumors to chemotherapy.<sup>184</sup>

### Annexin B1

Annexin B1 is a PS-binding protein isolated from the pork tapeworm (*Cysticercus cellulosae*, the larval stage of *Taenia solium*). The protein has a distinct N-terminus and only 32 to 44% homology to other annexins, including Annexin A5.<sup>185</sup> Radiolabeled Annexin B1 has been tested for SPECT and PET imaging of apoptosis (Table 3). [<sup>99m</sup>Tc]- and [<sup>18</sup>F]Annexin B1 showed predominantly renal clearance, like Annexin A5.

Although animal data indicate that apoptotic cells can be detected with radiolabeled Annexin B1, they have not demonstrated superiority of Annexin B1 over Annexin A5. Moreover, injection of a foreign protein like Annexin B1 may lead to an immune response in humans.

### Zinc coordination complexes

Zinc-dipicolylamine (Zn-DPA) coordination complexes contain two *meta*-oriented bivalent zinc cations and were created as mimetics to the domain of Annexin A5 which binds to PS via two bridging bivalent calcium cations.<sup>186</sup>

These small-molecule complexes associate with negatively-charged phosphorylated molecules, based on electrostatic interaction.<sup>187,188</sup> PSS-380 has a binding site with high and a binding site with low affinity for  $Zn^{2+}$ ; coordination of the second  $Zn^{2+}$  molecule occurs only after association of the probe with the anionic membrane surface.<sup>189</sup> PSS-380 has only been used in an in vitro setting. In vitro and in vivo studies with a similar NIR probe (PSS-794) demonstrated that Zn-DPA complexes can detect human cells dying by apoptosis or necrosis, and bacterial infections.<sup>190-193</sup>

The small molecular size of zinc coordination complexes could be an advantage and is one of the reasons why PET and SPECT analogues of these compounds were tested for apoptosis imaging (it could, e.g., lead to improved probe entry into tumor tissue). However, a high nonspecific binding of the labeled molecules in healthy tissue<sup>194</sup> and/or a high uptake and retention of radioactivity in liver and intestines<sup>195,196</sup> was found to limit the usefulness of Zn-DPA probes for visualization of cell death. Moreover, since Zn-DPA complexes can bind to all kinds of anionic surfaces, positive SPECT or PET signals may not always reflect exposed PS.

### Synaptotagmin I

Synaptotagmin I is a 65 kDa transmembrane protein primarily present in synaptic vesicles where it binds to negatively-charged phospholipids in a  $Ca^{2+}$ -dependent manner to facilitate vesicle fusion and recycling during neurotransmitter release.<sup>197-199</sup> The two cytoplasmic  $C_2$  domains ( $C_{2A}$  and  $C_{2B}$ ) of this protein have homology to PKC.<sup>198,199</sup> These domains interacting with  $Ca^{2+}$ , phospholipids, and soluble N-ethylmaleimide-sensitive factor attachment protein receptor are involved in membrane fusion during synaptic vesicle cycling.<sup>87</sup> Whereas the  $C_{2A}$  domain binds anionic phospholipids, such as PS ( $K_d = 15 - 40$  nM) and phosphatidylinositol, the  $C_{2B}$  domain interacts with calmodulin and phosphatidylinositol.<sup>200</sup> Imaging of apoptosis has been explored by labeling the 12 kDa  $C_{2A}$  domain with various fluorochromes, contrast agents (superparamagnetic iron oxide and Gd), and radionuclides ( $^{99m}Tc$  and  $^{18}F$ ). For this purpose, a  $C_{2A}$ -glutathione S-transferase fusion protein was synthesized to prevent chemical modification in the PS-binding site of  $C_{2A}$ . Unfortunately, this approach yielded a heterogeneous probe mixture as any of the 14 Lys residues in  $C_{2A}$  could be labeled resulting in a decrease of affinity to PS. Therefore, a single-site mutant of  $C_{2A}$  was developed ( $C_{2A}m$ , S78C) with a Cys residue suitable for labeling and distant from the PS-binding site.<sup>201</sup>

Initial experiments with a fluorescent probe showed that  $C_{2A}$  derivatives had much lower background binding in viable cells than Annexin A5 and were fourfold more specific in imaging cell death.<sup>201</sup> However, since the affinity of  $C_{2A}$  for PS-containing membranes ( $K_d = 20$  to  $71$  nM) is much lower than that of Annexin A5 ( $K_d = 1$  to  $7$  nM), a  $>50$  times higher protein concentration may be necessary for good images.<sup>201</sup> The preclinical imaging results described in Table 4 have indicated that  $C_{2A}$ -based probes are potentially useful for evaluation of antitumor treatment, but have also some drawbacks:

1. High levels of radioactivity in liver, kidney, and abdomen may complicate the evaluation of tracer uptake in these areas, particularly at short intervals after injection. The  $C_{2A}$  domain labeled with  $^{18}F$ <sup>202</sup> has shown a better clearance profile than the  $^{99m}Tc$ -labeled analogue.<sup>203</sup>
2. Because of the large size of the  $C_{2A}$  molecule, tracer uptake is limited by the rate of diffusion into tissue. Radiochemists could try to produce probes with a reduced size and charge which may show a more rapid tissue entry.
3. Although in vitro experiments indicated a low background binding of  $C_{2A}$  derivatives in viable cells, target-to-background ratios of the radiolabeled compounds in the mammalian body were rather unfavorable. These low ratios could be related to a low affinity of the probes to PS-containing membranes.  $C_{2A}$  domain probes with higher specificity and lower nonspecific retention have recently been developed, and as expected, these probes showed improved tumor-to-background ratios.<sup>204</sup>

### Lactadherin (MFG-E8, milk fat globule epidermal growth factor 8 protein)

MFG-E8, a 46 kDa extracellular glycoprotein, is secreted by a subset of macrophages and dendritic cells. As a soluble molecule, it participates in the opsonization of apoptotic cells and their phagocytosis, adhesion between sperm and the egg coat, repair of intestinal mucosa, mammary gland branching, morphogenesis, and angiogenesis.<sup>205</sup> The

protein acts as a potent anticoagulant in blood<sup>206</sup> and was linked to Alzheimer's disease and autoimmunity. It is a bridging molecule between apoptotic and phagocytic cells, has the ability to bind to integrins ( $\alpha_v\beta_3$  and  $\alpha_v\beta_5$ ) on immune cells via its arginyglycylaspartic acid motif of the glutamic acid-leucine-arginine domain,<sup>207</sup> and also binds to membrane PS on apoptotic cells (with preference to PS in membrane areas of spiky morphology). The binding to membrane PS occurs via its F5/8-type C1 and C2 domains ( $Kd_{C1C2} = 4.9$  nM,  $Kd_{C2} = 2.0$  nM) and does not require  $Ca^{2+}$ . The C2 domain has about 100-fold lower affinity toward soluble than membrane PS ( $Kd = 2.8$   $\mu$ M) and has a much higher affinity toward phosphatidyl-L-serine than phosphatidyl-D-serine.<sup>208</sup> Despite functional similarity of the C-domains present in synaptotagmin-1 and lactadherin, they do not share any sequence homology,<sup>207</sup> but there is homology between the C2 domains shared by lactadherin and blood coagulation factor VIII and V.<sup>209,210</sup> An in vitro study showed that lactadherin can specifically detect PS and has a higher affinity for PS than Annexin A5.<sup>211</sup> Imaging data for a SPECT tracer based on bovine lactadherin are presented in Table 4.

Lactadherin binding to apoptotic HL60 cells was reported to be related to PS exposure and not to an interaction of the probe with integrins.<sup>212</sup> However, the arginyglycylaspartic acid motif in lactadherin may bind to integrins throughout the body, which will likely complicate visualization of dying cells in living mammals. In future studies, lactadherin may be engineered in such a way that only the C2 domain, responsible for PS-binding, is used for labeling. A fluorescent derivative of the C2 domain has shown the ability to label different cellular pools of PS<sup>88,92</sup> and apoptotic tumor cells.<sup>208,213,214</sup>

### PS-binding peptides

Using phage display technology, peptides were identified which can bind with considerable affinity to exposed PS. Clusters of the basic amino acids Arg (R) and Lys (K) appeared to be critical for (ionic?) interaction with this phospholipid. A peptide called PSBP-6 has been radiolabeled for SPECT and PET imaging. The amino acid sequence of this peptide is based on the 14-amino-acid sequence from the C2 domain shared by PKC, PS decarboxylase, and synaptotagmin I.<sup>215</sup>

PS-binding peptides are in theory an attractive alternative to PS-binding proteins such as Annexin A5. The procedures for radiolabeling of peptides can be simpler, and the radioactive probes may show a more rapid entry into tumor tissue because of their smaller size. This reduced size can also result in a more rapid clearance of unbound probe from tissue and from blood. Moreover, peptides can be structurally modified, in order to improve their pharmacokinetic properties and metabolic stability. However, the currently available PS-binding peptides seem to have insufficient affinity<sup>216-220</sup> and/or specificity<sup>221</sup> for their target phospholipid (see Table 4).

### Bavituximab family of antibodies

An indirect option for imaging of externalized PS is provided by the generation of antibodies for  $\beta_2$ -glycoprotein 1. This protein is abundant in plasma and was shown to bind to negatively charged compounds, such as heparin, anionic phospholipids, and dextran sulfate. Two molecules of  $\beta_2$ -glycoprotein 1 are required for the interaction with PS ( $Kd \sim 1$  nM).<sup>222</sup> Several murine monoclonal antibodies (e.g., 3G4 and 2aG4),<sup>99,223-225</sup> a chimeric monoclonal antibody (mAb) (bavituximab),<sup>226</sup> and a human mAb (PGN635)<sup>227</sup> were generated to detect PS exposure on tumor vessels. All of these antibodies have been explored preclinically and in clinical trials for treatment of different types of malignancy. Radio-labeled bavituximab, PGN635, and PGN650 have been used for noninvasive in vivo imaging of PS exposure (Table 4).

Bavituximab (MW = 145.3 kDa) was constructed by fusion of variable (Fv) regions from the mouse 3G4 antibody and human immunoglobulin G1 $\kappa$  constant regions. The chimeric antibody cross-links and stabilizes a complex of two  $\beta_2$ -glycoprotein 1 molecules ( $Kd = 0.4$  nM, MW  $\sim 250$  kDa) attached to the cell surface pool of PS.

PGN635 is a first-in-class PS-targeting fully human mAb. The F(ab')<sub>2</sub> fragment of PGN635 was used to produce PGN650, which has similar affinity for PS- $\beta_2$ -glycoprotein 1 complexes as 3G4 and bavituximab.<sup>227</sup>

In an animal model of human prostate tumors,<sup>74</sup> As-bavituximab displayed very high tumor-to-muscle ratios and specific binding in the tumor (Table 4). Nonvascular staining of dead and dying cells in and around necrotic tumor regions was observed only sporadically, which may indicate a poor ability of bavituximab to penetrate tumor tissue. If this is the case, antibody fragments, such as PGN650 may show better penetration. An open-label, single-arm clinical

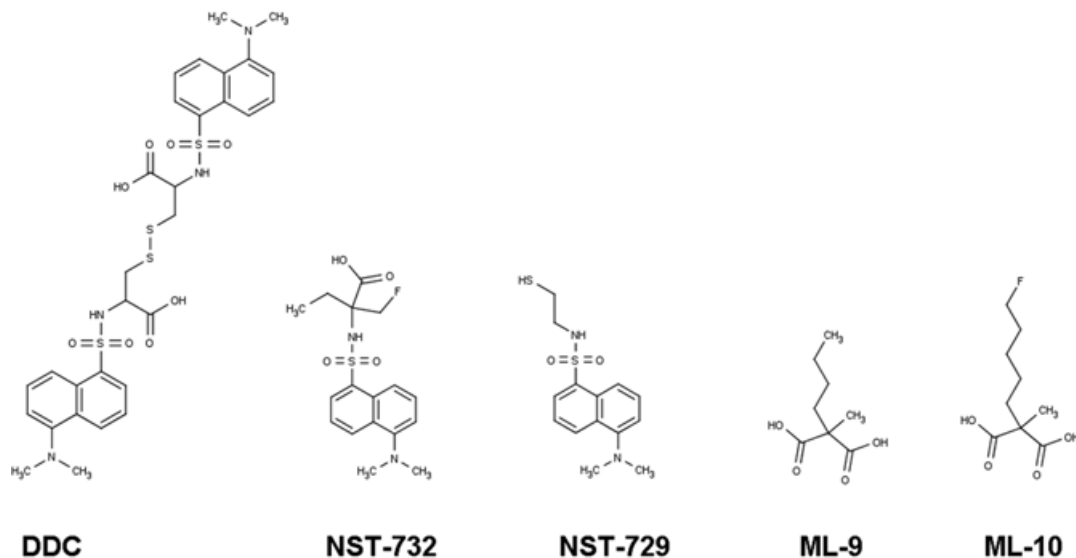


**FIGURE 2** Chemical structures of members of the ApoSense family of compounds

trial has been performed on 12 patients with advanced solid tumors, in which radioiodinated PGN650 was tested for tumor imaging, safety, and dosimetry. Unfortunately, the results of this trial have not yet been reported (Table 4).

### 'Betabodies'

'Betabodies' are fusion products based on the PS-binding domain(s) of  $\beta_2$ -glycoprotein 1 and the constant region of an antibody.<sup>228</sup> The recombinant 'betabody' KL15 is expressed in a dimeric form and consists of the domain I and V from  $\beta_2$ -glycoprotein 1 fused with the CH2 and CH3 constant (Fv) domains of a mouse IgG2a antibody. Only a few preclinical data concerning this probe have been published (see Table 4).

## 3.2 | Altered permeability of the cell membrane

### 3.2.1 | ApoSense family

The ApoSense family (Figure 2) is a group of small-molecule compounds (size 300 to 700 D) that can be used to detect altered membrane permeability in apoptotic cells. The family comprises two different generations of molecules. *N,N'*-Didansyl-L-cystine (DDC), (5-dimethylamino)-1-naphthalene-sulfonyl- $\alpha$ -ethyl-fluoroalanine (NST-732), and *N*-(2-mercaptoethyl)-dansylamide (NST-729) belong to the first generation. These molecules possess an amphiphatic structure, in which the hydrophobic moiety may provide a membrane anchor, while the charged moiety may prevent the compound from crossing healthy cell membranes. All contain a functional dansyl group with an inherent fluorescence. Butyl-2-methyl-malonic acid (ML-9) and pentyl-2-methyl-malonic acid (ML-10) belong to the second generation of the family. Their amphiphatic structure is based on an alkyl-malonate motif, which is derived from  $\gamma$ -carboxyglutamate-rich Vitamin K-dependent carboxylation/gamma-carboxyglutamic protein domain-containing proteins.<sup>229</sup> Vitamin K-dependent carboxylation/gamma-carboxyglutamic protein domain containing proteins (e.g., growth arrest-specific protein 6, coagulation factor X, vitamin K-dependent protein S, and prothrombin) bind anionic phospholipids and calcium ions and are an important component of the blood clotting cascade.

ApoSense molecules were initially thought to detect both apoptotic and necrotic cell damage, but later studies have suggested that they specifically accumulate in apoptotic cells.<sup>230</sup> Since ApoSense family members can cross the intact blood-brain barrier, they can be used to image the response of brain tumors to treatment, and loss of neurons after stroke or neurodegeneration in diseases like Alzheimer's disease. ApoSense compounds accumulate in the cytoplasm.<sup>231</sup>

Correlation between the *in vitro* uptake of DDC and Annexin A5 has suggested that scrambling processes in early apoptosis reduce the energetic barrier of the cell membrane and allow DDC to enter the cell. DDC uptake is thought to be the result of the following sequence of events:

Scrambling → membrane acidification → (mono)protonation of ApoSense molecules → flip-flop of the molecule through the membrane by active scramblases and cell membrane depolarization → binding of the molecule to cytoplasmic proteins.

However, this proposed mechanism is not yet fully supported by experimental data. Imaging results acquired with ApoSense probes are summarized in Table 5.

Advantages of the Aposense family of compounds are: their small molecular size, the minimal number of functional groups, and the absence of chemically reactive, undesired labeling sites.<sup>232</sup> Disadvantages are: the rather poorly defined mechanism of uptake and the requirement of a high administered dose. This last aspect raises concern about potential toxicity, since the dose is in the therapeutic rather than the tracer range. Some findings in animal models have suggested that the uptake of ML-10 is pH-sensitive.<sup>233</sup> If ML-10 uptake is indeed dependent on protonation, a decreased pH of the blood (e.g., due to failure of multiple organs after anti-Fas antibody treatment) may result in a high nonspecific uptake of ML-10 in viable tissues, whereas an increased extracellular pH (e.g., due to cyclophosphamide-induced necrosis in treated tumors) could be associated with a decrease of ML-10 uptake. Such factors may complicate the interpretation of PET images acquired with [<sup>18</sup>F]ML-10.

### 3.3 | Changes of mitochondrial transmembrane potential

Several lipophilic phosphonium cation-based tracers (arylphosphonium salts) have been developed for *in vivo* imaging of treatment-induced changes of MMP ( $\Delta\psi_m$ ).<sup>234</sup> Loss of negative charge at the inner mitochondrial membrane leads to reduced uptake of these lipophilic cationic tracers. Thus, radiolabeled arylphosphonium salts will generate a negative contrast.

#### 3.3.1 | [<sup>18</sup>F]fluorobenzyl triphenyl phosphonium

[<sup>18</sup>F]fluorobenzyl triphenyl phosphonium (FBnTP) accumulates in cells with normal mitochondrial potential and washes out when this potential is impaired by apoptosis. When the baseline uptake of the tracer in tumor tissue is low, another imaging modality must be used for tumor localization.<sup>235</sup> The signal of the tracer has been reported to be stable up to 45 min after injection.<sup>236</sup> Changes in [<sup>18</sup>F]FBnTP uptake may be difficult to interpret since the accumulation of this tracer can be affected by cellular efflux processes driven by multidrug-resistance proteins<sup>237</sup> and by tissue-dependent differences of background uptake. Various structural analogs of [<sup>18</sup>F]FBnTP have also been prepared, such as 4-[<sup>18</sup>F]-tetraphenylphosphonium (TPP),<sup>238–240</sup> ([<sup>18</sup>F]fluoropentyl)triphenylphosphonium,<sup>241</sup> and [<sup>18</sup>F]PEGylated-BnTP.<sup>242</sup> Uptake of these compounds is probably affected by the same processes as the tissue uptake of [<sup>18</sup>F]FBnTP.

#### 3.3.2 | [<sup>99m</sup>Tc]sesta-methoxyisobutylisonitrile

The SPECT perfusion tracer [<sup>99m</sup>Tc]sesta-methoxyisobutylisonitrile (mibi) has been tested as a probe of reduced membrane potential in dying cells. An early study reported that the uptake of this tracer in human breast cancer cells (MCF7) was reduced when cells were treated with a cytostatic agent (sodium phenylacetate), and the decline of tracer uptake was correlated to the fraction of apoptotic cells.<sup>243</sup> Another study reported that tumor uptake of [<sup>99m</sup>Tc]sestamibi was dose-dependently reduced in mice bearing Ehrlich carcinomas that were subjected to radiotherapy. At 24 hr after irradiation, tumor-to-background ratios were inversely correlated with apoptosis index and the percentage of necrotic area, but at longer intervals (72 hr and 144 hr post irradiation) these ratios were inversely correlated only with the percentage of necrotic area.<sup>244</sup> Although this study confirmed that [<sup>99m</sup>Tc]sestamibi is a “negative contrast tracer of dying cells,” another investigation performed in the same year showed that the absolute uptake values of [<sup>99m</sup>Tc]sestamibi in carcinomas are six- to eightfold smaller than those of a phosphonium cation like TPP.<sup>238</sup> Thus, [<sup>99m</sup>Tc]sestamibi scans will show a considerably lower signal-to-noise ratio than TPP scans.

TABLE 5 Probes targeting altered membrane permeability

Probe/label	Target	Preclinical evaluation	Human studies	Perspectives
DDC (fluorescent)	Membrane permeability (Ca <sup>2+</sup> dependent, ATP-independent uptake)	B16 (mouse melanoma cell line) tumors. <sup>387</sup> Mouse model of chemotherapy-induced enteropathy. <sup>388</sup> Uptake is specific for cells involved in apoptosis. <sup>388</sup>	None (fluorescent probes are only suitable for studies in cells and experimental animals).	Detects response of tumors (and rapidly dividing cells) to chemotherapy (uptake up to sevenfold increased).
NST-732 (fluorescent) <sup>18</sup> F	Membrane permeability	Jurkat cells, <sup>389</sup> LY-S (mouse lymphoma cell line) tumors. <sup>389</sup> Only results for fluorescent probe reported, not yet for the PET probe. <sup>390</sup>	None.	Detects response of tumors and tumor cells to radio- and immunotherapy (uptake up to 12-fold increased).
NST-729 (fluorescent)	Membrane permeability	Mouse models of Alzheimer's disease and ALS. <sup>391</sup>	None (fluorescent probes are only suitable for studies in cells and experimental animals).	Co-localizes with amyloid plaques in Alzheimer's disease and regions with axonal apoptosis in ALS.
ML-9 <sup>3</sup> H	Membrane permeability	Jurkat cells, <sup>229</sup> CT26 (mouse undifferentiated colon carcinoma cell line), xenografts. <sup>229</sup>	None (ML-9 cannot be labeled with a positron emitter. Its alkyl chain was modified in order to allow such labeling, resulting in the derivative ML-10).	Detects response of tumors and tumor cells to chemo- and immunotherapy (uptake up to 10.6-fold increased).
ML-10 <sup>3</sup> H <sup>18</sup> F, <sup>123</sup> I	Membrane permeability	Jurkat cells: response to anti-FAS mAb (monoclonal antibody) (ninefold increased uptake) is blocked by Z-valine-alanine-DL-aspartate-fluoromethyl ketone and specific for cells involved in apoptosis. <sup>392</sup> Colorectal tumor model with inbuilt doxocyclin-induced "death switch": strong apoptotic response clearly visible. <sup>52</sup> [ <sup>123</sup> I]ML-10 is rapidly degraded in living animals. <sup>393</sup>	8 volunteers: [ <sup>18</sup> F]ML-10 is metabolically stable, radiation dose (3.6 mSv) is acceptable, but hydration and bladder catheterization are necessary during the scan. <sup>392</sup> Ten patients with brain metastases; scanned shortly after radiotherapy: all lesions identified with MRI were detected, tracer uptake in tumors correlated with reduction of tumor size after 6–8 weeks. <sup>394</sup>	[ <sup>18</sup> F]ML-10 visualizes tumor response to therapy and may predict the therapeutic outcome. Accumulates in testes since spermatogenesis is accompanied by physiological apoptosis.

ALS, amyotrophic lateral sclerosis; Jurkat, immortalized line of human T lymphocytes.



In summary: PET and SPECT probes of mitochondrial transmembrane potential have shown limited success. The uptake of such tracers is affected by the activity of transporters involved in multidrug resistance and by changes of the physical properties of target tissue. Changes in the uptake of such probes after antitumor therapy may not always reflect changes in mitochondrial transmembrane potential of tumor cells.

### 3.4 | Increased proteolysis

Extrinsic and intrinsic apoptotic pathways converge at the level of caspase-3 and caspase-7 activation. The detection of activated caspases could be a valuable and specific tool for identifying dying cells before morphological features of cell death occur. Quantitative imaging of activated caspase-3 and -7 may be more useful for monitoring tumor responses to therapy than for diagnosis and localization of unknown tumors. In vivo imaging of activated caspases is possible via two different approaches:

1. use of caspase inhibitors (Z-valine-alanine-DL-aspartate or isatin-derivatives, for example, [ $^{18}\text{F}$ ]WC-II-89)<sup>245</sup>; and
2. use of caspase substrates (Z-aspartate-glutamate-valine-aspartate-derivatives, for example, [ $^{18}\text{F}$ ]CP18).<sup>246–248</sup>

The main benefits of radiolabeled substrates over radiolabeled inhibitors are (in theory): (a) no problem of saturation of the binding sites, and: (b) signal amplification. Since a single enzyme molecule can convert several substrate molecules within the time frame of a PET or SPECT scan, the use of a substrate may result in a higher sensitivity for the detection of an active enzyme. However, in a comparative study between a caspase substrate and activity-based probes (inhibitor-based), signal amplification at the site of proteolysis did not have a dramatic enhancing effect on imaging. The authors believe that this was due to slow diffusion of the substrates into tissues and cells.<sup>249</sup> In another study with inhibitor-based probes, the abundance of active proteases in tumor tissues was found to be sufficient for the generation of images with acceptable contrast, therefore no saturation of binding sites occurred.<sup>250</sup>

#### 3.4.1 | Caspase inhibitors

Radiolabeled inhibitors bind to a finite number of sites resulting in saturability of the probe binding.<sup>251–253</sup> The amount of accumulation is dependent on the ratio of the concentration of active caspases and the affinity of the inhibitor for these caspases ( $B_{\text{max}}/K_d$ ). The addition of a sulfonamide group confers isatins (i.e., derivatives of 1H-indole-2,3-dione) a high affinity for caspase-3 and -7.<sup>254</sup> The chemical structures of some isatin-based caspase inhibitors are shown in Figure 3, whereas imaging results acquired with these tracers are summarized in Table 6.

Radiolabeled isatins have been shown to bind specifically to activated caspases, but their sensitivity as PET probes was limited. [ $^{18}\text{F}$ ]WC-II-89 may be better than [ $^{11}\text{C}$ ]WC-98 or [ $^{18}\text{F}$ ]WC-IV-3 in discriminating the varying levels of active caspases in vivo. Although preclinical studies have indicated that [ $^{18}\text{F}$ ]ICMT-11 has potential for evaluation of the impact of antitumor therapy, clinical application of this tracer is not very easy. Because of a low baseline uptake of radioactivity, tumor outlines cannot be assessed by PET but should be determined from a CT scan. The low baseline uptake may be considered as a favorable property of a cell death tracer, since in patients only small fractions of apoptotic cells are expected in tumor tissues at all posttreatment scanning intervals. Thus, the use of a CT or MRI scan will possibly be always necessary to delineate the tumors. Since radioactivity accumulates in liver, kidneys, intestines, and urinary bladder, assessment of the uptake of [ $^{18}\text{F}$ ]ICMT-11 in abdominal tumors may be difficult or even impossible. Injected isatins can be trapped in blood (either due to apoptosis in lymphocytes, or to released, circulating caspases). Further optimization of the pharmacological properties of isatin-based caspase inhibitors seems therefore necessary, but unfortunately, literature indicates that the list of chemical alternatives for existing caspase-3/-7 tracers is almost exhausted.

**TABLE 6** Radiolabeled caspase inhibitors and substrates

Probe/label	Target/affinity	Preclinical evaluation	Human studies	Perspectives
IZ-VAD-fmk <sup>131</sup> I	Pan-caspase inhibitor Irreversible	Morris hepatoma cells. <sup>395</sup>	None	Low specific radioactivity, probe is mixture of two derivatives.
FB-VAD-fmk <sup>18</sup> F	Pan-caspase inhibitor, irreversible. IC <sub>50</sub> 225 nM (caspase-3).	SW620 (human colon carcinoma cell line), DLD-1, COLO-205, LIM-2405 (human caecal adenocarcinoma cell line) xenografts. <sup>396</sup>	None	Detects activated caspases after chemotherapy (single, multidrug). Predicts later tumor shrinking.
CBR <sup>18</sup> F	K <sub>i</sub> 36 nM (caspase-3), 93 nM (caspase-7)	NMRI (Naval Medical Research Institute [mouse strain]) nude mice: rapid clearance from blood and plasma (within 10 min). <sup>397</sup>	None	Probably not useful. No further data reported.
WC-II-89 <sup>18</sup> F	IC <sub>50</sub> 9.7 nM (caspase-3), 24 nM (caspase-7)	Rodent models of hepatic apoptosis. <sup>245,398</sup> No tumor model data. Improved synthesis reported. <sup>399</sup>	None	Detects activated caspases in apoptotic cells.
WC-98 <sup>11</sup> C	IC <sub>50</sub> 14.5 nM (caspase-3), 22 nM (caspase-7)	Rodent models of hepatic apoptosis. Observed increases were smaller than those of WC-II-89. <sup>399,400</sup>	None	Probe detects activated caspases but WC-II-89 should be preferred.
WC-IV-3 <sup>18</sup> F	IC <sub>50</sub> 8.6 nM (caspase-3), 26 nM (caspase-7)	Rodent models of hepatic apoptosis. <sup>245,400</sup> Observed increases were smaller than those of WC-II-89.	None	Probe detects activated caspases but WC-II-89 should be preferred.
ICMT-11 <sup>18</sup> F	IC <sub>50</sub> 0.5 nM (caspase-3), 2.5 nM (caspase-7)	RIF-1, LNM35 (human pulmonary carcinoma cell line), PC9, A549 (human lung adenocarcinoma cell line) cells. <sup>401,402</sup> RIF-1, 38C13 (mouse B-lymphoma cell line), HCT116 (human colon carcinoma cell line), MDA-MB-231 (human breast adenocarcinoma cell line), PC9 tumors. <sup>401-404</sup> Probe detects activated caspases. For proper analysis of PET data in tumors with necrotic centers, voxel-wise data analysis is a must.	Eight volunteers: eliminated via the hepatic and renal routes, acceptable dosimetry. <sup>405</sup>	Improved <sup>406</sup> and GMP (good manufacturing practice) synthesis of [ <sup>18</sup> F]ICMT-11 have been developed. <sup>407,408</sup> Further evaluation of [ <sup>18</sup> F]ICMT-11 in patients receiving antitumor therapy is required.

(Continues)

TABLE 6 (Continued)

Probe/label	Target/affinity	Preclinical evaluation	Human studies	Perspectives
WC-4-116 <sup>18F</sup>	IC <sub>50</sub> 4.5 nM (caspase-3)	EL4 (mouse lymphoma cell line) cells; <sup>409</sup> Colo205 (human colon carcinoma cell line) xenografts. <sup>409</sup> Plasma levels and nonspecific binding of tracer increase after immunotherapy.	None	Pharmacokinetics seem problematic.
Tat <sub>49-57</sub> -γ-DEVDG-NH <sub>2</sub> <sup>131I</sup>	Caspase-3 substrate	Jurkat J6 cells. <sup>255</sup> Peptide is fragmented; the radioactive G-NH <sub>2</sub> fragment is rapidly washed out.	None	Probe is not useful.
Tat <sub>57-49</sub> -γ-DEVDG-NH <sub>2</sub> <sup>131I</sup>	Caspase-3 substrate	Jurkat J6 cells. <sup>255</sup> Peptide is not fragmented, but the product of caspase cleavage is rapidly washed out.	None	Probe is not useful.
CP18 <sup>18F</sup>	Caspase-3 substrate (highly selective)	U87MG (human glioblastoma cell line), A498 (human kidney carcinoma cell line), A427 (human pulmonary carcinoma cell line), LnCap (human prostate carcinoma cell line), PC3 (human prostate carcinoma cell line), and Colo205 (human colon carcinoma cell line) xenografts. <sup>410-411</sup> Thymus apoptosis model. <sup>412</sup> Mouse model of doxorubicin cardiotoxicity. <sup>413</sup> CP18 may in colon cancer cells be a substrate for caspase-3 and caspase-9. <sup>411</sup>	Seven volunteers: cleared via kidneys, bladder dose can be reduced by frequent voiding <sup>414</sup>	Detects activated caspases after chemotherapy (see Figure 4). Considered suitable for patient studies. <sup>414</sup>

fmk, fluoromethyl ketone; Jurkat, immortalized line of human T lymphocytes; PC9, human lung adenocarcinoma cell line (differentiated); RIF-1, murine radiation-induced fibrosarcoma cell line.

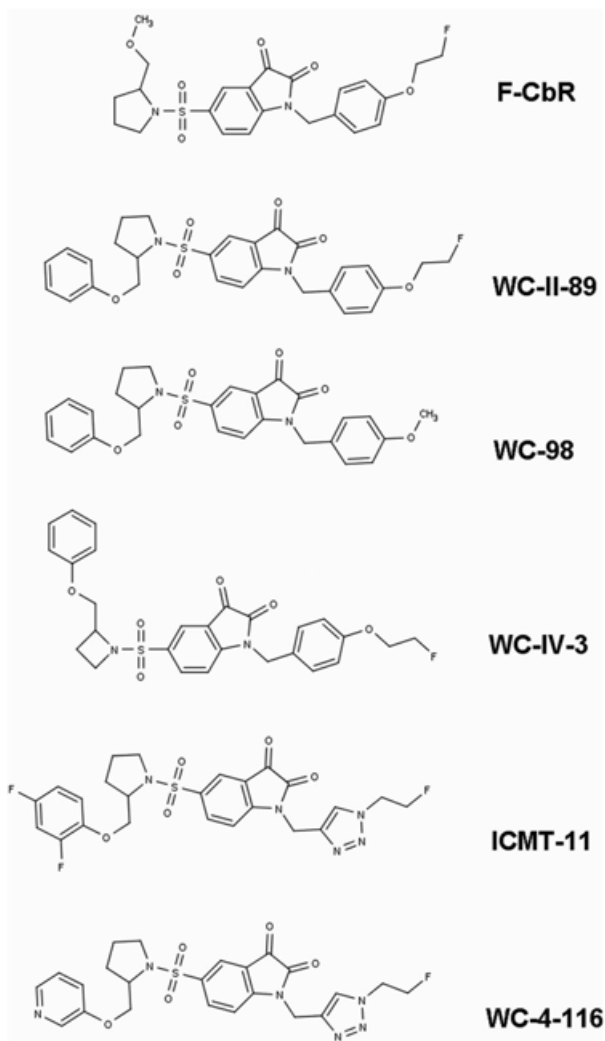


**FIGURE 3** Chemical structures of radiolabeled isatins which have been tested as PET probes for caspase-3

### 3.4.2 | Caspase substrates

The cellular trapping of radiolabeled caspase substrates is less sensitive to competition by physiological substances than the binding of radiolabeled caspase inhibitors, but intracellular retention of the cleaved substrate is necessary for successful imaging.

Currently used caspase substrates are based on the Z-aspartate-glutamate-valine-aspartate sequence. Since the inclusion of only a Aspartate, Glutamate, Valine, Aspartate, Glycine (DEVDG) or Asparagine, Glutamine, Valine, Asparagine, Glycine (NQVNG) amino acid sequence results in highly polar peptides, which do not cross cell membranes, some additional sequence should be attached to ensure membrane permeation. Membrane-penetrating peptide sequences which could be explored are the following:

- Multiple Antigenic Peptide (MAP) peptide (X-KLALKLALKALKKAALKLA)—group 1, bilateral transport;
- transportan—group 1, bilateral transport;
- Tat—group 2, unilateral trapping, suitable for labeling because of the presence of Tyr;
- penetratin—group 2, unilateral trapping, not suitable for labeling because of the presence of Met.

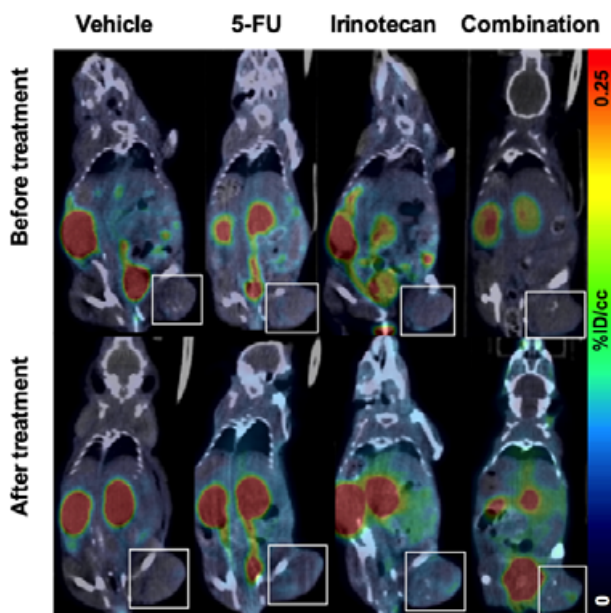


**FIGURE 4** In vivo [ $^{18}\text{F}$ ]CP18 scans of tumor-bearing mice (PET/CT images showing tracer uptake [ $\%ID/cm^3$ ] in vehicle, 5-FU (5-fluorouracil), irinotecan, and combination-treated animals (from left to right) before (upper panel) and after (lower panel) treatment. Tumors are indicated by white squares. Reproduced (with permission) from ref. 411

In the first attempts at probe development, a Tat sequence (e.g., Tat49-57, RKKRRQRRR) was added to ensure cellular uptake. It was demonstrated that insertion of yDEVG at the C-terminus of Tat was preferable, but the mechanism of uptake which is triggered by addition of that sequence is caspase-independent.<sup>255</sup>

An elegant solution to the problem of intracellular retention of the cleaved substrate has recently been provided by the so-called “smart probes” which display intramolecular macrocyclization and in situ nanoaggregation upon activation by caspase-3.<sup>256–258</sup> Due to sequence homology among the caspases, most caspase probes are not specific for caspase-3 or caspase-7. However, recent research on activity-based probes has shown that the selectivity of such probes for a single caspase can be greatly improved by introducing several unnatural amino acids in the peptide recognition sequence.<sup>259–262</sup>

Imaging results acquired with radiolabeled caspase substrates are presented in Figure 4 and Table 6. Although the preclinical data presented in Table 6 (particularly those of [ $^{18}\text{F}$ ]CP18) have indicated that it is possible to image apoptosis and therapy-induced increases of apoptosis with a radiolabeled substrate for caspase-3, concentrations of radioactivity in target tissues were usually very low. Thus, the currently available caspase substrates seem to have not fulfilled their promise of significant signal amplification with respect to radiolabeled caspase inhibitors.

### 3.5 | DNA damage and repair

As explained in Section 2.5 of this review, fragmentation of DNA is a process which accompanies both apoptosis and other forms of cell death. Environmental factors which may lead to the development of cancer, such as exposure to ultraviolet light, ionizing radiation, and carcinogenic substances, cause strand breaks in DNA. Moreover, many human cancers are characterized by deficiencies in DNA repair pathways compared to normal tissue. Finally, most forms of antitumor therapy induce damage to DNA. Many researchers have therefore attempted to develop radiopharmaceuticals which can visualize DNA damage and repair. Such tracers could be used to: (i) detect several forms of cancer at an early stage, (ii) evaluate the response of tumors to therapy, (iii) assess the biodistribution, pharmacokinetics, and target engagement of cytotoxic drugs aimed at inhibiting DNA repair, and (iv) select patients for treatment with such drugs. Results of attempts to visualize DNA damage and repair are summarized in Table 7.

TABLE 7 Probes targeting DNA damage and repair

Probe/label	Target	Preclinical evaluation	Human studies	Perspectives
PJ34 <sup>11</sup> C	PARP-1 (NAD <sup>+</sup> binding site, activated enzyme)	Rat model of diabetes. Pancreatic uptake correlates with PARP-1 expression in beta cells, reflects necrosis. <sup>415</sup>	None	Feasibility of PARP-1 imaging demonstrated.
BO <sup>18</sup> F	PARP-1 (olaparib derivative, IC <sub>50</sub> 17.9 nM)	MDA-MB-468, SKOV3, MIAPaCA-2 (human pancreatic carcinoma cell line), PANC-1 (human pancreatic epitheloid carcinoma cell line), A2780 (human ovarian carcinoma cell line) xenografts. <sup>416–418</sup>	None	Probe can quantify PARP-1 expression in tumor cells and occupancy of PARP-1 by olaparib.
PARPi-fluorescein <sup>18</sup> F	PARP-1 (olaparib derivative)	U87MG xenografts. <sup>419</sup> Probe allows both PET and fluorescent imaging.	None	Rapidly defluorinated in vivo, thus not useful for in vivo studies.
PARPi <sup>18</sup> F	PARP-1 (olaparib derivative, IC <sub>50</sub> 2.8 nM)	U251MG xenografts: > 85% specific binding, tumor-to-brain ratios about 50. High uptake in lymph nodes and spleen because of PARP-1 expression in immune cells. <sup>420</sup>	None	Good results. PARP-1 tracers bind not only to tumor cells with DNA damage but also to inflammatory cells.
I2-PARPi <sup>123</sup> I, <sup>124</sup> I, <sup>131</sup> I	PARP-1 (olaparib derivative, IC <sub>50</sub> 9 nM)	U251MG, U87MG xenografts: 50–77% specific binding. <sup>421,422</sup>	None	Probe visualizes target but shows smaller specific binding fraction than PARPi.
FTT (Fluor Thanatrace) <sup>18</sup> F	PARP-1 (IC <sub>50</sub> 6.3 nM)	Genetically engineered fibroblasts. <sup>423</sup> SNU-251 (human ovarian carcinoma cell line), SKOV3 cells. <sup>424</sup> MDA-MB-231 xenografts. <sup>423,425</sup> Probe does not bind to PARP-2, shows specific binding in lymph nodes and spine. <sup>426</sup>	Radiation dose 6.9 mSv for 370 MBq, spleen and pancreas get highest dose. <sup>426</sup>	Probe is specific for PARP-1. Can distinguish BRCA-1 mutant from BRCA-1 wild-type cells after radiotherapy.

(Continues)

TABLE 7 (Continued)

Probe/label	Target	Preclinical evaluation	Human studies	Perspectives
KX1 (FTT analog) <sup>125</sup> I	PARP-1 (IC <sub>50</sub> in nM range)	Genetically engineered fibroblasts, many cell lines, <sup>427</sup> HCC1937 (human breast carcinoma cell line), MDA-MB-231 xenografts; considerable uptake but NO reduction after pretreatment of animals with cold olaparib. <sup>427</sup>	None	Probe is specific for PARP-1. But its pharmacokinetics are not optimal (plasma levels of radioactivity and nonspecific binding are strongly increased after drug treatment; it is possibly a substrate for P-gp [P-glycoprotein]).
KX-02-019 (FTT analog) <sup>125</sup> I	PARP-1 PARP-2	Genetically engineered fibroblasts, <sup>428</sup> EMT6 (mouse mammary carcinoma cell line) tumors. <sup>428</sup>	None	Probe is not specific for PARP-1. Showed only moderate target-to-nontarget ratios.
Anti- $\gamma$ H2AX-TAT antibodies <sup>111</sup> In	$\gamma$ H2AX	MDA-MB-468 cells. <sup>429</sup> MDA-MB-468 xenografts. <sup>429</sup> Transgenic mouse model of HER2 (human epidermal growth factor receptor 2)/neu overexpression-driven breast cancer: tumor formation could be detected earlier with the SPECT probe (after 96 days) than with DCE-MRI (dynamic contrast enhanced magnetic resonance imaging) (after 120 days) or by palpation (after 131 days). <sup>430</sup>	None	DNA damage response in tumor after radio- or chemotherapy can be visualized. SPECT with these antibodies has potential for early detection of malignant lesions.
Anti- $\gamma$ H2AX-TAT antibodies <sup>89</sup> Zr	$\gamma$ H2AX	MDA-MB-468 cells. <sup>431</sup> MDA-MB-468 xenografts; 2.4-fold increased uptake after radiotherapy, about 60% specific binding. <sup>431</sup>	None	DNA damage response in tumor can be visualized.
ATRj <sup>18</sup> F	ATR kinase	U251MG xenografts. <sup>432</sup> Only minor decrease of target-to-nontarget ratio after target blocking.	None	Pharmacokinetics seem inappropriate for PET imaging.

BRCA1, breast cancer type 1 susceptibility protein; MDA-MB, human breast adenocarcinoma cell line; SKOV3, human ovary adenocarcinoma cell line; U251MG, human glioblastoma cell line; U87MG, human glioblastoma cell line.

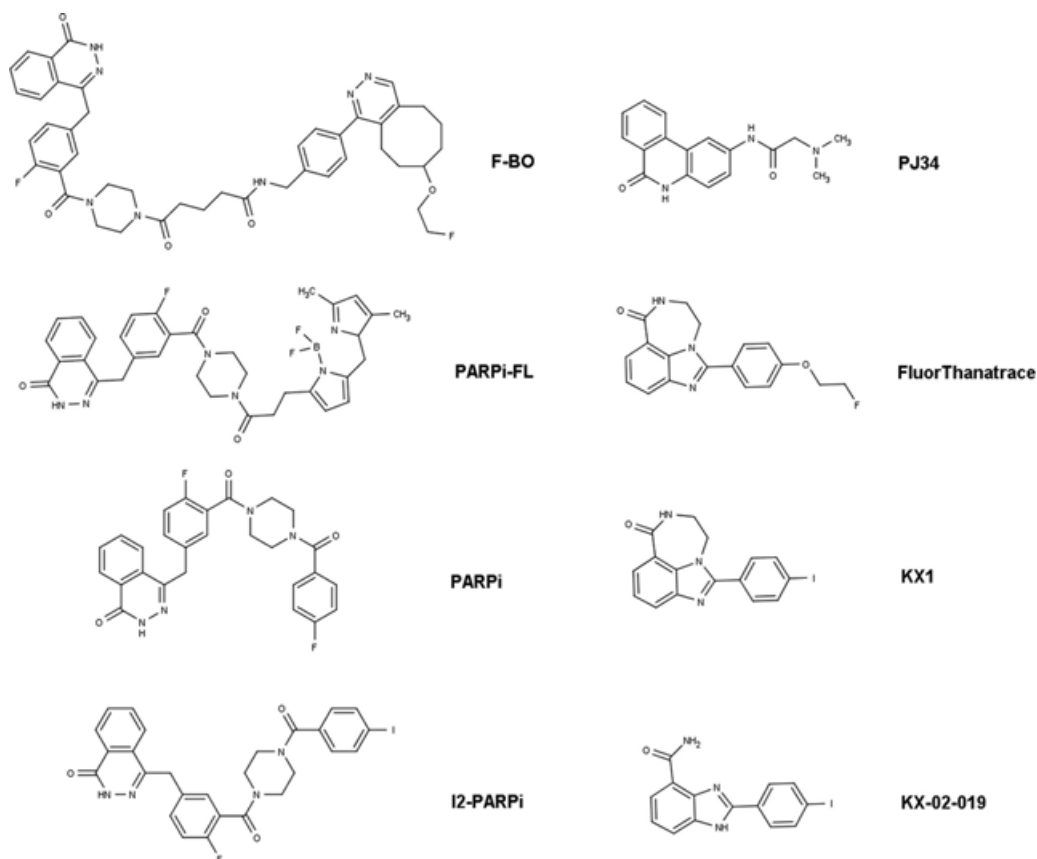


**FIGURE 5** Chemical structures of radiolabeled inhibitors which have been proposed for imaging of activated PARP-1

### 3.5.1 | Poly(ADP-ribose) polymerase-1

PARP-1 is an enzyme in the nucleus of eukaryotic cells. When single-strand breaks in DNA occur, PARP-1 transfers ADP-ribose units from NAD<sup>+</sup> to various proteins, such as DNA polymerase and histones. This action of the enzyme plays an important initiating role in the repair of DNA, but when PARP-1 is hyperactivated, cellular NAD<sup>+</sup> pools are depleted, resulting in a decline of the levels of ATP and necrosis. Radiopharmaceuticals which target the expression or the activity of PARP-1 have thus been used to evaluate target engagement of cytotoxic drugs. Such probes include radiolabeled analogs of the drug olaparib and derivatives of the benzimidazol carboxamide NU1085 (see Table 7 and Figure 5).

Some PET tracers for PARP-1 have shown very promising results in animal models, particularly [<sup>18</sup>F]PARPi. However, all radiolabeled PARP inhibitors which have been studied thus far are hepatobiliary cleared. It remains to be seen whether the high accumulation of radioactivity in liver, intestines, and gall bladder constitutes a problem for application of these tracers in patients with abdominal cancer. The use of radiolabeled PARP-1 inhibitors may be associated with two other complications: (i) Such probes may bind not only to dying tumor cells but also to immune cells, and (ii) DNA damage and repair will not always lead to cell death. Thus, PARP-1 inhibitors will have a limited specificity for dying cells.

### 3.5.2 | Phosphorylated X isoform of the histone H2A ( $\gamma$ H2AX)

When double-strand breaks in DNA occur, the X-form of histone H2A (H2AX) is phosphorylated ( $\gamma$ H2AX) and several hundreds of phosphorylated protein molecules accumulate around each break site. The formation and accumulation of



$\gamma$ H2AX is necessary for recruitment and activation of the subsequent processes of DNA repair. The expression levels of  $\gamma$ H2AX are very low under normal physiological conditions, but show a strong and rapid rise after the induction of DNA damage. For this reason,  $\gamma$ H2AX is an attractive target for SPECT and PET imaging. Imaging of this target may be used to visualize the impact of antitumor therapy.

Anti- $\gamma$ H2AX antibodies can be used to quantify phosphorylated H2AX in permeabilized or lysed cells, but are not useful in living cells since such antibodies do not cross intact cell membranes. However, when the antibodies are linked to a cell penetrating peptide ("TAT sequence"), they are internalized in living cells and targeted to the nucleus (see Table 7).

A recent review on imaging of the DNA damage response<sup>263</sup> concluded that several important issues still need to be addressed before anti- $\gamma$ H2AX-TAT antibodies can be applied in clinical studies:

1. A humanized version of the antibodies should be prepared, since the preclinically tested antibodies were raised in rabbits and will cause an immune response when they are injected in humans;
2. Since the currently used  $\gamma$ H2AX-TAT antibodies have a rather high nonspecific *in vivo* binding, it may be necessary to improve the target-to-nontarget ratio of these probes, for example, by using smaller antibody fragments rather than full antibodies, or by the application of a pretargeting strategy;
3. Quantification of the exact number of DNA double strand breaks may be difficult, since the local increase of  $\gamma$ H2AX is not directly or linearly related to the number of strand breaks. More information about the biology of  $\gamma$ H2AX is required to properly interpret PET or SPECT images acquired with anti- $\gamma$ H2AX-TAT.<sup>263</sup>

### 3.5.3 | Ataxia telangiectasia and Rad3-related threonine serine kinase

Another important enzyme involved in the initiation and orchestration of the repair of DNA damage is ataxia telangiectasia and Rad3-related threonine serine kinase (ATR kinase). A radiolabeled analog of the ATR kinase inhibitor Ve-821 has been prepared but the results were disappointing (Table 7). Apparently, the pharmacokinetic properties of radiolabeled ATR kinase inhibitors need to be improved before they can be applied as PET tracers.

## 3.6 | Other processes involved in cell death

Several imaging probes have been developed which may visualize necrosis. Imaging findings concerning these probes are summarized in Table 8 and the chemical structures of some probes are shown in Figure 6. The probes in question targeted the following processes:

### 3.6.1 | Exposure of histone H1

Apoptosis-targeting peptide-1 (ApoPep-1), a hexapeptide identified by phage display, binds in a  $\text{Ca}^{2+}$ -independent manner to histone H1, which is exposed by apoptotic cells or becomes accessible in the nucleus of necrotic cells.<sup>264</sup> The translocation of histone H1 during apoptosis proceeds in a caspase-dependent manner and occurs at the early stage of apoptosis (before DNA fragmentation). The R3 residue was shown to determine binding and the ApoPep-1 sequence was homologous to the G-protein-coupled receptor 83.

### 3.6.2 | Redistribution of La autoantigen

La autoantigen is a nuclear protein with an MW of 47 (or 48) kDa which is overexpressed in cancer cells with respect to cells of the tissue of origin. The La protein is cleaved by caspase-3 during apoptosis, resulting in translocation of the  $\text{NH}_2$  terminus part of the molecule (MW 43 kDa) to the cytoplasm<sup>265</sup> and accessibility of this part to anti-La antibodies.<sup>266</sup> Since the expression of the La autoantigen is selectively induced in dead or dying cancer cells after DNA-damaging chemotherapy, imaging of this target is an interesting strategy for the detection of tumors and the evaluation of anti-tumor therapy.<sup>267</sup>

TABLE 8 Probes targeting necrosis

Probe/label	Target	Preclinical evaluation/findings	Human studies/findings	Perspectives of the probe
ApoPep-1 <sup>124</sup> I, <sup>131</sup> I	Histone H1	A549 (human lung adenocarcinoma cell line), H460 (human nonsmall-cell lung cancer cell line) xenografts. <sup>464,433</sup> Can also be labeled with <sup>18</sup> F for PET imaging. <sup>434</sup>	None	Potentially useful for imaging of cell death. Cyclic peptide may be better than linear one. <sup>435</sup>
3B9 mAb (monoclonal antibody) <sup>14</sup> C, <sup>111</sup> In	La autoantigen	EL4 (mouse lymphoma cell line) tumors. <sup>436</sup>	None	Detects tumor response to chemotherapy. <sup>436</sup>
Antimyosin <sup>111</sup> In	Myosin heavy fragments	VX2, AH109A (rat hepatoma cell line) tumors <sup>437</sup> ; Probe shows nonspecific accumulation in inflammatory cells in and around tumors.	Patients with rhabdomyosarcoma, leiomyosarcoma, and neuroectodermal tumors. <sup>438–442</sup> Tumors lacking the target (myosin) can also accumulate the probe. <sup>443</sup>	Probe is not a specific marker for necrosis, or release of myosin.
Glucarate <sup>99m</sup> Tc	Unknown (histones?)	BT20, MCF7 (human breast cancer cell line), SUM190 (human breast cancer cell line), BxPC3 (human pancreatic adenocarcinoma cell line), HEK-293 (human embryonic kidney cell line), and HCT-116 xenografts. <sup>444–447</sup> Probe visualizes tumors and is not a substrate for P-gp (P-glycoprotein) or MRP-1 (multidrug resistance-associated protein 1).	Eleven patients with advanced head and neck cancer <sup>448</sup> and 47 patients with lung or head and neck cancer; both primary lesions and metastatic sites visible. <sup>449</sup> Tracer uptake after antitumor therapy correlated with later response. <sup>449</sup>	Probe may also accumulate in non-necrotic ischemic, hypoxic, and/or hypoglycemic tissues. <sup>450,451</sup> Uptake mechanism is poorly defined.
Hypericin <sup>131</sup> I <sup>64</sup> Cu-bis-DOTA (1,4,7,10-tetraazacyclododecane-1,4,7,10-tetraacetic acid)	Unknown but specific <sup>452</sup> (may bind to cholesterol, PE, PS, and/or E-DNA). <sup>453,454</sup>	BT474 (human breast carcinoma cell line) xenografts, <sup>455</sup> hepatic rhabdomyosarcomas, <sup>456</sup> and VX2 tumors. <sup>457</sup>	Duodenal drainage catheter is required to reduce the intestinal radiation dose. <sup>458–460</sup> The dose to thyroid and lungs is then still considerable. <sup>461</sup> Intratumoral tracer administration has been proposed to circumvent these problems. <sup>462</sup>	Formation of aggregates should be avoided by addition of PEG400 or sodium cholate. <sup>463–466</sup> Various hypericin analogs with better solubility have been proposed. <sup>454,467–469</sup> Uptake mechanism is poorly defined.
Pamoic acid <sup>99m</sup> Tc, <sup>68</sup> Ga	Unknown	Animal models of hepatic infarction, hepatic necrosis, and muscle necrosis. <sup>470–472</sup>	None.	Uptake mechanism is poorly defined.

VX2, rabbit anaplastic squamous cell carcinoma.

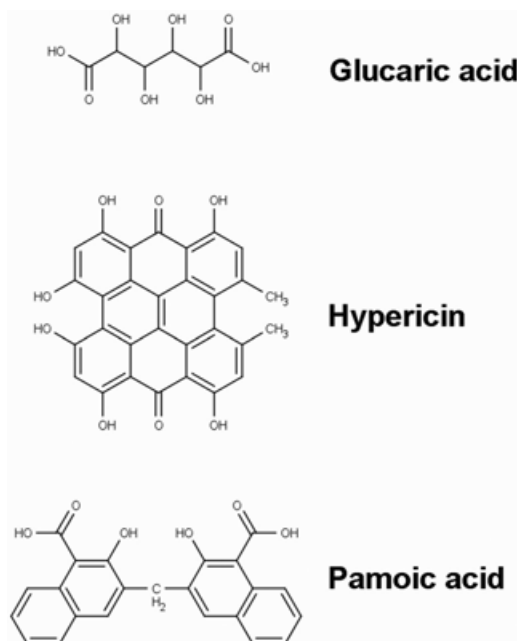


**FIGURE 6** Chemical structures of some compounds which have been used to target tissue necrosis

### 3.6.3 | Accessibility of myosin

Radiolabeled Fab fragments of monoclonal antibodies against myosin ( $[^{111}\text{In}]$ antimyosin) have been widely used for the detection of myocardial cell injury and necrosis. Membrane disruption of myocytes makes it possible for such fragments to enter the dying cell and to interact with myosin heavy fragments.

### 3.6.4 | Exposed histones

$[^{99\text{m}}\text{Tc}]$ Glucarate ( $[^{99\text{m}}\text{Tc}]$ -D-glucaric acid) is a six-carbon dicarboxylic acid with a structural similarity to fructose. This SPECT tracer has been reported to accumulate in areas of acute ischemic injury where necrosis occurs, both within the brain<sup>268</sup> and heart.<sup>269–272</sup> For this reason,  $[^{99\text{m}}\text{Tc}]$ glucarate has also been tested as a cell death tracer in animal models of human cancer and in cancer patients (see Table 8).

### 3.6.5 | Extracellular DNA

Hypericin is a red pigment with anthraquinone-like structure (MW 504 Da), which has been isolated from St. John's wort (*Hypericum perforatum*). Hypericin has been tested in many studies as a photosensitizer for photodynamic therapy. Since the compound accumulates in necrotic cells and tissues, hypericin has also been radioiodinated or labeled with  $^{64}\text{Cu}$  for the imaging of tumors and infarctions in experimental animals and humans (Table 8). Because of its polyphenolic polycyclic structure, hypericin has fluorescent properties and the compound can be detected in cell or preclinical experiments by optical imaging.<sup>273–275</sup>

### 3.6.6 | Unknown target (Pamoic acid derivatives)

The bis-DTPA derivative of pamoic acid (4,4'-methylenebis[3-hydroxy-2-naphthoic acid]) is a necrosis avid contrast agent. The mechanism underlying accumulation of this compound in necrotic tissue is unknown.<sup>276</sup> Various derivatives of pamoic acid have been radiolabeled and evaluated for visualization of necrosis with SPECT or PET (Table 8).

Unfortunately, most necrosis-targeting probes seem to lack adequate specificity (see Table 8). They may accumulate in tissues by mechanisms unrelated to cell death (e.g., inflammation, ischemia, hypoxia, or hypoglycemia), and the uptake mechanism of these probes is poorly defined. Only the peptide ApoPep-1 seems to deserve further evaluation.

## 4 | CONCLUSIONS AND PERSPECTIVES

Although a large number of PET and SPECT probes for imaging of cell death have been developed, only a few radiopharmaceuticals have proceeded to the clinical stage of testing, viz. radiolabeled Annexin A5, PGN650, ML-10, CP18, antimyosin antibodies, glucarate, and hypericin. Of these seven, the first four are the most likely candidates for translation to the clinic, and results of ongoing clinical trials with Annexin V-124 and PGN650 are eagerly awaited.

An important issue concerning cell death imaging is the question whether radiopharmaceuticals should be specific for a particular death mode and biochemical process (e.g., activated caspase-3 or caspase-7), or can have limited specificity (e.g., detect exposed PS or anionic phospholipids). The required specificity will probably depend on the intended use of the tracer. In a basic science setting (visualizing of dying cells in animal and in vitro models of human disease), specificity of the used probe is very important in order to acquire specific information about the mechanisms underlying cell death (apoptotic vs. nonapoptotic, noninflammatory, or pro-inflammatory, etc.). However, in a clinical setting (assessment of a patient's response to antitumor treatment), specificity of the probe may be of less importance. In this case, a probe with limited specificity that provides a stronger signal than a specific probe may be preferred. Here the main question to answer is whether cells have died. The question via which mechanism cell death was induced is then only a secondary issue.

In the extensive work performed with radiolabeled Annexin A5, two important difficulties were noted which will be of general concern in treatment response evaluation with any cell death tracer: (i) since the optimal timing of a post-therapy scan is frequently unknown or uncertain, a complex (multi-scan) protocol may be required for correct evaluation of tumor responses, and (ii) increases in cell death occur rapidly after the onset of therapy and correlate with early tumor shrinkage, but the magnitude of this early response to treatment is not always predictive for the long-term response of a tumor. For a few tracers (i.e., [<sup>99m</sup>Tc]Annexin A5, [<sup>18</sup>F]ML-10, [<sup>18</sup>F]FB-VAD-fluoromethyl ketone, [<sup>99m</sup>Tc]glucarate) and a few tumor models, data have been acquired demonstrating that the magnitude of early tracer uptake in the tumor corresponds to the extent of tumor shrinkage during follow-up. There is definitely a need for more information about this subject, since valid predictive tools will allow clinicians to change therapy in nonresponding patients at an early stage, avoiding unnecessary toxicity and increasing treatment efficacy.

Since a limited probe entry into tumor tissue was frequently encountered in previous research (probably due to a large molecular size of the probes), radiolabeled protein domains or antibody fragments may be more promising as tracers than full-length proteins or antibodies. Some novel potential tracer candidates have been identified in recent years, but have not yet been widely explored for PET and SPECT imaging. These include the Tim family of proteins which bind to PS via their IgV domain (but show a higher affinity to oxidized PS)<sup>277</sup>; Bai-1, which binds to PS via thrombospondin domains<sup>278</sup>; and sRAGE, which binds PS via a V-type domain.<sup>279</sup> Other possible candidates are: antibodies against CXCL1, which is released during the unfolded protein response,<sup>280</sup> the high mobility group box 1 (HMGB1) protein, which interacts with PS in an integrin-dependent manner,<sup>52</sup> and imaging of granzyme B, which may be a predictive biomarker of immunotherapy response.<sup>281</sup> The already wide field of cell death imaging may thus expand even further in the near future.

### ORCID

Aren van Waarde  <http://orcid.org/0000-0003-1183-1603>

### REFERENCES

1. Candi E, Schmidt R, Melino G. The cornified envelope: a model of cell death in the skin. *Nat Rev Mol Cell Biol.* 2005;6:328–340.
2. Meier P, Finch A, Evan G. Apoptosis in development. *Nature.* 2000;407:796–801.
3. Saxen L, Sariola H. Early organogenesis of the kidney. *Pediatr Nephrol.* 1987;1:385–392.
4. Freude B, Masters TN, Robicsek F, et al. Apoptosis is initiated by myocardial ischemia and executed during reperfusion. *J Mol Cell Cardiol.* 2000;32:197–208.
5. Hotchkiss RS, Tinsley KW, Karl IE. Role of apoptotic cell death in sepsis. *Scand J Infect Dis.* 2003;35:585–592.

6. Moriwaki M, Itoh N, Miyagawa J, et al. Fas and Fas ligand expression in inflamed islets in pancreas sections of patients with recent-onset Type I diabetes mellitus. *Diabetologia*. 1999;42:1332–1340.
7. Josien R, Muschen M, Gilbert E, et al. Fas ligand, tumor necrosis factor- $\alpha$  expression, and apoptosis during allograft rejection and tolerance. *Transplantation*. 1998;66:887–893.
8. Ethell DW, Buhler LA. Fas ligand-mediated apoptosis in degenerative disorders of the brain. *J Clin Immunol*. 2003;23:363–370.
9. Li CJ, Friedman DJ, Wang C, Metelev V, Pardee AB. Induction of apoptosis in uninfected lymphocytes by HIV-1 Tat protein. *Science*. 1995;268:429–431.
10. Hodge S, Hodge G, Holmes M, Reynolds PN. Increased peripheral blood T-cell apoptosis and decreased Bcl-2 in chronic obstructive pulmonary disease. *Immunol Cell Biol*. 2005;83:160–166.
11. Vignola AM, Chiappara G, Gagliardo R, et al. Apoptosis and airway inflammation in asthma. *Apoptosis*. 2000;5:473–485.
12. Sugiyama M, Tsukazaki T, Yonekura A, Matsuzaki S, Yamashita S, Iwasaki K. Localisation of apoptosis and expression of apoptosis related proteins in the synovium of patients with rheumatoid arthritis. *Ann Rheum Dis*. 1996;55:442–449.
13. Kerr JF, Winterford CM, Harmon BV. Apoptosis. Its significance in cancer and cancer therapy. *Cancer*. 1994;73:2013–2026.
14. Schweichel JU, Merker HJ. The morphology of various types of cell death in prenatal tissues. *Teratology*. 1973;7:253–266.
15. Galluzzi L, Bravo-San Pedro JM, Vitale I, et al. Essential versus accessory aspects of cell death: recommendations of the NCCD 2015. *Cell Death Differ*. 2015;22:58–73.
16. Kerr JF, Wyllie AH, Currie AR. Apoptosis: a basic biological phenomenon with wide-ranging implications in tissue kinetics. *Br J Cancer*. 1972;26:239–257.
17. Li P, Nijhawan D, Budihardjo I, et al. Cytochrome c and dATP-dependent formation of Apaf-1/caspase-9 complex initiates an apoptotic protease cascade. *Cell*. 1997;91:479–489.
18. Du C, Fang M, Li Y, Li L, Wang X. Smac, a mitochondrial protein that promotes cytochrome c-dependent caspase activation by eliminating IAP inhibition. *Cell*. 2000;102:33–42.
19. Verhagen AM, Ekert PG, Pakusch M, et al. Identification of DIABLO, a mammalian protein that promotes apoptosis by binding to and antagonizing IAP proteins. *Cell*. 2000;102:43–53.
20. Wajant H, Pfizenmaier K, Scheurich P. TNF-related apoptosis inducing ligand (TRAIL) and its receptors in tumor surveillance and cancer therapy. *Apoptosis*. 2002;7:449–459.
21. Micheau O, Shirley S, Dufour F. Death receptors as targets in cancer. *Br J Pharmacol*. 2013;169:1723–1744.
22. Goldschneider D, Mehlen P. Dependence receptors: a new paradigm in cell signaling and cancer therapy. *Oncogene*. 2010;29:1865–1882.
23. Irmiler M, Thome M, Hahne M, et al. Inhibition of death receptor signals by cellular FLIP. *Nature*. 1997;388:190–195.
24. Deveraux QL, Takahashi R, Salvesen GS, Reed JC. X-linked IAP is a direct inhibitor of cell-death proteases. *Nature*. 1997;388:300–304.
25. Kaufmann T, Strasser A, Jost PJ. Fas death receptor signalling: roles of Bid and XIAP. *Cell Death Differ*. 2012;19:42–50.
26. Kantari C, Walczak H. Caspase-8 and bid: caught in the act between death receptors and mitochondria. *Biochim Biophys Acta*. 2011;1813:558–563.
27. Elmore S. Apoptosis: a review of programmed cell death. *Toxicol Pathol*. 2007;35:495–516.
28. Brown JM, Attardi LD. The role of apoptosis in cancer development and treatment response. *Nat Rev Cancer*. 2005;5:231–237.
29. Liu Y, Levine B. Autosis and autophagic cell death: the dark side of autophagy. *Cell Death Differ*. 2015;22:367–376.
30. Abedin MJ, Wang D, McDonnell MA, Lehmann U, Kelekar A. Autophagy delays apoptotic death in breast cancer cells following DNA damage. *Cell Death Differ*. 2007;14:500–510.
31. Gonzalez-Polo RA, Niso-Santano M, Ortiz-Ortiz MA, et al. Inhibition of paraquat-induced autophagy accelerates the apoptotic cell death in neuroblastoma SH-SY5Y cells. *Toxicol Sci*. 2007;97:448–458.
32. Landowski TH, Escalante AM, Jefferson A, Dorr RT, Lynch R. Inhibition of autophagy promotes bortezomib-mediated cell death in myeloma cells. *Blood*. 2008;112:3677.
33. Ge PF, Zhang JZ, Wang XF, et al. Inhibition of autophagy induced by proteasome inhibition increases cell death in human SHG-44 glioma cells. *Acta Pharmacol Sin*. 2009;30:1046–1052.
34. Mishima Y, Santo L, Cirstea DD, et al. Inhibition of autophagy by ACY-1215, a selective HDAC6 inhibitor accelerates carfilzomib-induced cell death in multiple myeloma. *Blood*. 2013;122:4431.

35. Galluzzi L, Vitale I, Abrams JM, et al. Molecular definitions of cell death subroutines: recommendations of the Nomenclature Committee on Cell Death 2012. *Cell Death Differ.* 2012;19:107–120.
36. Shimizu S, Kanaseki T, Mizushima N, et al. Role of Bcl-2 family proteins in a non-apoptotic programmed cell death dependent on autophagy genes. *Nat Cell Biol.* 2004;6:1221–1228.
37. Yu L, Lenardo MJ, Baehrecke EH. Autophagy and caspases: a new cell death program. *Cell Cycle.* 2004;3:1124–1126.
38. Mizushima N, Levine B. Autophagy in mammalian development and differentiation. *Nat Cell Biol.* 2010;12:823–830.
39. Takamura A, Komatsu M, Hara T, et al. Autophagy-deficient mice develop multiple liver tumors. *Genes Dev.* 2011;25:795–800.
40. White E. The role for autophagy in cancer. *J Clin Invest.* 2015;125:42–46.
41. Mowers EE, Sharifi MN, Macleod KF. Autophagy in cancer metastasis. *Oncogene.* 2017;36:1619–1630.
42. Vandenabeele P, Galluzzi L, Vanden Berghe T, Kroemer G. Molecular mechanisms of necroptosis: an ordered cellular explosion. *Nat Rev Mol Cell Biol.* 2010;11:700–714.
43. Amaravadi RK, Thompson CB. The roles of therapy-induced autophagy and necrosis in cancer treatment. *Clin Cancer Res.* 2007;13:7271–7279.
44. Su Z, Yang Z, Xie L, DeWitt JP, Chen Y. Cancer therapy in the necroptosis era. *Cell Death Differ.* 2016;23:748–756.
45. Cho JS, Pietras EM, Garcia NC, et al. IL-17 is essential for host defense against cutaneous *Staphylococcus aureus* infection in mice. *J Clin Invest.* 2010;120:1762–1773.
46. Kaczmarek K, Morales A, Henderson AJ. T cell transcription factors and their impact on HIV expression. *Virology (Auckl).* 2013;2013:41–47.
47. Bizik J, Kankuri E, Ristimaki A, et al. Cell-cell contacts trigger programmed necrosis and induce cyclooxygenase-2 expression. *Cell Death Differ.* 2004;11:183–195.
48. Guo ZS, Bartlett DL. Oncolytic viruses as platform for multimodal cancer therapeutics: a promising land. *Cancer Gene Ther.* 2014;21:261–263.
49. Tait SW, Ichim G, Green DR. Die another way: non-apoptotic mechanisms of cell death. *J Cell Sci.* 2014;127:2135–2144.
50. Vakifahmetoglu H, Olsson M, Tamm C, Heidari N, Orrenius S, Zhivotovsky B. DNA damage induces two distinct modes of cell death in ovarian carcinomas. *Cell Death Differ.* 2008;15:555–566.
51. Surova O, Zhivotovsky B. Various modes of cell death induced by DNA damage. *Oncogene.* 2013;32:3789–3797.
52. Simpson KL, Cawthorne C, Zhou C, et al. A caspase-3 'death-switch' in colorectal cancer cells for induced and synchronous tumor apoptosis in vitro and in vivo facilitates the development of minimally invasive cell death biomarkers. *Cell Death Dis.* 2013;4:e613.
53. Leist M, Jaattela M. Four deaths and a funeral: from caspases to alternative mechanisms. *Nat Rev Mol Cell Biol.* 2001;2:589–598.
54. Kroemer G, Galluzzi L, Vandenabeele P, et al. Classification of cell death: recommendations of the Nomenclature Committee on Cell Death 2009. *Cell Death Differ.* 2009;16:3–11.
55. Vakifahmetoglu H, Olsson M, Zhivotovsky B. Death through a tragedy: mitotic catastrophe. *Cell Death Differ.* 2008;15:1153–1162.
56. Singer SJ, Nicolson GL. The fluid mosaic model of the structure of cell membranes. *Science.* 1972;175:720–731.
57. Weismann D, Binder CJ. The innate immune response to products of phospholipid peroxidation. *Biochim Biophys Acta.* 2012;1818:2465–2475.
58. Lentz BR. Exposure of platelet membrane phosphatidylserine regulates blood coagulation. *Prog Lipid Res.* 2003;42:423–438.
59. Wuthier RE, Lipscomb GF. Matrix vesicles: structure, composition, formation and function in calcification. *Front Biosci (Landmark Ed).* 2011;16:2812–2902.
60. Spector AA, Yorek MA. Membrane lipid composition and cellular function. *J Lipid Res.* 1985;26:1015–1035.
61. Andersen OS, Koeppe RE. Bilayer thickness and membrane protein function: an energetic perspective. *Annu Rev Biophys Biomol Struct.* 2007;36:107–130.
62. Zachowski A. Phospholipids in animal eukaryotic membranes: transverse asymmetry and movement. *Biochem J.* 1993;294(Pt 1):1–14.
63. Emoto K, Toyama-Sorimachi N, Karasuyama H, Inoue K, Umeda M. Exposure of phosphatidylethanolamine on the surface of apoptotic cells. *Exp Cell Res.* 1997;232:430–434.

64. Stafford JH, Thorpe PE. Increased exposure of phosphatidylethanolamine on the surface of tumor vascular endothelium. *Neoplasia*. 2011;13:299–308.
65. VanWijk MJ, VanBavel E, Sturk A, Nieuwland R. Microparticles in cardiovascular diseases. *Cardiovasc Res*. 2003;59:277–287.
66. Hanayama R, Tanaka M, Miwa K, Shinohara A, Iwamatsu A, Nagata S. Identification of a factor that links apoptotic cells to phagocytes. *Nature*. 2002;417:182–187.
67. Kagan VE, Borisenko GG, Serinkan BF, et al. Appetizing rancidity of apoptotic cells for macrophages: oxidation, externalization, and recognition of phosphatidylserine. *Am J Physiol Lung Cell Mol Physiol*. 2003;285:L1–L17.
68. Asano K, Miwa M, Miwa K, et al. Masking of phosphatidylserine inhibits apoptotic cell engulfment and induces autoantibody production in mice. *J Exp Med*. 2004;200:459–467.
69. Petrovski G, Zahuczky G, Katona K, et al. Clearance of dying autophagic cells of different origin by professional and non-professional phagocytes. *Cell Death Differ*. 2007;14:1117–1128.
70. Grzanka D, Stepień A, Grzanka A, Gackowska L, Helmin-Basa A, Szczepanski MA. Hyperthermia-induced reorganization of microtubules and microfilaments and cell killing in CHO AA8 cell line. *Neoplasma*. 2008;55:409–415.
71. Demeyere K, Remijns Q, Demon D, et al. *Escherichia coli* induces bovine neutrophil cell death independent from caspase-3/-7/-1, but with phosphatidylserine exposure prior to membrane rupture. *Vet Immunol Immunopathol*. 2013;153:45–56.
72. Wang Q, Imamura R, Motani K, Kushiyama H, Nagata S, Suda T. Pyroptotic cells externalize eat-me and release find-me signals and are efficiently engulfed by macrophages. *Int Immunol*. 2013;25:363–372.
73. Waring P, Lambert D, Sjaarda A, Hurne A, Beaver J. Increased cell surface exposure of phosphatidylserine on propidium iodide negative thymocytes undergoing death by necrosis. *Cell Death Differ*. 1999;6:624–637.
74. Vance JE. Phosphatidylserine and phosphatidylethanolamine in mammalian cells: two metabolically related aminophospholipids. *J Lipid Res*. 2008;49:1377–1387.
75. Van Meer G, de Kroon AI. Lipid map of the mammalian cell. *J Cell Sci*. 2011;124:5–8.
76. Li Z, Agellon LB, Allen TM, et al. The ratio of phosphatidylcholine to phosphatidylethanolamine influences membrane integrity and steatohepatitis. *Cell Metab*. 2006;3:321–331.
77. Umeda M, Emoto K. Membrane phospholipid dynamics during cytokinesis: regulation of actin filament assembly by redistribution of membrane surface phospholipid. *Chem Phys Lipids*. 1999;101:81–91.
78. Emoto K, Umeda M. An essential role for a membrane lipid in cytokinesis. Regulation of contractile ring disassembly by redistribution of phosphatidylethanolamine. *J Cell Biol*. 2000;149:1215–1224.
79. Thibault G, Shui G, Kim W, et al. The membrane stress response buffers lethal effects of lipid disequilibrium by reprogramming the protein homeostasis network. *Mol Cell*. 2012;48:16–27.
80. Zhixin L, Wells CW, North PE, et al. Phosphatidylethanolamine at the luminal endothelial surface: implications for hemostasis and thrombotic autoimmunity. *Clin Appl Thromb Hemost*. 2011;17:158–163.
81. Zhao M. Lantibiotics as probes for phosphatidylethanolamine. *Amino Acids*. 2011;41:1071–1079.
82. Audi S, Li Z, Capacete J, et al. Understanding the in vivo uptake kinetics of a phosphatidylethanolamine-binding agent (<sup>99m</sup>Tc-Duramycin. *Nucl Med Biol*. 2012;39:821–825.
83. Vance JE, Steenbergen R. Metabolism and functions of phosphatidylserine. *Prog Lipid Res*. 2005;44:207–234.
84. Ravichandran KS, Lorenz U. Engulfment of apoptotic cells: signals for a good meal. *Nat Rev Immunol*. 2007;7:964–974.
85. Cullis PR, de KB. Lipid polymorphism and the functional roles of lipids in biological membranes. *Biochim Biophys Acta*. 1979;559:399–420.
86. Van Dijck PW, de Kruijff B, Verkleij AJ, van Deenen LL, de Gier J. Comparative studies on the effects of pH and Ca<sup>2+</sup> on bilayers of various negatively charged phospholipids and their mixtures with phosphatidylcholine. *Biochim Biophys Acta*. 1978;512:84–96.
87. Zimmerberg J, Akimov SA, Frolov V. Synaptotagmin: fusogenic role for calcium sensor?. *Nat Struct Mol Biol*. 2006;13:301–303.
88. Fairn GD, Schieber NL, Ariotti N, et al. High-resolution mapping reveals topologically distinct cellular pools of phosphatidylserine. *J Cell Biol*. 2011;194:257–275.
89. Tait JF, Smith C, Wood BL. Measurement of phosphatidylserine exposure in leukocytes and platelets by whole-blood flow cytometry with Annexin V. *Blood Cells Mol Dis*. 1999;25:271–278.
90. Appelt U, Sheriff A, Gaipal US, Kalden JR, Voll RE, Herrmann M. Viable, apoptotic and necrotic monocytes expose phosphatidylserine: cooperative binding of the ligand Annexin V to dying but not viable cells and implications for PS-dependent clearance. *Cell Death Differ*. 2005;12:194–196.

91. Steinberg SF. Structural basis of protein kinase C isoform function. *Physiol Rev.* 2008;88:1341–1378.
92. Yeung T, Gilbert GE, Shi J, Silvius J, Kapus A, Grinstein S. Membrane phosphatidylserine regulates surface charge and protein localization. *Science.* 2008;319:210–213.
93. Hui E, Johnson CP, Yao J, Dunning FM, Chapman ER. Synaptotagmin-mediated bending of the target membrane is a critical step in Ca(2+)-regulated fusion. *Cell.* 2009;138:709–721.
94. Van den Eijnde SM, Lips J, Boshart L, et al. Spatiotemporal distribution of dying neurons during early mouse development. *Eur J Neurosci.* 1999;11:712–724.
95. Yoshida H, Kawane K, Koike M, Mori Y, Uchiyama Y, Nagata S. Phosphatidylserine-dependent engulfment by macrophages of nuclei from erythroid precursor cells. *Nature.* 2005;437:754–758.
96. Strauss HW, Narula J, Blankenberg FG. Radioimaging to identify myocardial cell death and probably injury. *Lancet.* 2000;356:180–181.
97. Yang MY, Chuang H, Chen RF, Yang KD. Reversible phosphatidylserine expression on blood granulocytes related to membrane perturbation but not DNA strand breaks. *J Leukoc Biol.* 2002;71:231–237.
98. Ran S, Thorpe PE. Phosphatidylserine is a marker of tumor vasculature and a potential target for cancer imaging and therapy. *Int J Radiat Oncol Biol Phys.* 2002;54:1479–1484.
99. Ran S, He J, Huang X, Soares M, Scothorn D, Thorpe PE. Antitumor effects of a monoclonal antibody that binds anionic phospholipids on the surface of tumor blood vessels in mice. *Clin Cancer Res.* 2005;11:1551–1562.
100. Zhou H, Stafford JH, Hallac RR, et al. Phosphatidylserine-targeted molecular imaging of tumor vasculature by magnetic resonance imaging. *J Biomed Nanotechnol.* 2014;10:846–855.
101. Greenberg ME, Sun M, Zhang R, Febbraio M, Silverstein R, Hazen SL. Oxidized phosphatidylserine-CD36 interactions play an essential role in macrophage-dependent phagocytosis of apoptotic cells. *J Exp Med.* 2006;203:2613–2625.
102. Borisenko GG, Iverson SL, Ahlberg S, Kagan VE, Fadeel B. Milk fat globule epidermal growth factor 8 (MFG-E8) binds to oxidized phosphatidylserine: implications for macrophage clearance of apoptotic cells. *Cell Death Differ.* 2004;11:943–945.
103. Frasn SC, Berry KZ, Fernandez-Boyanapalli R, et al. NADPH oxidase-dependent generation of lysophosphatidylserine enhances clearance of activated and dying neutrophils via G2A. *J Biol Chem.* 2008;283:33736–33749.
104. Hosono H, Aoki J, Nagai Y, et al. Phosphatidylserine-specific phospholipase A1 stimulates histamine release from rat peritoneal mast cells through production of 2-acyl-1-lysophosphatidylserine. *J Biol Chem.* 2001;276:29664–29670.
105. Aoki J, Nagai Y, Hosono H, Inoue K, Arai H. Structure and function of phosphatidylserine-specific phospholipase A1. *Biochim Biophys Acta.* 2002;1582:26–32.
106. Leventis PA, Grinstein S. The distribution and function of phosphatidylserine in cellular membranes. *Annu Rev Biophys.* 2010;39:407–427.
107. Mirnikjoo B, Balasubramanian K, Schroit AJ. Suicidal membrane repair regulates phosphatidylserine externalization during apoptosis. *J Biol Chem.* 2009;284:22512–22516.
108. Lee SH, Meng XW, Flatten KS, Loegering DA, Kaufmann SH. Phosphatidylserine exposure during apoptosis reflects bidirectional trafficking between plasma membrane and cytoplasm. *Cell Death Differ.* 2013;20:64–76.
109. Verhoven B, Schlegel RA, Williamson P. Mechanisms of phosphatidylserine exposure, a phagocyte recognition signal, on apoptotic T lymphocytes. *J Exp Med.* 1995;182:1597–1601.
110. Wolfs JL, Comfurios P, Rasmussen JT, et al. Activated scramblase and inhibited aminophospholipid translocase cause phosphatidylserine exposure in a distinct platelet fraction. *Cell Mol Life Sci.* 2005;62:1514–1525.
111. Balasubramanian K, Mirnikjoo B, Schroit AJ. Regulated externalization of phosphatidylserine at the cell surface: implications for apoptosis. *J Biol Chem.* 2007;282:18357–18364.
112. Hankins HM, Baldrige RD, Xu P, Graham TR. Role of flippases, scramblases and transfer proteins in phosphatidylserine subcellular distribution. *Traffic.* 2015;16:35–47.
113. Aussel C, Pelassy C, Breittmayer JP. CD95 (Fas/APO-1) induces an increased phosphatidylserine synthesis that precedes its externalization during programmed cell death. *FEBS Lett.* 1998;431:195–199.
114. Yu A, McMaster CR, Byers DM, Ridgway ND, Cook HW. Stimulation of phosphatidylserine biosynthesis and facilitation of UV-induced apoptosis in Chinese hamster ovary cells overexpressing phospholipid scramblase 1. *J Biol Chem.* 2003;278:9706–9714.
115. Elliott JI, Sardini A, Cooper JC, et al. Phosphatidylserine exposure in B lymphocytes: a role for lipid packing. *Blood.* 2006;108:1611–1617.



116. Suzuki J, Umeda M, Sims PJ, Nagata S. Calcium-dependent phospholipid scrambling by TMEM16F. *Nature*. 2010;468:834–838.
117. Bevers EM, Williamson PL. Phospholipid scramblase: an update. *FEBS Lett*. 2010;584:2724–2730.
118. Pomorski T, Holthuis JC, Herrmann A, van Meer G. Tracking down lipid flippases and their biological functions. *J Cell Sci*. 2004;117:805–813.
119. Tang X, Halleck MS, Schlegel RA, Williamson P. A subfamily of P-type ATPases with aminophospholipid transporting activity. *Science*. 1996;272:1495–1497.
120. Borisenko GG, Matsura T, Liu SX, et al. Macrophage recognition of externalized phosphatidylserine and phagocytosis of apoptotic Jurkat cells: existence of a threshold. *Arch Biochem Biophys*. 2003;413:41–52.
121. Kenis H, Zandbergen HR, Hofstra L, et al. Annexin A5 uptake in ischemic myocardium: demonstration of reversible phosphatidylserine externalization and feasibility of radionuclide imaging. *J Nucl Med*. 2010;51:259–267.
122. Mandal D, Mazumder A, Das P, Kundu M, Basu J. Fas-, caspase 8-, and caspase 3-dependent signaling regulates the activity of the aminophospholipid translocase and phosphatidylserine externalization in human erythrocytes. *J Biol Chem*. 2005;280:39460–39467.
123. Nagata S, Hanayama R, Kawane K. Autoimmunity and the clearance of dead cells. *Cell*. 2010;140:619–630.
124. Zang Y, Beard RL, Chandraratna RA, Kang JX. Evidence of a lysosomal pathway for apoptosis induced by the synthetic retinoid CD437 in human leukemia HL-60 cells. *Cell Death Differ*. 2001;8:477–485.
125. Bratton DL, Fadok VA, Richter DA, Kailey JM, Guthrie LA, Henson PM. Appearance of phosphatidylserine on apoptotic cells requires calcium-mediated nonspecific flip-flop and is enhanced by loss of the aminophospholipid translocase. *J Biol Chem*. 1997;272:26159–26165.
126. Martinez MC, Freyssinet JM. Deciphering the plasma membrane hallmarks of apoptotic cells: phosphatidylserine transverse redistribution and calcium entry. *BMC Cell Biol*. 2001;2:20.
127. Arachiche A, Kerbiriou-Nabias D, Garcin I, Letellier T, Dachary-Prigent J. Rapid procoagulant phosphatidylserine exposure relies on high cytosolic calcium rather than on mitochondrial depolarization. *Arterioscler Thromb Vasc Biol*. 2009;29:1883–1889.
128. Mirnikjoo B, Balasubramanian K, Schroit AJ. Mobilization of lysosomal calcium regulates the externalization of phosphatidylserine during apoptosis. *J Biol Chem*. 2009;284:6918–6923.
129. Daleke DL, Huestis WH, Newton AC. Protein kinase C as a measure of transbilayer phosphatidylserine asymmetry. *Anal Biochem*. 1994;217:33–40.
130. de Jong K, Rettig MP, Low PS, Kuypers FA. Protein kinase C activation induces phosphatidylserine exposure on red blood cells. *Biochemistry*. 2002;41:12562–12567.
131. Suzuki J, Denning DP, Imanishi E, Horvitz HR, Nagata S. Xk-related protein 8 and CED-8 promote phosphatidylserine exposure in apoptotic cells. *Science*. 2013;341:403–406.
132. Segawa K, Suzuki J, Nagata S. Flippases and scramblases in the plasma membrane. *Cell Cycle*. 2014;13:2990–2991.
133. Segawa K, Suzuki J, Nagata S. Constitutive exposure of phosphatidylserine on viable cells. *Proc Natl Acad Sci U S A*. 2011;108:19246–19251.
134. Simhadri VR, Andersen JF, Calvo E, Choi SC, Coligan JE, Borrego F. Human CD300a binds to phosphatidylethanolamine and phosphatidylserine, and modulates the phagocytosis of dead cells. *Blood*. 2012;119:2799–2809.
135. Borrego F. The CD300 molecules: an emerging family of regulators of the immune system. *Blood*. 2013;121:1951–1960.
136. Hammill AK, Uhr JW, Scheuermann RH. Annexin V staining due to loss of membrane asymmetry can be reversible and precede commitment to apoptotic death. *Exp Cell Res*. 1999;251:16–21.
137. Martin S, Pombo I, Poncet P, David B, Arock M, Blank U. Immunologic stimulation of mast cells leads to the reversible exposure of phosphatidylserine in the absence of apoptosis. *Int Arch Allergy Immunol*. 2000;123:249–258.
138. Bevers EM, Comfurius P, Dekkers DW, Zwaal RF. Lipid translocation across the plasma membrane of mammalian cells. *Biochim Biophys Acta*. 1999;1439:317–330.
139. Bortner CD, Gomez-Angelats M, Cidlowski JA. Plasma membrane depolarization without repolarization is an early molecular event in anti-Fas-induced apoptosis. *J Biol Chem*. 2001;276:4304–4314.
140. Nishi T, Forgac M. The vacuolar (H<sup>+</sup>)-ATPases—nature's most versatile proton pumps. *Nat Rev Mol Cell Biol*. 2002;3:94–103.
141. Strasser B, Iwaszkiewicz J, Michielin O, Mayer A. The V-ATPase proteolipid cylinder promotes the lipid-mixing stage of SNARE-dependent fusion of yeast vacuoles. *EMBO J*. 2011;30:4126–4141.

142. Counis MF, Torriglia A. Acid DNases and their interest among apoptotic endonucleases. *Biochimie*. 2006;88:1851–1858.
143. Dussmann H, Rehm M, Kogel D, Prehn JH. Outer mitochondrial membrane permeabilization during apoptosis triggers caspase-independent mitochondrial and caspase-dependent plasma membrane potential depolarization: a single-cell analysis. *J Cell Sci*. 2003;116:525–536.
144. Rizzuto R, Marchi S, Bonora M, et al. Ca(2+) transfer from the ER to mitochondria: when, how and why. *Biochim Biophys Acta*. 2009;1787:1342–1351.
145. Gogvadze V, Orrenius S. Mitochondrial regulation of apoptotic cell death. *Chem Biol Interact*. 2006;163:4–14.
146. Wang C, Youle RJ. The role of mitochondria in apoptosis. *Annu Rev Genet*. 2009;43:95–118.
147. Kroemer G. The pharmacology of T cell apoptosis. *Adv Immunol*. 1995;58:211–296.
148. Lindsay J, Esposti MD, Gilmore AP. Bcl-2 proteins and mitochondria: specificity in membrane targeting for death. *Biochim Biophys Acta*. 2011;1813:532–539.
149. White RJ, Reynolds JJ. Mitochondrial depolarization in glutamate-stimulated neurons: an early signal specific to excitotoxin exposure. *J Neurosci*. 1996;16:5688–5697.
150. Perry SW, Norman JP, Litzburg A, Zhang D, Dewhurst S, Gelbard HA. HIV-1 transactivator of transcription protein induces mitochondrial hyperpolarization and synaptic stress leading to apoptosis. *J Immunol*. 2005;174:4333–4344.
151. Yang J, Liu X, Bhalla K, et al. Prevention of apoptosis by Bcl-2: release of cytochrome c from mitochondria blocked. *Science*. 1997;275:1129–1132.
152. Crawford ED, Wells JA. Caspase substrates and cellular remodeling. *Annu Rev Biochem*. 2011;80:1055–1087.
153. Arntzen MO, Thiede B. ApoptoProteomics, an integrated database for analysis of proteomics data obtained from apoptotic cells. *Mol Cell Proteomics*. 2012;11. <https://doi.org/10.1074/mcp.M111.010447>
154. Chang HY, Yang X. Proteases for cell suicide: functions and regulation of caspases. *Microbiol Mol Biol Rev*. 2000;64:821–846.
155. Rosado JA, Lopez JJ, Gomez-Arteta E, Redondo PC, Salido GM, Pariente JA. Early caspase-3 activation independent of apoptosis is required for cellular function. *J Cell Physiol*. 2006;209:142–152.
156. Julien O, Wells JA. Caspases and their substrates. *Cell Death Differ*. 2017;24:1380–1389.
157. Poreba M, Strozky A, Salvesen GS, Drag M. Caspase substrates and inhibitors. *Cold Spring Harb Perspect Biol*. 2013;5:a008680.
158. Sanchez-Osuna M, Yuste VJ. AChE for DNA degradation. *Cell Res*. 2015;25:653–654.
159. Errami Y, Naura AS, Kim H, et al. Apoptotic DNA fragmentation may be a cooperative activity between caspase-activated deoxyribonuclease and the poly(ADP-ribose) polymerase-regulated DNAS1L3, an endoplasmic reticulum-localized endonuclease that translocates to the nucleus during apoptosis. *J Biol Chem*. 2013;288:3460–3468.
160. Widlak P, Li LY, Wang X, Garrard WT. Action of recombinant human apoptotic endonuclease G on naked DNA and chromatin substrates: cooperation with exonuclease and DNase I. *J Biol Chem*. 2001;276:48404–48409.
161. Widlak P, Garrard WT. Discovery, regulation, and action of the major apoptotic nucleases DFF40/CAD and endonuclease G. *J Cell Biochem*. 2005;94:1078–1087.
162. Fulda S, Debatin KM. Extrinsic versus intrinsic apoptosis pathways in anticancer chemotherapy. *Oncogene*. 2006;25:4798–4811.
163. Akematsu T, Pearlman RE, Endoh H. Gigantic macroautophagy in programmed nuclear death of *Tetrahymena thermophila*. *Autophagy*. 2010;6:901–911.
164. Zhdanov DD, Fahmi T, Wang X, et al. Regulation of apoptotic endonucleases by EndoG. *DNA Cell Biol*. 2015;34:316–326.
165. Scovassi AI, Torriglia A. Activation of DNA-degrading enzymes during apoptosis. *Eur J Histochem*. 2003;47:185–194.
166. Gavrieli Y, Sherman Y, Ben-Sasson SA. Identification of programmed cell death in situ via specific labeling of nuclear DNA fragmentation. *J Cell Biol*. 1992;119:493–501.
167. Emoto K, Kobayashi T, Yamaji A, et al. Redistribution of phosphatidylethanolamine at the cleavage furrow of dividing cells during cytokinesis. *Proc Natl Acad Sci U S A*. 1996;93:12867–12872.
168. Nakamura S, Racker E. Inhibitory effect of duramycin on partial reactions catalyzed by (Na+,K+)-adenosinetriphosphatase from dog kidney. *Biochemistry*. 1984;23:385–389.
169. Hayashi F, Nagashima K, Terui Y, Kawamura Y, Matsumoto K, Itazaki H. The structure of PA48009: the revised structure of duramycin. *J Antibiot (Tokyo)*. 1990;43:1421–1430.
170. Navarro J, Chabot J, Sherrill K, Aneja R, Zahler SA, Racker E. Interaction of duramycin with artificial and natural membranes. *Biochemistry*. 1985;24:4645–4650.

171. Zhao M, Li Z, Bugenhagen S.  $^{99m}\text{Tc}$ -labeled duramycin as a novel phosphatidylethanolamine-binding molecular probe. *J Nucl Med.* 2008;49:1345–1352.
172. Iwamoto K, Hayakawa T, Murate M, et al. Curvature-dependent recognition of ethanolamine phospholipids by duramycin and cinnamycin. *Biophys J.* 2007;93:1608–1619.
173. Boucrot E, Pick A, Camdere G, et al. Membrane fission is promoted by insertion of amphipathic helices and is restricted by crescent BAR domains. *Cell.* 2012;149:124–136.
174. Bohn H. Placental and pregnancy proteins. In: Lehman FG, ed. *Carcino-Embryonic Proteins*. Amsterdam, the Netherlands: Elsevier-North Holland Biomedical Press; 1979:289–299.
175. Boersma HH, Kietselaer BL, Stolk LM, et al. Past, present, and future of Annexin A5: from protein discovery to clinical applications. *J Nucl Med.* 2005;46:2035–2050.
176. Reutelingsperger CP, Hornstra G, Hemker HC. Isolation and partial purification of a novel anticoagulant from arteries of human umbilical cord. *Eur J Biochem.* 1985;151:625–629.
177. Stuart MC, Reutelingsperger CP, Frederik PM. Binding of Annexin V to bilayers with various phospholipid compositions using glass beads in a flow cytometer. *Cytometry.* 1998;33:414–419.
178. Balasubramanian K, Bevers EM, Willems GM, Schroit AJ. Binding of Annexin V to membrane products of lipid peroxidation. *Biochemistry.* 2001;40:8672–8676.
179. Wen Y, Edelman JL, Kang T, Sachs G. Lipocortin V may function as a signaling protein for vascular endothelial growth factor receptor-2/Flk-1. *Biochem Biophys Res Commun.* 1999;258:713–721.
180. Andersen MH, Berglund L, Petersen TE, Rasmussen JT. Annexin-V binds to the intracellular part of the beta(5) integrin receptor subunit. *Biochem Biophys Res Commun.* 2002;292:550–557.
181. Kartachova MS, Verheij M, van Eck BL, Hoefnagel CA, Olmos RA. Radionuclide imaging of apoptosis in malignancies: promise and pitfalls of TC-hyinc-RH-Annexin V imaging. *Clin Med Oncol.* 2008;2:319–325.
182. Grosse J, Grimm D, Westphal K, et al. Radiolabeled Annexin V for imaging apoptosis in irradiated human follicular thyroid carcinomas: is an individualized protocol necessary? *Nucl Med Biol.* 2009;36:89–98.
183. Yang TJ, Haimovitz-Friedman A, Verheij M. Anticancer therapy and apoptosis imaging. *Exp Oncol.* 2012;34:269–276.
184. Blankenberg F. To scan or not to scan, it is a question of timing: technetium- $^{99m}$ -Annexin V radionuclide imaging assessment of treatment efficacy after one course of chemotherapy. *Clin Cancer Res.* 2002;8:2757–2758.
185. Hongli Y, Shuhan S, Ruiwen C, Yingjun G. Cloning and functional identification of a novel annexin subfamily in *Cysticercus cellulosae*. *Mol Biochem Parasitol.* 2002;119:1–5.
186. Koulov AV, Stucker KA, Lakshmi C, Robinson JP, Smith BD. Detection of apoptotic cells using a synthetic fluorescent sensor for membrane surfaces that contain phosphatidylserine. *Cell Death Differ.* 2003;10:1357–1359.
187. Hanshaw RG, Lakshmi C, Lambert TN, Johnson JR, Smith BD. Fluorescent detection of apoptotic cells by using zinc coordination complexes with a selective affinity for membrane surfaces enriched with phosphatidylserine. *ChemBioChem.* 2005;6:2214–2220.
188. Quinti L, Weissleder R, Tung CH. A fluorescent nanosensor for apoptotic cells. *Nano Lett.* 2006;6:488–490.
189. Hanshaw RG, Smith BD. New reagents for phosphatidylserine recognition and detection of apoptosis. *Bioorg Med Chem.* 2005;13:5035–5042.
190. Smith BA, Akers WJ, Leevy WM, et al. Optical imaging of mammary and prostate tumors in living animals using a synthetic near infrared zinc(II)-dipicolylamine probe for anionic cell surfaces. *J Am Chem Soc.* 2010;132:67–69.
191. Leevy WM, Johnson JR, Lakshmi C, Morris J, Marquez M, Smith BD. Selective recognition of bacterial membranes by zinc(II)-coordination complexes. *Chem Commun (Camb).* 2006:1595–1597.
192. Leevy WM, Gammon ST, Johnson JR, et al. Noninvasive optical imaging of *Staphylococcus aureus* bacterial infection in living mice using a Bis-dipicolylamine-Zinc(II) affinity group conjugated to a near-infrared fluorophore. *Bioconjug Chem.* 2008;19:686–692.
193. Liu X, Cheng D, Gray BD, et al. Radiolabeled Zn-DPA as a potential infection imaging agent. *Nucl Med Biol.* 2012;39:709–714.
194. Wyffels L, Gray BD, Barber C, et al. Synthesis and preliminary evaluation of radiolabeled bis(zinc(II)-dipicolylamine) coordination complexes as cell death imaging agents. *Bioorg Med Chem.* 2011;19:3425–3433.
195. Chen K, Yap LP, Park R, Gray B, Pak K, Conti P. Evaluation of  $^{64}\text{Cu}$ -labeled dipicolylamine (DPA) as a small-molecule PET probe for in vivo imaging of phosphatidylserine exposure. *J Nucl Med.* 2011;52:1502.
196. Wang H, Tang X, Tang G, et al. Noninvasive positron emission tomography imaging of cell death using a novel small-molecule probe, (18)F labeled bis(zinc(II)-dipicolylamine) complex. *Apoptosis.* 2013;18:1017–1027.

197. Brose N, Petrenko AG, Sudhof TC, Jahn R. Synaptotagmin: a calcium sensor on the synaptic vesicle surface. *Science*. 1992;256:1021–1025.
198. Davletov BA, Sudhof TC. A single C2 domain from synaptotagmin I is sufficient for high affinity Ca<sup>2+</sup>/phospholipid binding. *J Biol Chem*. 1993;268:26386–26390.
199. Chapman ER, Jahn R. Calcium-dependent interaction of the cytoplasmic region of synaptotagmin with membranes. Autonomous function of a single C2-homologous domain. *J Biol Chem*. 1994;269:5735–5741.
200. Fukuda M, Aruga J, Niinobe M, Aimoto S, Mikoshiba K. Inositol-1,3,4,5-tetrakisphosphate binding to C2B domain of IP4BP/synaptotagmin II. *J Biol Chem*. 1994;269:29206–29211.
201. Alam IS, Neves AA, Witney TH, Boren J, Brindle KM. Comparison of the C2A domain of synaptotagmin-I and Annexin-V as probes for detecting cell death. *Bioconjug Chem*. 2010;21:884–891.
202. Wang F, Fang W, Zhang MR, et al. Evaluation of chemotherapy response in VX2 rabbit lung cancer with 18F-labeled C2A domain of synaptotagmin I. *J Nucl Med*. 2011;52:592–599.
203. Fang W, Wang F, Ji S, et al. SPECT imaging of myocardial infarction using 99mTc-labeled C2A domain of synaptotagmin I in a porcine ischemia-reperfusion model. *Nucl Med Biol*. 2007;34:917–923.
204. Neves AA, Xie B, Fawcett S, et al. Rapid imaging of tumor cell death in vivo using the C2A domain of Synaptotagmin-I. *J Nucl Med*. 2017;58:881–887.
205. Raymond A, Ensslin MA, Shur BD. SED1/MFG-E8: a bi-motif protein that orchestrates diverse cellular interactions. *J Cell Biochem*. 2009;106:957–966.
206. Hou J, Fu Y, Zhou J, et al. Lactadherin functions as a probe for phosphatidylserine exposure and as an anticoagulant in the study of stored platelets. *Vox Sang*. 2011;100:187–195.
207. Andersen MH, Graversen H, Fedosov SN, Petersen TE, Rasmussen JT. Functional analyses of two cellular binding domains of bovine lactadherin. *Biochemistry*. 2000;39:6200–6206.
208. Shi J, Heegaard CW, Rasmussen JT, Gilbert GE. Lactadherin binds selectively to membranes containing phosphatidyl-L-serine and increased curvature. *Biochim Biophys Acta*. 2004;1667:82–90.
209. Lin L, Huai Q, Huang M, Furie B, Furie BC. Crystal structure of the bovine lactadherin C2 domain, a membrane binding motif, shows similarity to the C2 domains of factor V and factor VIII. *J Mol Biol*. 2007;371:717–724.
210. Shao C, Novakovic VA, Head JF, Seaton BA, Gilbert GE. Crystal structure of lactadherin C2 domain at 1.7Å resolution with mutational and computational analyses of its membrane-binding motif. *J Biol Chem*. 2008;283:7230–7241.
211. Dasgupta SK, Guchhait P, Thiagarajan P. Lactadherin binding and phosphatidylserine expression on cell surface—comparison with Annexin A5. *Transl Res*. 2006;148:19–25.
212. Waehrens LN, Rasmussen JT, Heegaard CW, Falborg L. Preparation and in vitro evaluation of 99mTc-labelled bovine lactadherin as a novel radioligand for apoptosis detection. *J Labelled Comp Radiopharm*. 2007;50:211–217.
213. Shi J, Shi Y, Waehrens LN, Rasmussen JT, Heegaard CW, Gilbert GE. Lactadherin detects early phosphatidylserine exposure on immortalized leukemia cells undergoing programmed cell death. *Cytometry A*. 2006;69:1193–1201.
214. Hu T, Shi J, Jiao X, Zhou J, Yin X. Measurement of Annexin V uptake and lactadherin labeling for the quantification of apoptosis in adherent Tca8113 and ACC-2 cells. *Braz J Med Biol Res*. 2008;41:750–757.
215. Igarashi K, Kaneda M, Yamaji A, et al. A novel phosphatidylserine-binding peptide motif defined by an anti-idiotypic monoclonal antibody. Localization of phosphatidylserine-specific binding sites on protein kinase C and phosphatidylserine decarboxylase. *J Biol Chem*. 1995;270:29075–29078.
216. Laumonier C, Segers J, Laurent S, et al. A new peptidic vector for molecular imaging of apoptosis, identified by phage display technology. *J Biomol Screen*. 2006;11:537–545.
217. Segers J, Laumonier C, Burtea C, Laurent S, Elst LV, Muller RN. From phage display to magnetophage, a new tool for magnetic resonance molecular imaging. *Bioconjug Chem*. 2007;18:1251–1258.
218. Perreault A, Richter S, Bergman C, Wuest M, Wuest F. Targeting phosphatidylserine with a 64Cu-labeled peptide for molecular imaging of apoptosis. *Mol Pharm*. 2016;13:3564–3577.
219. Kapyt J, Banman S, Goping IS, Mercer JR. Evaluation of phosphatidylserine-binding peptides targeting apoptotic cells. *J Biomol Screen*. 2012;17:1293–1301.
220. Wuest M, Perreault A, Kapyt J, et al. Radiopharmacological evaluation of (18)F-labeled phosphatidylserine-binding peptides for molecular imaging of apoptosis. *Nucl Med Biol*. 2015;42:864–874.
221. Shao R, Xiong C, Wen X, Gelovani JG, Li C. Targeting phosphatidylserine on apoptotic cells with phages and peptides selected from a bacteriophage display library. *Mol Imaging*. 2007;6:417–426.

222. Luster TA, He J, Huang X, et al. Plasma protein beta-2-glycoprotein 1 mediates interaction between the anti-tumor monoclonal antibody 3G4 and anionic phospholipids on endothelial cells. *J Biol Chem*. 2006;281:29863–29871.
223. Huang X, Bennett M, Thorpe PE. A monoclonal antibody that binds anionic phospholipids on tumor blood vessels enhances the antitumor effect of docetaxel on human breast tumors in mice. *Cancer Res*. 2005;65:4408–4416.
224. He J, Luster TA, Thorpe PE. Radiation-enhanced vascular targeting of human lung cancers in mice with a monoclonal antibody that binds anionic phospholipids. *Clin Cancer Res*. 2007;13:5211–5218.
225. He J, Yin Y, Luster TA, Watkins L, Thorpe PE. Antiphosphatidylserine antibody combined with irradiation damages tumor blood vessels and induces tumor immunity in a rat model of glioblastoma. *Clin Cancer Res*. 2009;15:6871–6880.
226. Jennewein M, Lewis MA, Zhao D, et al. Vascular imaging of solid tumors in rats with a radioactive arsenic-labeled antibody that binds exposed phosphatidylserine. *Clin Cancer Res*. 2008;14:1377–1385.
227. Gong J, Archer R, Brown M, et al. Measuring response to therapy by near-infrared imaging of tumors using a phosphatidylserine-targeting antibody fragment. *Mol Imaging*. 2013;12:244–256.
228. Huang X, Ye D, Luster T, Thorpe PE. Phosphatidylserine-targeting “betabodies” for the treatment of cancer. *Cancer Res*. 2012;72:4632.
229. Grimberg H, Levin G, Shirvan A, et al. Monitoring of tumor response to chemotherapy in vivo by a novel small-molecule detector of apoptosis. *Apoptosis*. 2009;14:257–267.
230. Reshef A, Shirvan A, Waterhouse RN, et al. Molecular imaging of neurovascular cell death in experimental cerebral stroke by PET. *J Nucl Med*. 2008;49:1520–1528.
231. Damianovich M, Ziv I, Heyman SN, et al. ApoSense: a novel technology for functional molecular imaging of cell death in models of acute renal tubular necrosis. *Eur J Nucl Med Mol Imaging*. 2006;33:281–291.
232. Cohen A, Shirvan A, Levin G, Grimberg H, Reshef A, Ziv I. From the Gla domain to a novel small-molecule detector of apoptosis. *Cell Res*. 2009;19:625–637.
233. Bauwens M, De Saint-Hubert M, Cleynhens J, et al. Radioiodinated phenylalkyl malonic acid derivatives as pH-sensitive SPECT tracers. *PLoS One*. 2012;7:e38428.
234. Madar I, Ravert H, Nelkin B, et al. Characterization of membrane potential-dependent uptake of the novel PET tracer 18F-fluorobenzyl triphenylphosphonium cation. *Eur J Nucl Med Mol Imaging*. 2007;34:2057–2065.
235. Madar I, Huang Y, Ravert H, et al. Detection and quantification of the evolution dynamics of apoptosis using the PET voltage sensor 18F-fluorobenzyl triphenyl phosphonium. *J Nucl Med*. 2009;50:774–780.
236. Higuchi T, Fukushima K, Rischpler C, et al. Stable delineation of the ischemic area by the PET perfusion tracer 18F-fluorobenzyl triphenyl phosphonium after transient coronary occlusion. *J Nucl Med*. 2011;52:965–969.
237. Tait JF. Imaging of apoptosis. *J Nucl Med*. 2008;49:1573–1576.
238. Madar I, Weiss L, Izbicki G. Preferential accumulation of (3)H-tetraphenylphosphonium in non-small cell lung carcinoma in mice: comparison with (99m)Tc-MIBI. *J Nucl Med*. 2002;43:234–238.
239. Min JJ, Biswal S, Deroose C, Gambhir SS. Tetraphenylphosphonium as a novel molecular probe for imaging tumors. *J Nucl Med*. 2004;45:636–643.
240. Gurm GS, Danik SB, Shoup TM, et al. 4-[18F]-tetraphenylphosphonium as a PET tracer for myocardial mitochondrial membrane potential. *JACC Cardiovasc Imaging*. 2012;5:285–292.
241. Kim DY, Kim HS, Le UN, et al. Evaluation of a mitochondrial voltage sensor, (18F-fluoropentyl)triphenylphosphonium cation, in a rat myocardial infarction model. *J Nucl Med*. 2012;53:1779–1785.
242. Tominaga T, Ito H, Ishikawa Y, Iwata R, Ishiwata K, Furumoto S. Radiosynthesis and preliminary biological evaluation of a new (18)F-labeled triethylene glycol derivative of triphenylphosphonium. *J Labelled Comp Radiopharm*. 2016;59:117–123.
243. Vergote J, Di BM, Moretti JL, et al. Could 99mTc-MIBI be used to visualize the apoptotic MCF7 human breast cancer cells? *Cell Mol Biol (Noisy-le-grand)*. 2001;47:467–471.
244. Zhu X, Wu H, Xia J, Zhao M, Xianyu Z. The relationship between (99m)Tc-MIBI uptakes and tumor cell death/proliferation state under irradiation. *Cancer Lett*. 2002;182:217–222.
245. Chen DL, Zhou D, Chu W, et al. Radiolabeled isatin binding to caspase-3 activation induced by anti-Fas antibody. *Nucl Med Biol*. 2012;39:137–144.
246. Kolb H, Szardenings K, Mocharla V, et al. Preclinical evaluation of 18F-CP18, a substrate-based apoptosis imaging agent, in various apoptotic tissues. *Eur J Nucl Med Mol Imaging*. 2011;38:S183.
247. Kolb H, Walsh J, Gangadharmath U, Mu F, Mocharla V, Chaudhary A. Synthesis of an 18F-labeled CP18 peptide as a potential apoptosis biomarker in PET imaging. *J Nucl Med*. 2011;52:1430.

248. Kolb H, Walsh J, Mocharla V, Liang Q, Zhao T, Gomez F. 18F-CP18: a novel DEVD containing peptide substrate for imaging apoptosis via caspase-3 activity. *J Nucl Med*. 2011;52:350.
249. Blum G, Weimer RM, Edgington LE, Adams W, Bogyo M. Comparative assessment of substrates and activity based probes as tools for non-invasive optical imaging of cysteine protease activity. *PLoS One*. 2009;4:e6374.
250. Blum G, von Degenfeld G, Merchant MJ, Blau HM, Bogyo M. Noninvasive optical imaging of cysteine protease activity using fluorescently quenched activity-based probes. *Nat Chem Biol*. 2007;3:668–677.
251. Garcia-Calvo M, Peterson EP, Leiting B, Ruel R, Nicholson DW, Thornberry NA. Inhibition of human caspases by peptide-based and macromolecular inhibitors. *J Biol Chem*. 1998;273:32608–32613.
252. Thimister PW, Hofstra L, Liem IH, et al. In vivo detection of cell death in the area at risk in acute myocardial infarction. *J Nucl Med*. 2003;44:391–396.
253. Lahorte CM, Vanderheyden JL, Steinmetz N, Van de Wiele C, Dierckx RA, Slegers G. Apoptosis-detecting radioligands: current state of the art and future perspectives. *Eur J Nucl Med Mol Imaging*. 2004;31:887–919.
254. Lee D, Long SA, Murray JH, et al. Potent and selective nonpeptide inhibitors of caspases 3 and 7. *J Med Chem*. 2001;44:2015–2026.
255. Bauer C, Bauder-Wuest U, Mier W, Haberkorn U, Eisenhut M. 131I-labeled peptides as caspase substrates for apoptosis imaging. *J Nucl Med*. 2005;46:1066–1074.
256. Shen B, Jeon J, Palner M, et al. Positron emission tomography imaging of drug-induced tumor apoptosis with a caspase-triggered nanoaggregation probe. *Angew Chem Int Ed Engl*. 2013;52:10511–10514.
257. Witney TH, Hoehne A, Reeves RE, et al. A systematic comparison of 18F-c-snat to established radiotracer imaging agents for the detection of tumor response to treatment. *Clin Cancer Res*. 2015;21:3896–3905.
258. Palner M, Shen B, Jeon J, Lin J, Chin FT, Rao J. Preclinical kinetic analysis of the caspase-3/7 pet tracer 18F-c-snat: quantifying the changes in blood flow and tumor retention after chemotherapy. *J Nucl Med*. 2015;56:1415–1421.
259. Vickers CJ, Gonzalez-Paez GE, Wolan DW. Discovery of a highly selective caspase-3 substrate for imaging live cells. *ACS Chem Biol*. 2014;9:2199–2203.
260. Vickers CJ, Gonzalez-Paez GE, Litwin KM, Umotoy JC, Coutusias EA, Wolan DW. Selective inhibition of initiator versus executioner caspases using small peptides containing unnatural amino acids. *ACS Chem Biol*. 2014;9:2194–2198.
261. Vickers CJ, Gonzalez-Paez GE, Wolan DW. Selective detection and inhibition of active caspase-3 in cells with optimized peptides. *J Am Chem Soc*. 2013;135:12869–12876.
262. Vickers CJ, Gonzalez-Paez GE, Wolan DW. Selective detection of caspase-3 versus caspase-7 using activity-based probes with key unnatural amino acids. *ACS Chem Biol*. 2013;8:1558–1566.
263. Knight JC, Koustoulidou S, Cornelissen B. Imaging the DNA damage response with PET and SPECT. *Eur J Nucl Med Mol Imaging*. 2017;44:1065–1078.
264. Wang K, Purushotham S, Lee JY, et al. In vivo imaging of tumor apoptosis using histone H1-targeting peptide. *J Control Release*. 2010;148:283–291.
265. Ayukawa K, Taniguchi S, Masumoto J, et al. La autoantigen is cleaved in the COOH terminus and loses the nuclear localization signal during apoptosis. *J Biol Chem*. 2000;275:34465–34470.
266. Neufing PJ, Clancy RM, Jackson MW, Tran HB, Buyon JP, Gordon TP. Exposure and binding of selected immunodominant La/SSB epitopes on human apoptotic cells. *Arthritis Rheum*. 2005;52:3934–3942.
267. Al-Ejeh F, Darby JM, Brown MP. The La autoantigen is a malignancy-associated cell death target that is induced by DNA-damaging drugs. *Clin Cancer Res*. 2007;13:5509s–5518s.
268. Yaoita H, Uehara T, Brownell AL, et al. Localization of technetium-99m-glucarate in zones of acute cerebral injury. *J Nucl Med*. 1991;32:272–278.
269. Ohtani H, Callahan RJ, Khaw BA, Fishman AJ, Wilkinson RA, Strauss HW. Comparison of technetium-99m-glucarate and thallium-201 for the identification of acute myocardial infarction in rats. *J Nucl Med*. 1992;33:1988–1993.
270. Narula J, Petrov A, Pak KY, Lister BC, Khaw BA. Very early noninvasive detection of acute experimental nonreperfused myocardial infarction with 99mTc-labeled glucarate. *Circulation*. 1997;95:1577–1584.
271. Johnson LL, Schofield L, Mastrofrancesco P, Donahay T, Farb A, Khaw BA. Technetium-99m glucarate uptake in a swine model of limited flow plus increased demand. *J Nucl Cardiol*. 2000;7:590–598.
272. Liu Z, Barrett HH, Stevenson GD, et al. High-resolution imaging with (99m)Tc-glucarate for assessing myocardial injury in rat heart models exposed to different durations of ischemia with reperfusion. *J Nucl Med*. 2004;45:1251–1259.

273. Van de Putte M, Wang H, Chen F, de Witte PA, Ni Y. Hypericin as a marker for determination of tissue viability after intratumoral ethanol injection in a murine liver tumor model. *Acad Radiol.* 2008;15:107–113.
274. Van de Putte M, Wang H, Chen F, de Witte PA, Ni Y. Hypericin as a marker for determination of tissue viability after radiofrequency ablation in a murine liver tumor model. *Oncol Rep.* 2008;19:927–932.
275. Jiang C, Li Y, Jiang X, et al. Hypericin as a marker for determination of myocardial viability in a rat model of myocardial infarction. *Photochem Photobiol.* 2014;90:867–872.
276. Ni Y, Bormans G, Chen F, Verbruggen A, Marchal G. Necrosis avid contrast agents: functional similarity versus structural diversity. *Invest Radiol.* 2005;40:526–535.
277. Tietjen GT, Gong Z, Chen CH, et al. Molecular mechanism for differential recognition of membrane phosphatidylserine by the immune regulatory receptor Tim4. *Proc Natl Acad Sci U S A.* 2014;111:E1463–E1472.
278. Bevers EM, Williamson PL. Getting to the outer leaflet: physiology of phosphatidylserine exposure at the plasma membrane. *Physiol Rev.* 2016;96:605–645.
279. He M, Kubo H, Morimoto K, et al. Receptor for advanced glycation end products binds to phosphatidylserine and assists in the clearance of apoptotic cells. *EMBO Rep.* 2011;12:358–364.
280. Rufo N, Garg AD, Agostinis P. The unfolded protein response in immunogenic cell death and cancer immunotherapy. *Trends Cancer.* 2017;3:643–658.
281. Larimer BM, Wehrenberg-Klee E, Dubois F, et al. Granzyme B PET imaging as a predictive biomarker of immunotherapy response. *Cancer Res.* 2017;77:2318–2327.
282. Palchaudhuri R, Lambrecht MJ, Botham RC, et al. A small molecule that induces intrinsic pathway apoptosis with unparalleled speed. *Cell Rep.* 2015;13:2027–2036.
283. Liu G, Zou H, Luo T, et al. Caspase-dependent and caspase-independent pathways are involved in cadmium-induced apoptosis in primary rat proximal tubular cell culture. *PLoS One.* 2016;11:e0166823.
284. Fombonne J, Bissey PA, Guix C, Sadoul R, Thibert C, Mehlen P. Patched dependence receptor triggers apoptosis through ubiquitination of caspase-9. *Proc Natl Acad Sci U S A.* 2012;109:10510–10515.
285. He S, Huang S, Shen Z. Biomarkers for the detection of necroptosis. *Cell Mol Life Sci.* 2016;73:2177–2181.
286. de Gassart A, Martinon F. Pyroptosis: caspase-11 unlocks the gates of death. *Immunity.* 2015;43:835–837.
287. Shi J, Zhao Y, Wang K, et al. Cleavage of GSDMD by inflammatory caspases determines pyroptotic cell death. *Nature.* 2015;526:660–665.
288. Vitale I, Galluzzi L, Castedo M, Kroemer G. Mitotic catastrophe: a mechanism for avoiding genomic instability. *Nat Rev Mol Cell Biol.* 2011;12:385–392.
289. Toledo L, Neelsen KJ, Lukas J. Replication catastrophe: when a checkpoint fails because of exhaustion. *Mol Cell.* 2017;66:735–749.
290. Girnius N, Davis RJ. JNK promotes epithelial cell anoikis by transcriptional and post-translational regulation of BH3-only proteins. *Cell Rep.* 2017;21:1910–1921.
291. Wang X, Lin G, Martins-Taylor K, Zeng H, Xu RH. Inhibition of caspase-mediated anoikis is critical for basic fibroblast growth factor-sustained culture of human pluripotent stem cells. *J Biol Chem.* 2009;284:34054–34064.
292. Eckhart L, Lippens S, Tschachler E, Declercq W. Cell death by cornification. *Biochim Biophys Acta.* 2013;1833:3471–3480.
293. Gupta AK, Giaglis S, Hasler P, Hahn S. Efficient neutrophil extracellular trap induction requires mobilization of both intracellular and extracellular calcium pools and is modulated by cyclosporine A. *PLoS One.* 2014;9:e97088.
294. Wang Y, An R, Umanah GK, et al. A nuclease that mediates cell death induced by DNA damage and poly(ADP-ribose) polymerase-1. *Science.* 2016;354. <https://doi.org/10.1126/science.aad6872>
295. Hamann JC, Surcel A, Chen R, et al. Entosis is induced by glucose starvation. *Cell Rep.* 2017;20:201–210.
296. Vanden Berghe T, Vanlangenakker N, Parthoens E, et al. Necroptosis, necrosis and secondary necrosis converge on similar cellular disintegration features. *Cell Death Differ.* 2010;17:922–930.
297. Peters AA, Jamaludin SYN, Yapa KTDS, et al. Oncosis and apoptosis induction by activation of an overexpressed ion channel in breast cancer cells. *Oncogene.* 2017;36:6490–6500.
298. Dixon SJ, Lemberg KM, Lamprecht MR, et al. Ferroptosis: an iron-dependent form of nonapoptotic cell death. *Cell.* 2012;149:1060–1072.
299. Machaidze G, Ziegler A, Seelig J. Specific binding of Ro 09–0198 (cinnamycin) to phosphatidylethanolamine: a thermodynamic analysis. *Biochemistry.* 2002;41:1965–1971.

300. Makino A, Baba T, Fujimoto K, et al. Cinnamycin (Ro 09-0198) promotes cell binding and toxicity by inducing transbilayer lipid movement. *J Biol Chem*. 2003;278:3204–3209.
301. Elvas F, Vangestel C, Rapic S, et al. Characterization of [(99m)Tc]Duramycin as a SPECT imaging agent for early assessment of tumor apoptosis. *Mol Imaging Biol*. 2015;17:838–847.
302. Elvas F, Vangestel C, Pak K, et al. Early prediction of tumor response to treatment: preclinical validation of 99mTc-Duramycin. *J Nucl Med*. 2016;57:805–811.
303. Luo R, Niu L, Qiu F, et al. Monitoring apoptosis of breast cancer xenograft after paclitaxel treatment with 99mTc-labeled duramycin SPECT/CT. *Mol Imaging*. 2016;15. <https://doi.org/10.1177/1536012115624918>
304. Elvas F, Boddaert J, Vangestel C, et al. 99mTc-Duramycin SPECT imaging of early tumor response to targeted therapy: a comparison with 18F-FDG PET. *J Nucl Med*. 2017;58:665–670.
305. Zhao M, Li Z. A single-step kit formulation for the (99m)Tc-labeling of HYNIC-Duramycin. *Nucl Med Biol*. 2012;39:1006–1011.
306. Yao S, Hu K, Tang G, et al. Positron emission tomography imaging of cell death with [(18)F]FPDduramycin. *Apoptosis*. 2014;19:841–850.
307. Tait JF, Gibson D, Fujikawa K. Phospholipid binding properties of human placental anticoagulant protein-I, a member of the lipocortin family. *J Biol Chem*. 1989;264:7944–7949.
308. Cao W, Huang J, Wu J, et al. Study of 99mTc-Annexin V uptake in apoptotic cell models of Parkinson's disease. *Nucl Med Commun*. 2007;28:895–901.
309. Blankenberg FG, Katsikis PD, Tait JF, et al. In vivo detection and imaging of phosphatidylserine expression during programmed cell death. *Proc Natl Acad Sci U S A*. 1998;95:6349–6354.
310. Mochizuki T, Kuge Y, Zhao S, et al. Detection of apoptotic tumor response in vivo after a single dose of chemotherapy with 99mTc-Annexin V. *J Nucl Med*. 2003;44:92–97.
311. Kim W, Yoon JH, Jeong JM, et al. Apoptosis-inducing antitumor efficacy of hexokinase II inhibitor in hepatocellular carcinoma. *Mol Cancer Ther*. 2007;6:2554–2562.
312. Wong E, Kumar V, Howman-Giles RB, Vanderheyden JL. Imaging of therapy-induced apoptosis using (99m)Tc-HYNIC-Annexin V in thymoma tumor-bearing mice. *Cancer Biother Radiopharm*. 2008;23:715–726.
313. Ohtsuki K, Akashi K, Aoka Y, et al. Technetium-99m HYNIC-Annexin V: a potential radiopharmaceutical for the in-vivo detection of apoptosis. *Eur J Nucl Med*. 1999;26:1251–1258.
314. Guo MF, Zhao Y, Tian R, et al. In vivo 99mTc-HYNIC-Annexin V imaging of early tumor apoptosis in mice after single dose irradiation. *J Exp Clin Cancer Res*. 2009;28:136.
315. Yang DJ, Azhdarinia A, Wu P, et al. In vivo and in vitro measurement of apoptosis in breast cancer cells using 99mTc-EC-Annexin V. *Cancer Biother Radiopharm*. 2001;16:73–83.
316. Takei T, Kuge Y, Zhao S, et al. Enhanced apoptotic reaction correlates with suppressed tumor glucose utilization after cytotoxic chemotherapy: use of 99mTc-Annexin V, 18F-FDG, and histologic evaluation. *J Nucl Med*. 2005;46:794–799.
317. Vangestel C, Van de Wiele C, Mees G, et al. Single-photon emission computed tomographic imaging of the early time course of therapy-induced cell death using technetium 99m tricarbonyl His-Annexin A5 in a colorectal cancer xenograft model. *Mol Imaging*. 2012;11:135–147.
318. Mandl SJ, Mari C, Edinger M, et al. Multi-modality imaging identifies key times for Annexin V imaging as an early predictor of therapeutic outcome. *Mol Imaging*. 2004;3:1–8.
319. Erba PA, Manfredi C, Lazzeri E, et al. Time course of Paclitaxel-induced apoptosis in an experimental model of virus-induced breast cancer. *J Nucl Med*. 2010;51:775–781.
320. Beekman CA, Buckle T, van Leeuwen AC, et al. Questioning the value of (99m)Tc-HYNIC-Annexin V based response monitoring after docetaxel treatment in a mouse model for hereditary breast cancer. *Appl Radiat Isot*. 2011;69:656–662.
321. Subbarayan M, Hafeli UO, Feyes DK, Unnithan J, Emancipator SN, Mukhtar H. A simplified method for preparation of 99mTc-Annexin V and its biologic evaluation for in vivo imaging of apoptosis after photodynamic therapy. *J Nucl Med*. 2003;44:650–656.
322. Wen X, Wu QP, Ke S, et al. Improved radiolabeling of PEGylated protein: pEGylated Annexin V for noninvasive imaging of tumor apoptosis. *Cancer Biother Radiopharm*. 2003;18:819–827.
323. Ke S, Wen X, Wu QP, et al. Imaging taxane-induced tumor apoptosis using PEGylated, 111In-labeled Annexin V. *J Nucl Med*. 2004;45:108–115.
324. Kratz H, Haeckel A, Michel R, et al. Straightforward thiol-mediated protein labelling with DTPA: synthesis of a highly active 111In-Annexin A5-DTPA tracer. *EJNMMI Res*. 2012;2:17.



325. van Tilborg GA, Mulder WJ, Deckers N, Storm G, Reutelingsperger CP, Strijkers GJ, Nicolay K. Annexin A5-functionalized bimodal lipid-based contrast agents for the detection of apoptosis. *Bioconjug Chem*. 2006;17:741–749.
326. Zhang R, Lu W, Wen X, et al. Annexin A5-conjugated polymeric micelles for dual SPECT and optical detection of apoptosis. *J Nucl Med*. 2011;52:958–964.
327. Belhocine T, Steinmetz N, Hustinx R, et al. Increased uptake of the apoptosis-imaging agent ( $^{99m}\text{Tc}$ ) recombinant human Annexin V in human tumors after one course of chemotherapy as a predictor of tumor response and patient prognosis. *Clin Cancer Res*. 2002;8:2766–2774.
328. Kartachova M, Haas RL, Olmos RA, Hoebbers FJ, van Zandwijk N, Verheij M. In vivo imaging of apoptosis by  $^{99m}\text{Tc}$ -Annexin V scintigraphy: visual analysis in relation to treatment response. *Radiother Oncol*. 2004;72:333–339.
329. Rottey S, Slegers G, Van Belle S, Goethals I, Van de Wiele C. Sequential  $^{99m}\text{Tc}$ -hydrazinonicotinamide-Annexin V imaging for predicting response to chemotherapy. *J Nucl Med*. 2006;47:1813–1818.
330. Kartachova M, van Zandwijk N, Burgers S, van Tinteren H, Verheij M, Valdes Olmos RA. Prognostic significance of  $^{99m}\text{Tc}$  HYNIC-rh-Annexin V scintigraphy during platinum-based chemotherapy in advanced lung cancer. *J Clin Oncol*. 2007;25:2534–2539.
331. Kartachova MS, Valdes Olmos RA, Haas RL, Hoebbers FJ, van Herk M, Verheij M.  $^{99m}\text{Tc}$ -HYNIC-rh-Annexin-V scintigraphy: visual and quantitative evaluation of early treatment-induced apoptosis to predict treatment outcome. *Nucl Med Commun*. 2008;29:39–44.
332. Rottey S, Loose D, Vakaet L, et al.  $^{99m}\text{Tc}$ -HYNIC Annexin-V imaging of tumors and its relationship to response to radiotherapy and/or chemotherapy. *Q J Nucl Med Mol Imaging*. 2007;51:182–188.
333. Loose D, Vermeersch H, De Vos F, Deron P, Slegers G, Van de Wiele C. Prognostic value of  $^{99m}\text{Tc}$ -HYNIC Annexin-V imaging in squamous cell carcinoma of the head and neck. *Eur J Nucl Med Mol Imaging*. 2008;35:47–52.
334. Vermeersch H, Loose D, Lahorte C, et al.  $^{99m}\text{Tc}$ -HYNIC Annexin-V imaging of primary head and neck carcinoma. *Nucl Med Commun*. 2004;25:259–263.
335. Van de Wiele C, Lahorte C, Vermeersch H, et al. Quantitative tumor apoptosis imaging using technetium- $^{99m}$ -HYNIC Annexin V single photon emission computed tomography. *J Clin Oncol*. 2003;21:3483–3487.
336. Vermeersch H, Mervillie K, Lahorte C, et al. Relationship of  $^{99m}\text{Tc}$ -HYNIC Annexin V uptake to microvessel density, FasL and MMP-9 expression, and the number of tumour-infiltrating lymphocytes in head and neck carcinoma. *Eur J Nucl Med Mol Imaging*. 2004;31:1016–1021.
337. Vermeersch H, Ham H, Rottey S, et al. Intraobserver, interobserver, and day-to-day reproducibility of quantitative  $^{99m}\text{Tc}$ -HYNIC Annexin-V imaging in head and neck carcinoma. *Cancer Biother Radiopharm*. 2004;19:205–210.
338. Biechlin ML, Bonmartin A, Gilly FN, Fraysse M, du Moulinet d'Hardemare A. Radiolabeling of Annexin A5 with ( $^{99m}\text{Tc}$ ): comparison of HYNIC-Tc vs. iminothiolane-Tc-tricarbonyl conjugates. *Nucl Med Biol*. 2008;35:679–687.
339. De Saint-Hubert M, Mottaghy FM, Vunckx K, et al. Site-specific labeling of 'second generation' Annexin V with  $^{99m}\text{Tc}(\text{CO})_3$  for improved imaging of apoptosis in vivo. *Bioorg Med Chem*. 2010;18:1356–1363.
340. Vangestel C, Peeters M, Oltenfreiter R, et al. In vitro and in vivo evaluation of [ $^{99m}\text{Tc}$ ]-labeled tricarbonyl His-Annexin A5 as an imaging agent for the detection of phosphatidylserine-expressing cells. *Nucl Med Biol*. 2010;37:965–975.
341. Vangestel C, Van de Wiele C, Van Damme N, et al. ( $^{99m}\text{Tc}$ )-(CO) $_3$  His-Annexin A5 micro-SPECT demonstrates increased cell death by irinotecan during the vascular normalization window caused by bevacizumab. *J Nucl Med*. 2011;52:1786–1794.
342. Lin KJ, Wu CC, Pan YH, et al. In vivo imaging of radiation-induced tissue apoptosis by ( $^{99m}\text{Tc}$ )-his (6)-Annexin A5. *Ann Nucl Med*. 2012;26:272–280.
343. Tait JF, Brown DS, Gibson DF, Blankenberg FG, Strauss HW. Development and characterization of Annexin V mutants with endogenous chelation sites for ( $^{99m}\text{Tc}$ ). *Bioconjug Chem*. 2000;11:918–925.
344. Mukherjee A, Kothari K, Toth G, et al.  $^{99m}\text{Tc}$ -labeled Annexin V fragments: a potential SPECT radiopharmaceutical for imaging cell death. *Nucl Med Biol*. 2006;33:635–643.
345. Tait JF, Smith C, Blankenberg FG. Structural requirements for in vivo detection of cell death with  $^{99m}\text{Tc}$ -Annexin V. *J Nucl Med*. 2005;46:807–815.
346. Fonge H, de Saint HM, Vunckx K, et al. Preliminary in vivo evaluation of a novel  $^{99m}\text{Tc}$ -labeled HYNIC-cys-Annexin A5 as an apoptosis imaging agent. *Bioorg Med Chem Lett*. 2008;18:3794–3798.
347. Greupink R, Sio CF, Ederveen A, Orsel J. Evaluation of a  $^{99m}\text{Tc}$ -labeled AnnexinA5 variant for non-invasive SPECT imaging of cell death in liver, spleen and prostate. *Pharm Res*. 2009;26:2647–2656.

348. Ye F, Fang W, Wang F, Hua ZC, Wang Z, Yang X. Evaluation of adenosine preconditioning with  $^{99m}\text{Tc}$ -His10-Annexin V in a porcine model of myocardium ischemia and reperfusion injury: preliminary study. *Nucl Med Biol.* 2011;38:567–574.
349. Lu C, Jiang Q, Hu M, et al. Preliminary biological evaluation of novel ( $^{99m}\text{Tc}$ )-Cys-Annexin A5 as a apoptosis imaging agent. *Molecules.* 2013;18:6908–6918.
350. Benali K, Louedec L, Azzouna RB, et al. Preclinical validation of  $^{99m}\text{Tc}$ -Annexin A5-128 in experimental autoimmune myocarditis and infective endocarditis: comparison with  $^{99m}\text{Tc}$ -HYNIC-Annexin A5. *Mol Imaging.* 2014;13. <https://doi.org/10.2310/7290.2014.00049>
351. Tait JF, Smith C, Levashova Z, Patel B, Blankenberg FG, Vanderheyden JL. Improved detection of cell death in vivo with Annexin V radiolabeled by site-specific methods. *J Nucl Med.* 2006;47:1546–1553.
352. Thiagarajan P, Tait JF. Binding of Annexin V/placental anticoagulant protein I to platelets. Evidence for phosphatidylserine exposure in the procoagulant response of activated platelets. *J Biol Chem.* 1990;265:17420–17423.
353. Lahorte C, Slegers G, Philippe J, Van de Wiele C, Dierckx RA. Synthesis and in vitro evaluation of  $^{123}\text{I}$ -labelled human recombinant Annexin V. *Biomol Eng.* 2001;17:51–53.
354. Lahorte CM, Van de Wiele C, Bacher K, et al. Biodistribution and dosimetry study of  $^{123}\text{I}$ -rh-Annexin V in mice and humans. *Nucl Med Commun.* 2003;24:871–880.
355. Russell J, O'Donoghue JA, Finn R, et al. Iodination of Annexin V for imaging apoptosis. *J Nucl Med.* 2002;43:671–677.
356. Cornelissen B, Lahorte C, Kersemans V, et al. In vivo apoptosis detection with radioiodinated Annexin V in LoVo tumour-bearing mice following Tipifarnib (Zarnestra, R115777) farnesyltransferase inhibitor therapy. *Nucl Med Biol.* 2005;32:233–239.
357. Watanabe H, Murata Y, Miura M, Hasegawa M, Kawamoto T, Shibuya H. In-vivo visualization of radiation-induced apoptosis using ( $^{125}\text{I}$ )-Annexin V. *Nucl Med Commun.* 2006;27:81–89.
358. Dekker B, Keen H, Lyons S, et al. MBP-Annexin V radiolabeled directly with iodine-124 can be used to image apoptosis in vivo using PET. *Nucl Med Biol.* 2005;32:241–252.
359. Glaser M, Collingridge DR, Aboagye EO, et al. Iodine-124 labelled Annexin-V as a potential radiotracer to study apoptosis using positron emission tomography. *Appl Radiat Isot.* 2003;58:55–62.
360. Keen HG, Dekker BA, Disley L, et al. Imaging apoptosis in vivo using  $^{124}\text{I}$ -Annexin V and PET. *Nucl Med Biol.* 2005;32:395–402.
361. Dekker B, Keen H, Shaw D, et al. Functional comparison of Annexin V analogues labeled indirectly and directly with iodine-124. *Nucl Med Biol.* 2005;32:403–413.
362. Collingridge DR, Glaser M, Osman S, et al. In vitro selectivity, in vivo biodistribution and tumour uptake of Annexin V radiolabelled with a positron emitting radioisotope. *Br J Cancer.* 2003;89:1327–1333.
363. Hu S, Kiesewetter DO, Zhu L, et al. Longitudinal PET imaging of doxorubicin-induced cell death with  $^{18}\text{F}$ -Annexin V. *Mol Imaging Biol.* 2012;14:762–770.
364. Perreault A, Knight JC, Wang M, Way J, Wuest F.  $^{18}\text{F}$ -Labeled wild-type Annexin V: comparison of random and site-selective radiolabeling methods. *Amino Acids.* 2016;48:65–74.
365. Yagle KJ, Eary JF, Tait JF, et al. Evaluation of  $^{18}\text{F}$ -Annexin V as a PET imaging agent in an animal model of apoptosis. *J Nucl Med.* 2005;46:658–666.
366. Zhang X, Paule MG, Newport GD, et al. A minimally invasive, translational biomarker of ketamine-induced neuronal death in rats: microPET imaging using  $^{18}\text{F}$ -Annexin V. *Toxicol Sci.* 2009;111:355–361.
367. Zijlstra S, Gunawan J, Burchert W. Synthesis and evaluation of a  $^{18}\text{F}$ -labelled recombinant Annexin-V derivative, for identification and quantification of apoptotic cells with PET. *Appl Radiat Isot.* 2003;58:201–207.
368. Toretsky J, Levenson A, Weinberg IN, Tait JF, Uren A, Mease RC. Preparation of F-18 labeled Annexin V: a potential PET radiopharmaceutical for imaging cell death. *Nucl Med Biol.* 2004;31:747–752.
369. Qin H, Zhang MR, Xie L, et al. PET imaging of apoptosis in tumor-bearing mice and rabbits after paclitaxel treatment with ( $^{18}\text{F}$ )-Labeled recombinant human His10-Annexin V. *Am J Nucl Med Mol Imaging.* 2015;5:27–37.
370. Li X, Link JM, Stekhova S, et al. Site-specific labeling of Annexin V with F-18 for apoptosis imaging. *Bioconjug Chem.* 2008;19:1684–1688.
371. Luo QY, Wang F, Zhang ZY, et al. Preparation and bioevaluation of ( $^{99m}\text{Tc}$ )-HYNIC-Annexin B1 as a novel radioligand for apoptosis imaging. *Apoptosis.* 2008;13:600–608.
372. Luo QY, Zhang ZY, Wang F, Lu HK, Guo YZ, Zhu RS. Preparation, in vitro and in vivo evaluation of ( $^{99m}\text{Tc}$ )-Annexin B1: a novel radioligand for apoptosis imaging. *Biochem Biophys Res Commun.* 2005;335:1102–1106.

373. Wang MW, Wang F, Zheng YJ, et al. An in vivo molecular imaging probe (18)F-Annexin B1 for apoptosis detection by PET/CT: preparation and preliminary evaluation. *Apoptosis*. 2013;18:238–247.
374. Zhao M, Zhu X, Ji S, et al. 99mTc-labeled C2A domain of synaptotagmin I as a target-specific molecular probe for noninvasive imaging of acute myocardial infarction. *J Nucl Med*. 2006;47:1367–1374.
375. Wang F, Fang W, Zhao M, et al. Imaging paclitaxel (chemotherapy)-induced tumor apoptosis with 99mTc C2A, a domain of synaptotagmin I: a preliminary study. *Nucl Med Biol*. 2008;35:359–364.
376. Tavare R, De Rosales TMR, Blower PJ, Mullen GE. Efficient site-specific radiolabeling of a modified C2A domain of synaptotagmin I with [99mTc(CO)3]+: a new radiopharmaceutical for imaging cell death. *Bioconjug Chem*. 2009;20:2071–2081.
377. Huetting R, Tavare R, Dilworth JR, Mullen GE. Copper-64 radiolabelling of the C2A domain of synaptotagmin I using a functionalised bis(thiosemicarbazone): a pre- and post-labelling comparison. *J Inorg Biochem*. 2013;128:108–111.
378. Falborg L, Waehrens LN, Alsner J, et al. Biodistribution of 99mTc-HYNIC-lactadherin in mice: a potential tracer for visualizing apoptosis in vivo. *Scand J Clin Lab Invest*. 2010;70:209–216.
379. Waehrens LN, Heegaard CW, Gilbert GE, Rasmussen JT. Bovine lactadherin as a calcium-independent imaging agent of phosphatidylserine expressed on the surface of apoptotic HeLa cells. *J Histochem Cytochem*. 2009;57:907–914.
380. Poulsen RH, Rasmussen JT, Ejlersen JA, et al. Pharmacokinetics of the phosphatidylserine tracers 99mTc-lactadherin and 99mTc-Annexin V in pigs. *EJNMMI Res*. 2013;3:15.
381. Xiong C, Brewer K, Song S, et al. Peptide-based imaging agents targeting phosphatidylserine for the detection of apoptosis. *J Med Chem*. 2011;54:1825–1835.
382. Song S, Xiong C, Lu W, Ku G, Huang G, Li C. Apoptosis imaging probe predicts early chemotherapy response in preclinical models: a comparative study with 18F-FDG PET. *J Nucl Med*. 2013;54:104–110.
383. Gerber DE, Hao G, Watkins L, et al. Tumor-specific targeting by Bavituximab, a phosphatidylserine-targeting monoclonal antibody with vascular targeting and immune modulating properties, in lung cancer xenografts. *Am J Nucl Med Mol Imaging*. 2015;5:493–503.
384. Kumar A, Hao G, Liu L, et al. Click-chemistry strategy for labeling antibodies with copper-64 via a cross-bridged tetraaza-macrocyclic chelator scaffold. *Bioconjug Chem*. 2015;26:782–789.
385. Ogasawara A, Tinianow JN, Vanderbilt AN, et al. ImmunoPET imaging of phosphatidylserine in pro-apoptotic therapy treated tumor models. *Nucl Med Biol*. 2013;40:15–22.
386. Stafford JH, Hao G, Best AM, Sun X, Thorpe PE. Highly specific PET imaging of prostate tumors in mice with an iodine-124-labeled antibody fragment that targets phosphatidylserine. *PLoS One*. 2013;8:e84864.
387. Cohen A, Ziv I, Aloya T, et al. Monitoring of chemotherapy-induced cell death in melanoma tumors by N,N'-Didansyl-L-cystine. *Technol Cancer Res Treat*. 2007;6:221–234.
388. Levin G, Shirvan A, Grimberg H, et al. Novel fluorescence molecular imaging of chemotherapy-induced intestinal apoptosis. *J Biomed Opt*. 2009;14:054019.
389. Aloya R, Shirvan A, Grimberg H, et al. Molecular imaging of cell death in vivo by a novel small molecule probe. *Apoptosis*. 2006;11:2089–2101.
390. Basuli F, Wu H, Shi ZD, et al. Synthesis of ApoSense compound [18F]2-(5-(dimethylamino)naphthalene-1-sulfonamido)-2-(fluoromethyl)butanoic acid ([18F]NST732) by nucleophilic ring opening of an aziridine precursor. *Nucl Med Biol*. 2012;39:687–696.
391. Shirvan A, Reshef A, Yogev-Falach M, Ziv I. Molecular imaging of neurodegeneration by a novel cross-disease biomarker. *Exp Neurol*. 2009;219:274–283.
392. Hoglund J, Shirvan A, Antoni G, et al. 18F-ML-10, a PET tracer for apoptosis: first human study. *J Nucl Med*. 2011;52:720–725.
393. Bauwens M, De Saint-Hubert M, Cleynhens J, Vandeputte C, Li J, Devos E. In vitro and in vivo comparison of 18F and 123I-labeled ML10 with 68Ga-Cys2-AnxA5 for molecular imaging of apoptosis. *Q J Nucl Med Mol Imaging*. 2013;57:187–200.
394. Allen AM, Ben-Ami M, Reshef A, et al. Assessment of response of brain metastases to radiotherapy by PET imaging of apoptosis with (1)(8)F-ML-10. *Eur J Nucl Med Mol Imaging*. 2012;39:1400–1408.
395. Haberkorn U, Kinscherf R, Krammer PH, Mier W, Eisenhut M. Investigation of a potential scintigraphic marker of apoptosis: radioiodinated Z-Val-Ala-DL-Asp(O-methyl)-fluoromethyl ketone. *Nucl Med Biol*. 2001;28:793–798.
396. Hight MR, Cheung YY, Nickels ML, et al. A peptide-based positron emission tomography probe for in vivo detection of caspase activity in apoptotic cells. *Clin Cancer Res*. 2014;20:2126–2135.

397. Faust A, Wagner S, Law MP, et al. The nonpeptidyl caspase binding radioligand (S)-1-(4-(2-[<sup>18</sup>F]fluoroethoxy)-benzyl)-5-[1-(2-methoxymethylpyrrolidinyl)sulfonyl]isatin ([<sup>18</sup>F]CbR) as potential positron emission tomography-compatible apoptosis imaging agent. *Q J Nucl Med Mol Imaging*. 2007;51:67–73.
398. Zhou D, Chu W, Rothfuss J, et al. Synthesis, radiolabeling, and in vivo evaluation of an 18F-labeled isatin analog for imaging caspase-3 activation in apoptosis. *Bioorg Med Chem Lett*. 2006;16:5041–5046.
399. Zhou D, Chu W, Chen DL, et al. [<sup>18</sup>F]- and [<sup>11</sup>C]-labeled N-benzyl-isatin sulfonamide analogues as PET tracers for apoptosis: synthesis, radiolabeling mechanism, and in vivo imaging study of apoptosis in Fas-treated mice using [<sup>11</sup>C]WC-98. *Org Biomol Chem*. 2009;7:1337–1348.
400. Chen DL, Zhou D, Chu W, et al. Comparison of radiolabeled isatin analogs for imaging apoptosis with positron emission tomography. *Nucl Med Biol*. 2009;36:651–658.
401. Nguyen QD, Smith G, Glaser M, Perumal M, Arstad E, Aboagye EO. Positron emission tomography imaging of drug-induced tumor apoptosis with a caspase-3/7 specific [<sup>18</sup>F]-labeled isatin sulfonamide. *Proc Natl Acad Sci USA*. 2009;106:16375–16380.
402. Witney TH, Fortt R, Aboagye EO. Preclinical assessment of carboplatin treatment efficacy in lung cancer by 18F-ICMT-11-positron emission tomography. *PLoS One*. 2014;9:e91694.
403. Smith G, Glaser M, Perumal M, et al. Design, synthesis, and biological characterization of a caspase 3/7 selective isatin labeled with 2-[<sup>18</sup>F]fluoroethylazide. *J Med Chem*. 2008;51:8057–8067.
404. Nguyen QD, Lavdas I, Gubbins J, et al. Temporal and spatial evolution of therapy-induced tumor apoptosis detected by caspase-3-selective molecular imaging. *Clin Cancer Res*. 2013;19:3914–3924.
405. Challapalli A, Kenny LM, Hallett WA, et al. 18F-ICMT-11, a caspase-3-specific PET tracer for apoptosis: biodistribution and radiation dosimetry. *J Nucl Med*. 2013;54:1551–1556.
406. Glaser M, Goggi J, Smith G, et al. Improved radiosynthesis of the apoptosis marker 18F-ICMT11 including biological evaluation. *Bioorg Med Chem Lett*. 2011;21:6945–6949.
407. Fortt R, Smith G, Awais RO, Luthra SK, Aboagye EO. Automated GMP synthesis of [(18)F]ICMT-11 for in vivo imaging of caspase-3 activity. *Nucl Med Biol*. 2012;39:1000–1005.
408. Nguyen QD, Challapalli A, Smith G, Fortt R, Aboagye EO. Imaging apoptosis with positron emission tomography: 'bench to bedside' development of the caspase-3/7 specific radiotracer [(18)F]ICMT-11. *Eur J Cancer*. 2012;48:432–440.
409. Chen DL, Engle JT, Griffin EA, et al. Imaging caspase-3 activation as a marker of apoptosis-targeted treatment response in cancer. *Mol Imaging Biol*. 2015;17:384–393.
410. Xia CF, Chen G, Gangadharmath U, et al. In vitro and in vivo evaluation of the caspase-3 substrate-based radiotracer [(18)F]-CP18 for PET imaging of apoptosis in tumors. *Mol Imaging Biol*. 2013;15:748–757.
411. Ropic S, Vangestel C, Elvas F, et al. Evaluation of [<sup>18</sup>F]CP18 as a substrate-based apoptosis imaging agent for the assessment of early treatment response in oncology. *Mol Imaging Biol*. 2017;19:560–569.
412. Su H, Chen G, Gangadharmath U, et al. Evaluation of [(18)F]-CP18 as a PET imaging tracer for apoptosis. *Mol Imaging Biol*. 2013;15:739–747.
413. Su H, Gorodny N, Gomez LF, et al. Noninvasive molecular imaging of apoptosis in a mouse model of anthracycline-induced cardiotoxicity. *Circ Cardiovasc Imaging*. 2015;8:e001952.
414. Doss M, Kolb HC, Walsh JC, et al. Biodistribution and radiation dosimetry of 18F-CP-18, a potential apoptosis imaging agent, as determined from PET/CT scans in healthy volunteers. *J Nucl Med*. 2013;54:2087–2092.
415. Tu Z, Chu W, Zhang J, Dence CS, Welch MJ, Mach RH. Synthesis and in vivo evaluation of [<sup>11</sup>C]PJ34, a potential radiotracer for imaging the role of PARP-1 in necrosis. *Nucl Med Biol*. 2005;32:437–443.
416. Keliher EJ, Reiner T, Turetsky A, Hilderbrand SA, Weissleder R. High-yielding, two-step 18F labeling strategy for 18F-PARP1 inhibitors. *Chem Med Chem*. 2011;6:424–427.
417. Reiner T, Keliher EJ, Earley S, Marinelli B, Weissleder R. Synthesis and in vivo imaging of a 18F-labeled PARP1 inhibitor using a chemically orthogonal scavenger-assisted high-performance method. *Angew Chem Int Ed Engl*. 2011;50:1922–1925.
418. Reiner T, Lacy J, Keliher EJ, et al. Imaging therapeutic PARP inhibition in vivo through bioorthogonally developed companion imaging agents. *Neoplasia*. 2012;14:169–177.
419. Carlucci G, Carney B, Brand C, et al. Dual-modality optical/PET imaging of PARP1 in glioblastoma. *Mol Imaging Biol*. 2015;17:848–855.
420. Carney B, Carlucci G, Salinas B, et al. Non-invasive PET imaging of PARP1 expression in glioblastoma models. *Mol Imaging Biol*. 2016;18:386–392.

421. Salinas B, Irwin CP, Kossatz S, et al. Radioiodinated PARP1 tracers for glioblastoma imaging. *EJNMMI Res.* 2015;5:123.
422. Zmuda F, Malviya G, Blair A, et al. Synthesis and evaluation of a radioiodinated tracer with specificity for poly(ADP-ribose) polymerase-1 (PARP-1) in vivo. *J Med Chem.* 2015;58:8683–8693.
423. Edmonds CE, Makvandi M, Lieberman BP, et al. [(18)F]FluorThanatrace uptake as a marker of PARP1 expression and activity in breast cancer. *Am J Nucl Med Mol Imaging.* 2016;6:94–101.
424. Sander Effron S, Makvandi M, Lin L, et al. PARP-1 expression quantified by [18f]fluorothantrace: a biomarker of response to parp inhibition adjuvant to radiation therapy. *Cancer Biother Radiopharm.* 2017;32:9–15.
425. Zhou D, Chu W, Xu J, et al. Synthesis, [(18)F] radiolabeling, and evaluation of poly (ADP-ribose) polymerase-1 (PARP-1) inhibitors for in vivo imaging of PARP-1 using positron emission tomography. *Bioorg Med Chem.* 2014;22:1700–1707.
426. Michel LS, Dyroff S, Brooks FJ, et al. PET of poly (ADP-Ribose) polymerase activity in cancer: preclinical assessment and first in-human studies. *Radiology.* 2017;282:453–463.
427. Makvandi M, Xu K, Lieberman BP, et al. A radiotracer strategy to quantify PARP-1 expression in vivo provides a biomarker that can enable patient selection for PARP inhibitor therapy. *Cancer Res.* 2016;76:4516–4524.
428. Anderson RC, Makvandi M, Xu K, et al. Iodinated benzimidazole PARP radiotracer for evaluating PARP1/2 expression in vitro and in vivo. *Nucl Med Biol.* 2016;43:752–758.
429. Cornelissen B, Kersemans V, Darbar S, et al. Imaging DNA damage in vivo using gammaH2AX-targeted immunoconjugates. *Cancer Res.* 2011;71:4539–4549.
430. Cornelissen B, Able S, Kartsonaki C, et al. Imaging DNA damage allows detection of preneoplasia in the BALB-neuT model of breast cancer. *J Nucl Med.* 2014;55:2026–2031.
431. Knight JC, Topping C, Mosley M, et al. PET imaging of DNA damage using (89)Zr-labelled anti-gammaH2AX-TAT immunoconjugates. *Eur J Nucl Med Mol Imaging.* 2015;42:1707–1717.
432. Carlucci G, Carney B, Sadique A, Vansteene A, Tang J, Reiner T. Evaluation of [18F]-ATRi as PET tracer for in vivo imaging of ATR in mouse models of brain cancer. *Nucl Med Biol.* 2017;48:9–15.
433. Kwak W, Ha YS, Soni N, et al. Apoptosis imaging studies in various animal models using radio-iodinated peptide. *Apoptosis.* 2015;20:110–121.
434. Sachin K, Jadhav VH, Kim EM, et al. F-18 labeling protocol of peptides based on chemically orthogonal strain-promoted cycloaddition under physiologically friendly reaction conditions. *Bioconjug Chem.* 2012;23:1680–1686.
435. Jung HK, Wang K, Jung MK, Kim IS, Lee BH. In vivo near-infrared fluorescence imaging of apoptosis using histone H1-targeting peptide probe after anti-cancer treatment with cisplatin and cetuximab for early decision on tumor response. *PLoS One.* 2014;9:e100341.
436. Al-Ejeh F, Darby JM, Pensa K, Diener KR, Hayball JD, Brown MP. In vivo targeting of dead tumor cells in a murine tumor model using a monoclonal antibody specific for the La autoantigen. *Clin Cancer Res.* 2007;13:5519s–5527s.
437. Kubota K, Ishiwata K, Kubota R, Yamada S. Investigation of tumor invasion with [111In]antimyosin. *Nucl Med Biol.* 1994;21:239–244.
438. Cox PH, Verweij J, Pillay M, Stoter G, Schonfeld D. Indium 111 antimyosin for the detection of leiomyosarcoma and rhabdomyosarcoma. *Eur J Nucl Med.* 1988;14:50–52.
439. Hoefnagel CA, Kapucu O, de Kraker J, van Dongen A, Voute PA. Radioimmunoscintigraphy using [111In]antimyosin Fab fragments for the diagnosis and follow-up of rhabdomyosarcoma. *Eur J Cancer.* 1993;29A:2096–2100.
440. Kairemo KJ, Lehtovirta P. Radioimmunodetection of uterine leiomyosarcoma with 111In-labeled monoclonal antimyosin antibody Fab fragments. *Gynecol Oncol.* 1990;36:417–422.
441. Koscielniak E, Reuland P, Schilling F, Feine U, Treuner J. Radio-immunodetection of myosarcoma using 111indium antimyosin. *Klin Padiatr.* 1990;202:230–234.
442. Reuland P, Koscielniak E, Ruck P, Treuner J, Feine U. Application of an anti-myosin antibody for scintigraphic differential diagnosis of infantile tumors. *Int J Rad Appl Instrum B.* 1991;18:89–93.
443. Kairemo KJ, Wiklund TA, Liewendahl K, et al. Imaging of soft-tissue sarcomas with indium-111-labeled monoclonal antimyosin Fab fragments. *J Nucl Med.* 1990;31:23–31.
444. Petrov AD, Narula J, Nakazawa A, Pak KY, Khaw BA. Targeting human breast tumour in xeno-grafted SCID mice with 99Tcm-glucarate. *Nucl Med Commun.* 1997;18:241–251.
445. Perek N, Le Jeune N, Denoyer D, Dubois F. MRP-1 protein expression and glutathione content of in vitro tumor cell lines derived from human glioma carcinoma U-87-MG do not interact with 99mTc-glucarate uptake. *Cancer Biother Radiopharm.* 2005;20:391–400.

446. Cheng D, Ruszkowski M, Wang Y, et al. A brief evaluation of tumor imaging in mice with  $^{99m}\text{Tc}$ -glucarate including a comparison with  $^{18}\text{F}$ -FDG. *Curr Radiopharm*. 2011;4:5–9.
447. Gambini JP, Cabral P, Alonso O, et al. Evaluation of  $^{99m}\text{Tc}$ -glucarate as a breast cancer imaging agent in a xenograft animal model. *Nucl Med Biol*. 2011;38:255–260.
448. Gambini JP, Nunez M, Cabral P, et al. Evaluation of patients with head and neck cancer by means of  $^{99m}\text{Tc}$ -glucarate. *J Nucl Med Technol*. 2009;37:229–232.
449. Choudhury PS, Savio E, Solanki KK, et al. ( $^{99m}\text{Tc}$ ) glucarate as a potential radiopharmaceutical agent for assessment of tumor viability: from bench to the bed side. *World J Nucl Med*. 2012;11:47–56.
450. Okada DR, Johnson G, III, Liu Z, et al. Myocardial kinetics of Tc- $^{99m}$  glucarate in low flow, hypoxia, and aglycemia. *J Nucl Cardiol*. 2003;10:168–176.
451. Ballinger JR, Hsue V, Rauth AM. Accumulation of technetium- $^{99m}$  glucarate: in vitro cell cultures and in vivo tumour models. *Nucl Med Commun*. 2003;24:597–606.
452. Van de Putte M, Ni Y, de Witte PA. Exploration of the mechanism underlying the tumor necrosis avidity of hypericin. *Oncol Rep*. 2008;19:921–926.
453. Jiang B, Wang J, Ni Y, Chen F. Necrosis avidity: a newly discovered feature of hypericin and its preclinical applications in necrosis imaging. *Theranostics*. 2013;3:667–676.
454. Duan X, Yin Z, Jiang C, et al. Radioiodinated hypericin disulfonic acid sodium salts as a DNA-binding probe for early imaging of necrotic myocardium. *Eur J Pharm Biopharm*. 2017;117:151–159.
455. Song S, Xiong C, Zhou M, et al. Small-animal PET of tumor damage induced by photothermal ablation with  $^{64}\text{Cu}$ -bis-DOTA-hypericin. *J Nucl Med*. 2011;52:792–799.
456. Li J, Cona MM, Chen F, et al. Exploring theranostic potentials of radioiodinated hypericin in rodent necrosis models. *Theranostics*. 2012;2:1010–1019.
457. Shao H, Zhang J, Sun Z, et al. Necrosis targeted radiotherapy with iodine-131-labeled hypericin to improve anticancer efficacy of vascular disrupting treatment in rabbit VX2 tumor models. *Oncotarget*. 2015;6:14247–14259.
458. Cona MM, Feng Y, Li Y, et al. Comparative study of iodine-123-labeled hypericin and ( $^{99m}\text{Tc}$ )-labeled hexakis [2-methoxy isobutyl isonitrile] in a rabbit model of myocardial infarction. *J Cardiovasc Pharmacol*. 2013;62:304–311.
459. Qi X, Shao H, Zhang J, Sun Z, Ni Y, Xu K. Radiopharmaceutical study on Iodine-131-labelled hypericin in a canine model of hepatic RFA-induced coagulative necrosis. *Radiol Med*. 2015;120:213–221.
460. Cona MM, Feng Y, Verbruggen A, Oyen R, Ni Y. Improved clearance of radioiodinated hypericin as a targeted anticancer agent by using a duodenal drainage catheter in rats. *Exp Biol Med (Maywood)*. 2013;238:1437–1449.
461. Cona MM, Koole M, Feng Y, et al. Biodistribution and radiation dosimetry of radioiodinated hypericin as a cancer therapeutic. *Int J Oncol*. 2014;44:819–829.
462. Liu W, Zhang D, Feng Y, et al. Biodistribution and anti-tumor efficacy of intratumorally injected necrosis-avid theranostic agent radioiodinated hypericin in rodent tumor models. *J Drug Target*. 2015;23:371–379.
463. Liu X, Jiang C, Li Y, et al. Evaluation of hypericin: effect of aggregation on targeting biodistribution. *J Pharm Sci*. 2015;104:215–222.
464. Cona MM, Alpizar YA, Li J, et al. Radioiodinated hypericin: its biodistribution, necrosis avidity and therapeutic efficacy are influenced by formulation. *Pharm Res*. 2014;31:278–290.
465. Ji Y, Zhan Y, Jiang C, et al. Improvement of solubility and targetability of radioiodinated hypericin by using sodium cholate based solvent in rat models of necrosis. *J Drug Target*. 2014;22:304–312.
466. Cona MM, Feng Y, Zhang J, et al. Sodium cholate, a solubilizing agent for the necrosis avid radioiodinated hypericin in rabbits with acute myocardial infarction. *Drug Deliv*. 2015;22:427–435.
467. Liu X, Feng Y, Jiang C, et al. Radiopharmaceutical evaluation of ( $^{131}\text{I}$ )-protohypericin as a necrosis avid compound. *J Drug Target*. 2015;23:417–426.
468. Wang Q, Yang S, Jiang C, et al. Discovery of radioiodinated monomeric anthraquinones as a novel class of necrosis avid agents for early imaging of necrotic myocardium. *Sci Rep*. 2016;6:21341.
469. Li J, Zhang J, Yang S, et al. Synthesis and preclinical evaluation of radioiodinated hypericin dicarboxylic acid as a necrosis avid agent in rat models of induced hepatic, muscular, and myocardial necroses. *Mol Pharm*. 2016;13:232–240.
470. Fonge H, Chitneni SK, Lixin J, et al. Necrosis avidity of ( $^{99m}\text{Tc}$ )(CO) $_3$ -labeled pamoic acid derivatives: synthesis and preliminary biological evaluation in animal models of necrosis. *Bioconjug Chem*. 2007;18:1924–1934.
471. Prinsen K, Li J, Vanbilloen H, et al. Development and evaluation of a  $^{68}\text{Ga}$  labeled pamoic acid derivative for in vivo visualization of necrosis using positron emission tomography. *Bioorg Med Chem*. 2010;18:5274–5281.

472. Prinsen K, Cona MM, Cleynhens BJ, et al. Synthesis and biological evaluation of  $^{68}\text{Ga}$ -bis-DOTA-PA as a potential agent for positron emission tomography imaging of necrosis. *Nucl Med Biol.* 2013;40:816–822.

## AUTHOR'S BIOGRAPHIES

**Anna A. Rybczynska** acquired a bachelor in biotechnology at the Institute of Biochemistry and Molecular Biology, University of Wrocław (Wrocław, Poland), in 2005, and a master of medical biotechnology at the same institution in 2007. From 2006 to 2007, she worked as an Erasmus exchange student at the Department of Molecular Neurobiology, University of Groningen (Groningen, the Netherlands), under the supervision of professor Paul Luiten, and from 2007 to 2011, she performed Ph.D. research at the Department of Nuclear Medicine and Molecular Imaging (University Medical Center Groningen, the Netherlands). Her Ph.D. project concerned the development of an imaging technique for visualization of cancer and evaluation of the metabolic and molecular responses of tumors to anticancer drug treatment, using sigma receptor ligands. After 2011, Anna performed postdoctoral research on mechanisms of cell death at the Division of Molecular Internal Medicine, University of Würzburg (Würzburg, Germany), and the Department of Nuclear Medicine and Molecular Imaging (University Medical Center Groningen, the Netherlands). Anna is currently employed as a research scientist at the Department of Genetics (University Medical Center Groningen, the Netherlands), where she is developing a diagnostic assay to facilitate treatment decisions in lung cancer patients.

**Hendrikus H. Boersma** studied pharmacy and was employed at Tramarko (Almere, the Netherlands) and the Slotervaart Hospital (Amsterdam, the Netherlands) in the late 1990s. From 1999 to 2005, he performed Ph.D. research at the Department of Human Biology, University of Maastricht (Maastricht, the Netherlands) under the supervision of professor C.P.M. Reutelingsperger. The title of his Ph.D. thesis was: "Annexin A5: Pharmacology, radiopharmaceutical aspects and cell death imaging." During the same period he was trained in clinical pharmacology and licensed as a hospital pharmacist. Near the end of his Ph.D. period, he worked as a visiting scientist at the Department of Cardiology, University of California, Irvine, CA, USA (2004–2005). Since 2007, Hendrikus is a senior staff member at the Departments of Clinical Pharmacy & Pharmacology and Nuclear Medicine & Molecular Imaging at the University Medical Center Groningen (Groningen, the Netherlands) and since 2013, he is also appointed as an assistant professor at the Faculty of Medicine, University of Groningen. Hendrikus has supervised several joint Ph.D. projects in cooperation with the Department of Cardiology, Mount Sinai Medical Center (New York, NY, USA, Dr. Jagat Narula), and several master projects in cooperation with Yale University (New Haven, CT, USA) and Karolinska Institute (Stockholm, Sweden). Some of these projects involved cell death in a cardiovascular setting.

**Steven de Jong** studied biology at the University of Groningen (the Netherlands) and acquired his Ph.D. degree in 1991. Mechanisms of drug resistance in small cell lung cancer were the subject of his thesis, which focused on DNA topoisomerases. From 1991 to 1995, Steven performed postdoctoral research on bacterial topoisomerases in the Department of Molecular Genetics, University of Groningen. In 2002–2003, he was a visiting scientist at the Burnham Institute (La Jolla, CA, USA; laboratory of professor John.C. Reed). Steven was appointed as a professor of preclinical and translational oncology in 2011. His research is directed at exploring novel rational options to enhance the therapeutic efficacy of cancer treatment. It is focused on induction of apoptosis, inhibition of pro-survival mechanisms and metabolism in tumor cells and patient-derived xenografts. Moreover, Steven is interested in gaining better understanding of the chemosensitivity and resistance of ovarian cancer and testicular germ cell tumors.

**Jourik A. Gietema** is professor of medical oncology at the University Medical Center Groningen (Groningen, the Netherlands). His research is focused on effect-driven systemic therapy of cancer and late effects of cancer treatment. Recent projects from his research group concerned: cardiovascular morbidity and mortality in breast cancer survivors; cardiovascular morbidity in testicular cancer survivors (a case-control study of risk factors and assessment of pharmacogenomic determinants of toxicity); and: increased incidence of cardiovascular morbidity in patients cured from

disseminated testicular cancer (What is the pathogenesis and how can it be prevented?). Professor Gietema is an expert in the treatment of testicular cancer. He is a member of the scientific advisory board of the Dutch Cancer Society (KWF).

**Walter Noordzij** studied medical imaging and radiation therapy at the Hanzehogeschool (University of applied sciences, Groningen, the Netherlands) and medicine at the University of Utrecht (Utrecht, the Netherlands). He acquired his MD in 2008. From 2008 to 2010, he worked as a research fellow at the Department of Cardiology, University Medical Center Groningen, and as resident not-in-training at the Department of Internal Medicine, Scheper Hospital (Emmen, the Netherlands). Walter was subsequently trained as a nuclear medicine physician at the Department of Nuclear Medicine and Molecular Imaging, University Medical Center Groningen (2010–2014), where he also performed Ph.D. research. The title of his Ph.D. thesis is: "SPECT and PET in Cardiac Sympathetic Innervation." Since 2014, Walter is a staff member at the Department of Nuclear Medicine and Molecular Imaging. Besides his work as a nuclear medicine physician with special interest in oncology and radionuclide therapy, he is the coordinator of the research lines "nuclear intervention" and "medical education."

**Rudi A. J. O. Dierckx** studied medicine and neuropsychiatry at the Free University of Brussels. He was trained as a nuclear medicine physician at the University of Antwerp (1988–1994). Rudi has headed the Department of Nuclear Medicine at the University Hospital of Ghent (Belgium) from 1994 to 2004, and has acquired a Master of Business Administration (MBA) at the Vlerick School of Management in Leuven (2004, cum laude). Since 2005 he is head of the Department of Nuclear Medicine and Molecular Imaging at University Medical Center Groningen (UMCG) in the Netherlands. In 2013, he was also appointed as head of the Medical Imaging Center, and as Chairman ad interim of the Department of Radiology at UMCG. His primary research interests are PET studies of the human brain.

**Philip H. Elsinga** was trained in radiochemistry at the Departments of Organic Chemistry and Nuclear Medicine at Groningen University (the Netherlands). Since 1995 he is the chief radiochemist of the Department of Nuclear Medicine and Molecular Imaging at the same university. Philip was a visiting scientist at the Imaging Research Lab (University of Washington, Seattle, USA) in 1998 and at the Tokyo Metropolitan Institute of Gerontology (Japan) in 2000. Since 2007 he is a visiting professor at the University of Ghent in Belgium and in 2012 he was appointed as full professor of Radiopharmaceutical Chemistry at the University of Groningen. Philip is president and co-founder of the Dutch Society for Clinical Radiochemistry, member of the Board of Directors of the Society of Radiopharmaceutical Sciences, and Editor-in-Chief of EJNMMI Radiopharmacy and Chemistry.

**Aren van Waarde** studied biology and received a Ph.D. degree from Leiden University in the Netherlands. He worked as a postdoctoral research associate in the Department of Molecular Biophysics and Biochemistry at Yale University (1986–1988). After his return from the United States, he was appointed in Leiden as a fellow of the Royal Dutch Academy of Sciences and worked on in vivo NMR spectroscopy of aquatic animals. For this research he received an award (C.J. Kok prize, Leiden University). Since 1991 he is a member of the permanent staff of the Department of Nuclear Medicine and Molecular Imaging (formerly: PET Center) at the University Medical Center Groningen (the Netherlands), and is involved in the preclinical evaluation of novel radiopharmaceuticals.

**How to cite this article:** Rybczynska AA, Boersma HH, de Jong S, et al. Avenues to molecular imaging of dying cells: Focus on cancer. *Med Res Rev.* 2018;38:1713–1768. <https://doi.org/10.1002/med.21495>